CR 137658

AVAILABLE TO THE PUBLIC

Performance of Convolutional Codes on Fading Channels Typical of Planetary Entry Missions

J.W. Modestino, S.Y. Mui, T.J. Reale

Communication and Information Processing Group

Systems Engineering Division
Rensselaer Polytechnic Institute
Troy, New York 12181

This work was performed under Contract No. NGR33-018-188 for the National Aeronautics and Space Administration, Ames Research Center, Moffett Field, California.

Period Covered

June 1, 1973 to May 31, 1974

ABSTRACT

The performance of convolutional codes in fading channels typical of the planetary entry channel is examined in detail. Here the signal fading is due primarily to turbulent atmospheric scattering of the RF signal transmitted from an entry probe through a planetary atmosphere. The primary motivation is in support of the Pioneer-Venus mission although the results should have wider applicability. Short constraint length convolutional codes are considered in conjunction with binary phase-shift keyed (BPSK) modulation and Viterbi maximum likelihood decoding while for longer constraint length codes we consider sequential decoding utilizing both the Fano and Zigangirov-Jelinek (ZJ) algorithms. Careful consideration is given to the modeling of the channel in terms of a few meaningful parameters which can be correlated closely with theoretical propagation studies. For short constraint length codes we are primarily interested in the bit error probability performance as a function of E_b/N_o parameterized by the fading channel parameters. For longer constraint length codes interest will center on the effect of the fading channel parameters on the computational requirements of both the Fano and ZJ algorithms. In either case the effects of simple block interleaving in combatting the memory of the channel is thoroughly explored. The approach is analytic where possible otherwise resort is made to digital computer simulation.

1.0 Introduction

The use of convolutional codes in conjunction with coherent binary phase-shift keyed (BPSK) modulation has proven to be an effective and efficient means of obtaining error control on the classical deep space channel. Recent work by Heller and Jacobs [1] has discussed the performance of short constraint length convolutional codes in conjunction with coherent BPSK modulation and Viterbi maximum likelihood decoding (cf. [2], [3]) while Jacobs [4] has treated the performance of longer constraint length convolutional codes utilizing sequential decoding (cf. [5], [6]). Again these works have been confined to the classical deep space channel where the net effect of the channel is simply the introduction of an additive white Gaussian noise (AWGN) component. In future planetary entry missions, however, the classical deep space channel provides an inappropriate model of the actual propagation environment experienced by an entry probe in transmitting an RF signal through a planetary atmosphere. Here it is expected that the signal will undergo fading due to a number of causes most notable of which appear to be: entry probe dynamics; effects of oscillator instabilities which become pronounced at the typically low bit rates associated with planetary entry missions; multipath reflections off the planet surface; turbulent atmospheric scattering of the RF signal within the planetary atmosphere. Our interest is primarily with this latter problem although the approach is purposely quite general and can be easily modified to apply to more general fading channel conditions. Unfortunately little is known concerning the performance of convolutional codes in fading channel environments typical of the planetary entry channel. The present study has been addressed to this problem. The primary motivation is in support of the Pioneer-Venus mission although the results should have wider applicability. In particular, we consider coherent BPSK modulation

in conjunction with Viterbi maximum likelihood decoding for short constraint length codes while sequential decoding strategies are employed for the longer constraint length codes. In the latter case both the Fano and Zigangirov-Jelinek (ZJ) algorithms are considered. Careful consideration is given to the modeling of the channel in terms of a few meaningful parameters which can be correlated closely with theoretical propagation studies. For short constraint length codes we are primarily interested in the bit error probability performance as a function of E_b/N_o parameterized by the fading channel parameters. For longer constraint length codes interest will center on the effect of the fading channel parameters on the computational requirements of both the Fano and ZJ algorithms. In either case the effects of simple block interleaving in combatting the memory of the channel is thoroughly explored. The approach is analytic where possible otherwise resort is made to digital computer simulation.

2.0 Preliminaries

Before proceeding to a discussion of binary convolutional code performance on fading channels typical of planetary entry missions, let us first consider the performance afforded by the use of coherent BPSK modulation on the additive white Gaussian noise (AWGN) channel. This will not only serve to introduce the results to follow but will allow a check on the accuracy of the various channel/decoder simulation programs employed. Consider then the communications system illustrated in Figure 2-1. Here the binary data stream $\{a_i\}$ is applied to a binary convolutional encoder resulting in a binary sequence $\{x_i\}$ (actually ± 1) at its output which is in turn applied to a modulator/transmitter producing at its output the analog channel waveform.

$$s(t) = \sqrt{2E_s} \cos(\omega_o t + \theta) \sum_i x_i p(t - i T_s) \qquad (2.1)$$

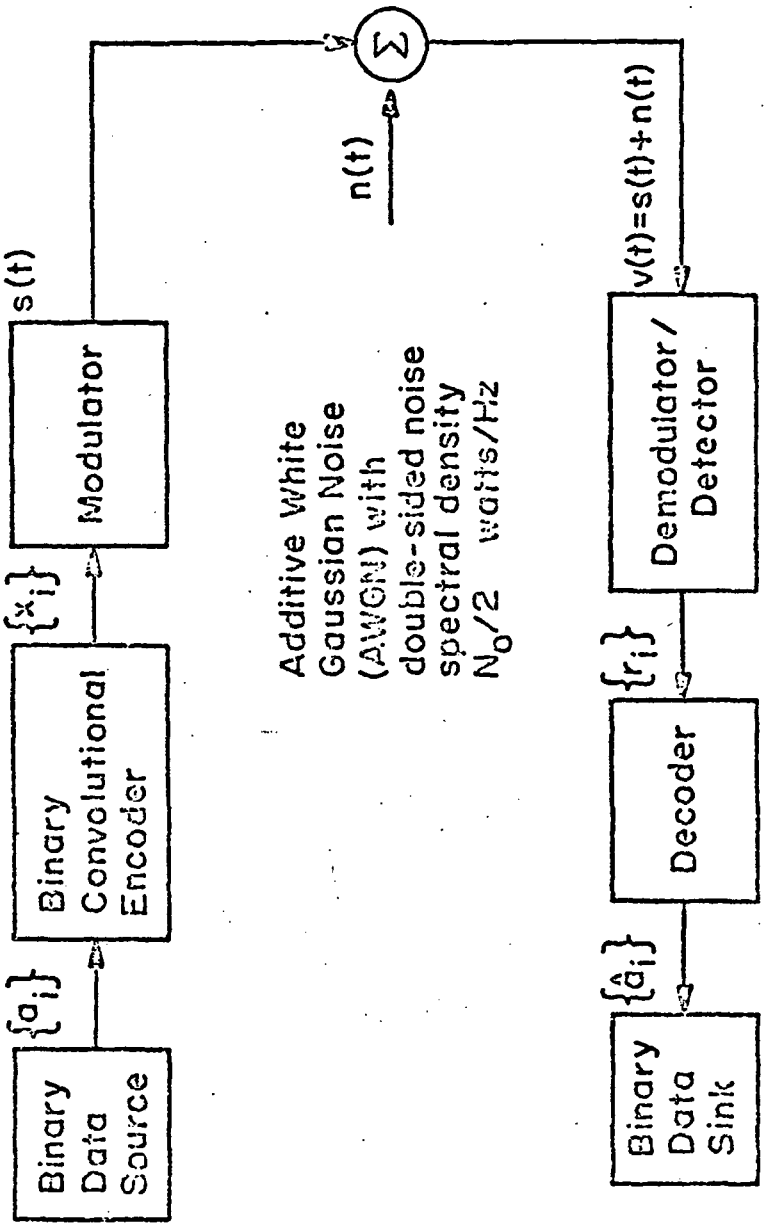

Figure 2-1

Data Communications System Employing Binary Convolutional Coding

where ω_o is the carrier frequency, Θ the carrier phase assumed known at the receiver, and p(t) a pulse-like waveform of duration T_s seconds satisfying

$$\int_0^{T_s} p^2(t)\, dt = 1 \tag{2.2}$$

so that E_s can be interpreted as the signal energy per transmitted channel symbol. The quantity E_s is related to the energy per transmitted information bit E_b by

$$E_s = R\, E_b \tag{2.3}$$

where R is the rate of the binary convolutional code. We have been concerned only with codes for which R = 1/n where n is the number of transmitted channel symbols per information bit. In some cases the binary information sequence $\{a_i\}$ must be blocked into segments or frames of length N bits to each of which K-1 (K is the code constraint length) tail zeros are added which, of course, carry no information. Such a procedure is not necessary for Viterbi decoding but is required with sequential decoding to facilitate decoder synchronization and/or restart after buffer overflow. The effect of the tail zeros is to reduce the energy available for information transmission resulting in a relationship between E_s and E_b given by

$$E_s = R\left(\frac{N}{N+K-1}\right) E_b \tag{2.4}$$

so that if $N >> K$ as in most cases of interest, we have $E_s \approx RE_b$ as in (2.3).

Due to the presence of additive channel noise, the channel output is

$$v(t) = s(t) + n(t) \tag{2.5}$$

where n(t) is zero-mean AWGN with double-sided noise spectral density $N_o/2$ watts/Hz. We will assume that the receiver utilizes a coherent matched filter matched to the pulse p(t). As a result, the receiver output after suitable normalization is the sequence of real numbers $\{r_i\}$ where

$$r_i = x_i \sqrt{\frac{2E_s}{N_o}} + n_i \; ; \qquad i = 1, 2, \ldots \tag{2.6}$$

and, as before, $\{x_i\}$ is a sequence of ± 1 values determined by the actual information sequence and the specific structure of the binary convolution code employed. The sequence $\{n_i\}$, on the other hand, is a sequence of independent and identically distributed (i.i.d.) random variables with zero mean and unit variance. The decoder processes the sequence $\{r_i\}$ to produce at its output the sequence $\{\hat{a}_i\}$ where $\hat{a}_i$ is an estimate of the i^{th} transmitted information bit a_i. Let us consider first the bit error probability performance of this system employing short constraint length binary convolutional codes and Viterbi maximum likelihood decoding.

2.1 Viterbi Decoding

Recently Viterbi [3] has provided a rather complete analysis of binary convolution codes and their performance in typical communication systems. His work has shown the utility of the state diagram and associated generating function approach to analyzing such problems. We will assume knowledge of this approach in what follows. Of immediate interest is the fact, as Viterbi has shown, that a tight upper bound on bit error probability can be obtained in terms of the generating function T(D, N) (see Ref. [3] for definitions) associated with a particular binary convolutional code. In particular, if d_f is the free distance of a code of rate R and with associated generating function T(D, N), then a tight upper bound on the resulting bit error probability is provided by the expression

$$P_b < \operatorname{erfc}\left(\sqrt{\frac{2d_f RE_b}{N_o}}\right) \exp\left\{\frac{d_f RE_b}{N_o}\right\} \left.\frac{dT(D, N)}{dN}\right|_{N=1,\ D=\exp\left\{-\frac{RE_b}{N_o}\right\}} \tag{2.7}$$

An efficient computer program (cf. [7]) has been written to evaluate this bound for arbitrary binary convolutional codes specified only in terms of their code connection vectors. Odenwalder [8] and more recently Larsen [9] have tabulated a number of good codes which, among other things, possess the desirable property of maximizing the free distance d_f for a given rate and constraint length. In particular, Odenwalder lists codes for rates R = 1/2 and 1/3 and constraint lengths $K \leq 9$, while Larsen has extended this tabulation to R = 1/2, 1/3 and 1/4 for constraint lengths $K \leq 24$. The upper bound given by (2.7) has been evaluated for the Larsen codes for rates R = 1/2, 1/3 and 1/4 and constraint lengths $K \leq 10$. The results are illustrated in Figures 2-2 through 2-4. The simulated bit error probability performance for selected R = 1/2 and 1/3 codes for various degrees of receiver output quantization are illustrated in Figures 2-5 through 2-8. The random number generator used in these simulations is one developed and tested previously at Lincoln Laboratory [10]. The path memory of the Viterbi decoder was chosen long enough to render negligible the effects of memory truncation (approximately 10 constraint lengths in each case). In all cases we have used uniform quantization of the matched filter outputs. More specifically, assume that there are Q distinct quantization levels* $\{q_1, q_2, \ldots, q_Q\}$ where Q is some power of 2. Then if I_j represents the upper endpoint of the j^{th} quantization interval j = 1, 2,...,Q we shall assume

$$I_{Q/2} = 0 \tag{2.8a}$$

$$I_{Q-j} = -I_j \; ; \qquad j = 1, 2, \ldots, \frac{Q}{2} - 1 \tag{2.8b}$$

with the additional assignments

$$I_Q = +\infty \; ; \qquad I_o = -\infty \tag{2.8c}$$

*The quantization levels are taken as the integers $\pm 1, \pm 2, \ldots, \pm Q/2$

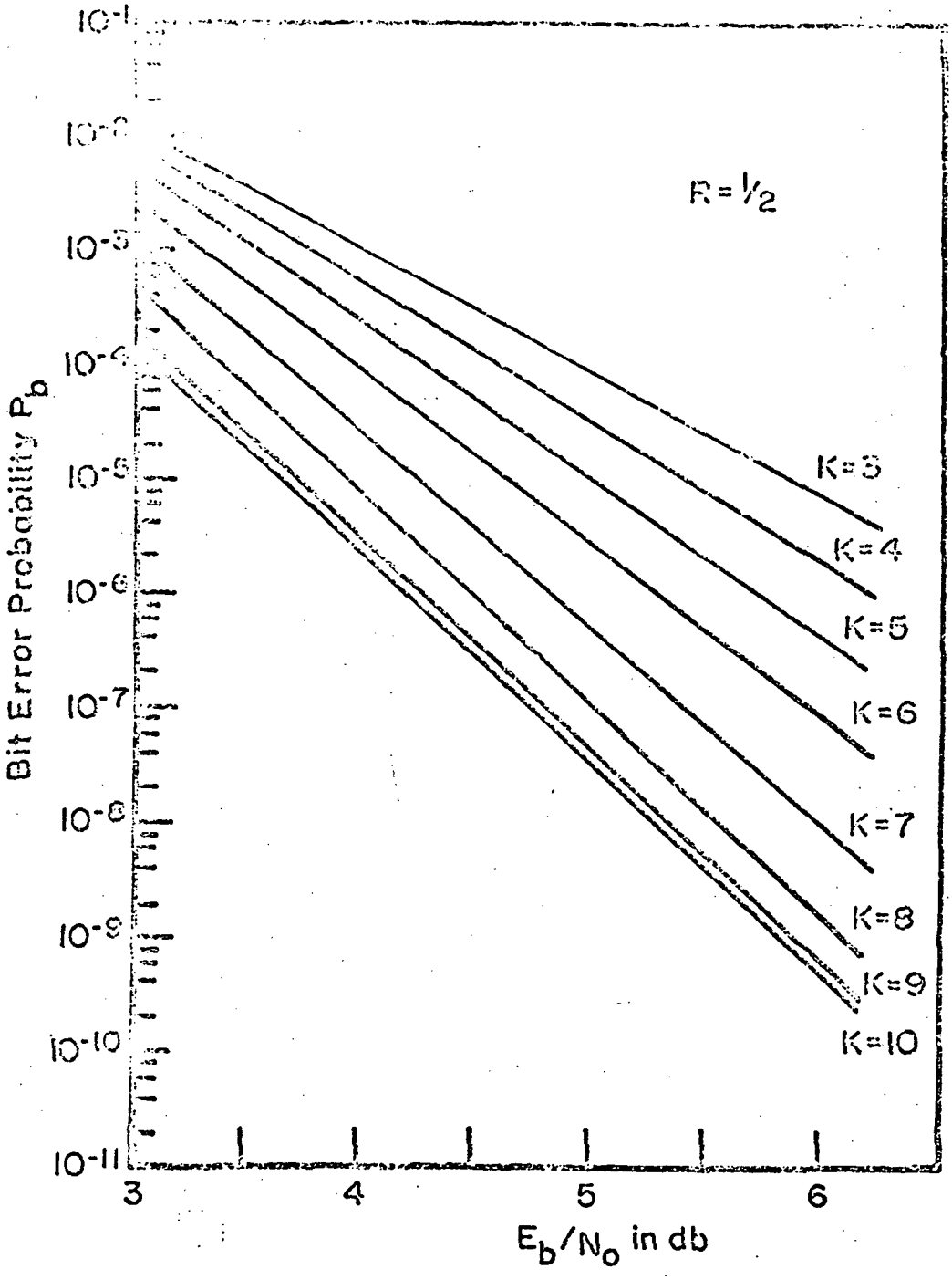

ORIGINAL PAGE IS
OF POOR QUALITY

Figure 2-2

Upper Bound on Bit Error Probability
for BPSK Modulation on AWGN
Channel with R=1/2

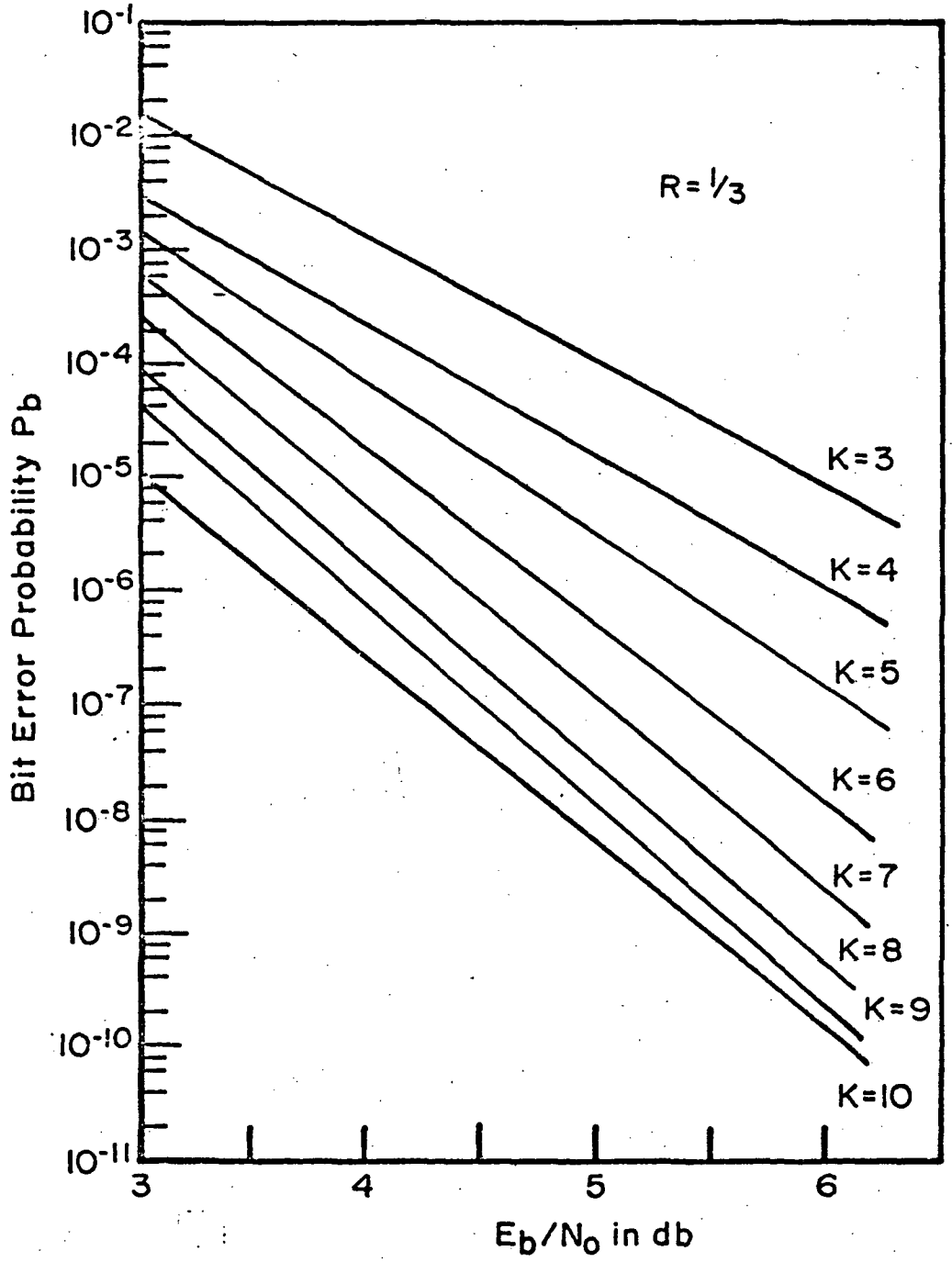

Figure 2-3

Upper Bound on Bit Error Probability for
BPSK Modulation on AWGN
Channel with R=1/3

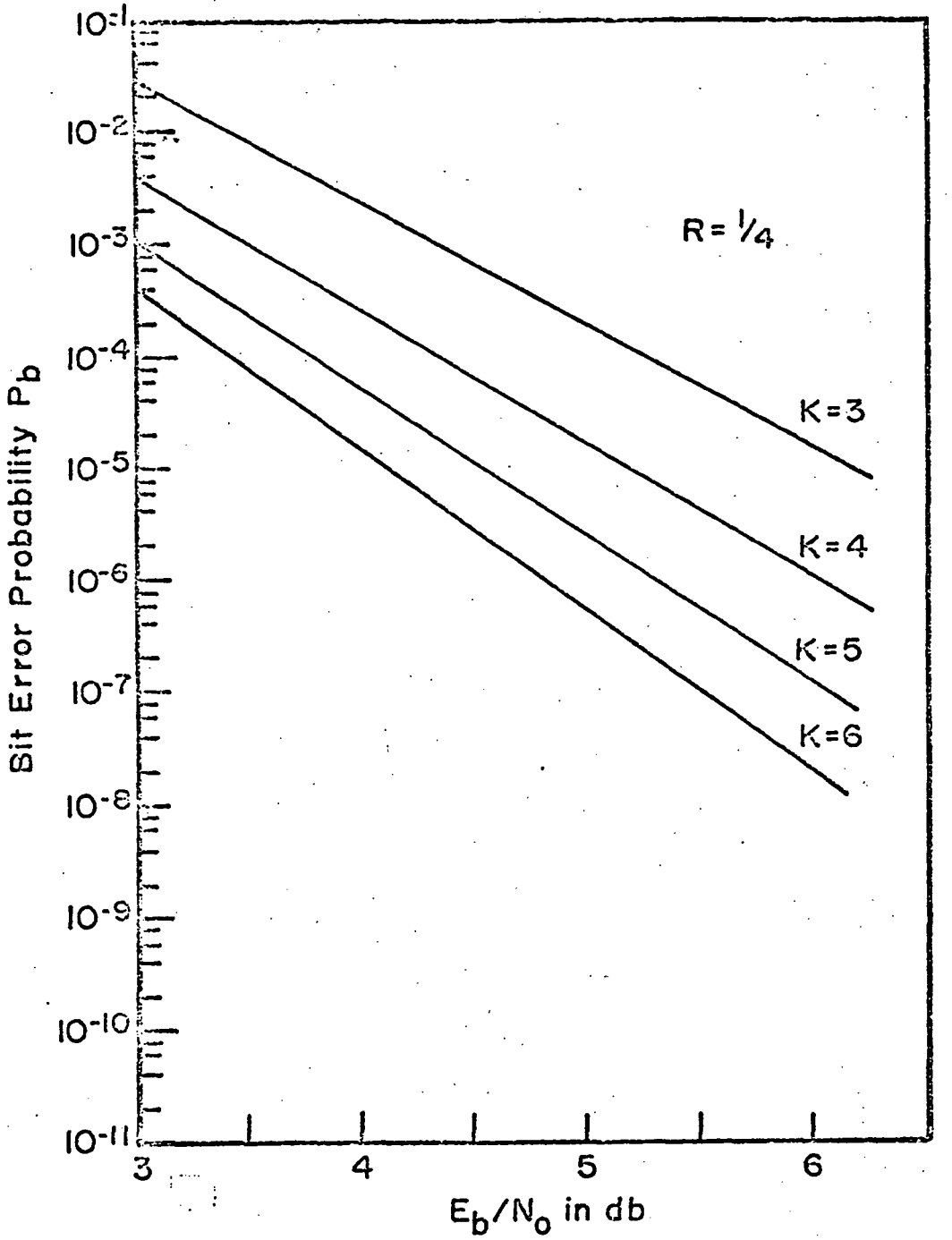

Figure 2-4

Upper Bound on Bit Error Probability for
BPSK Modulation on AWGN
Channel with R=1/4

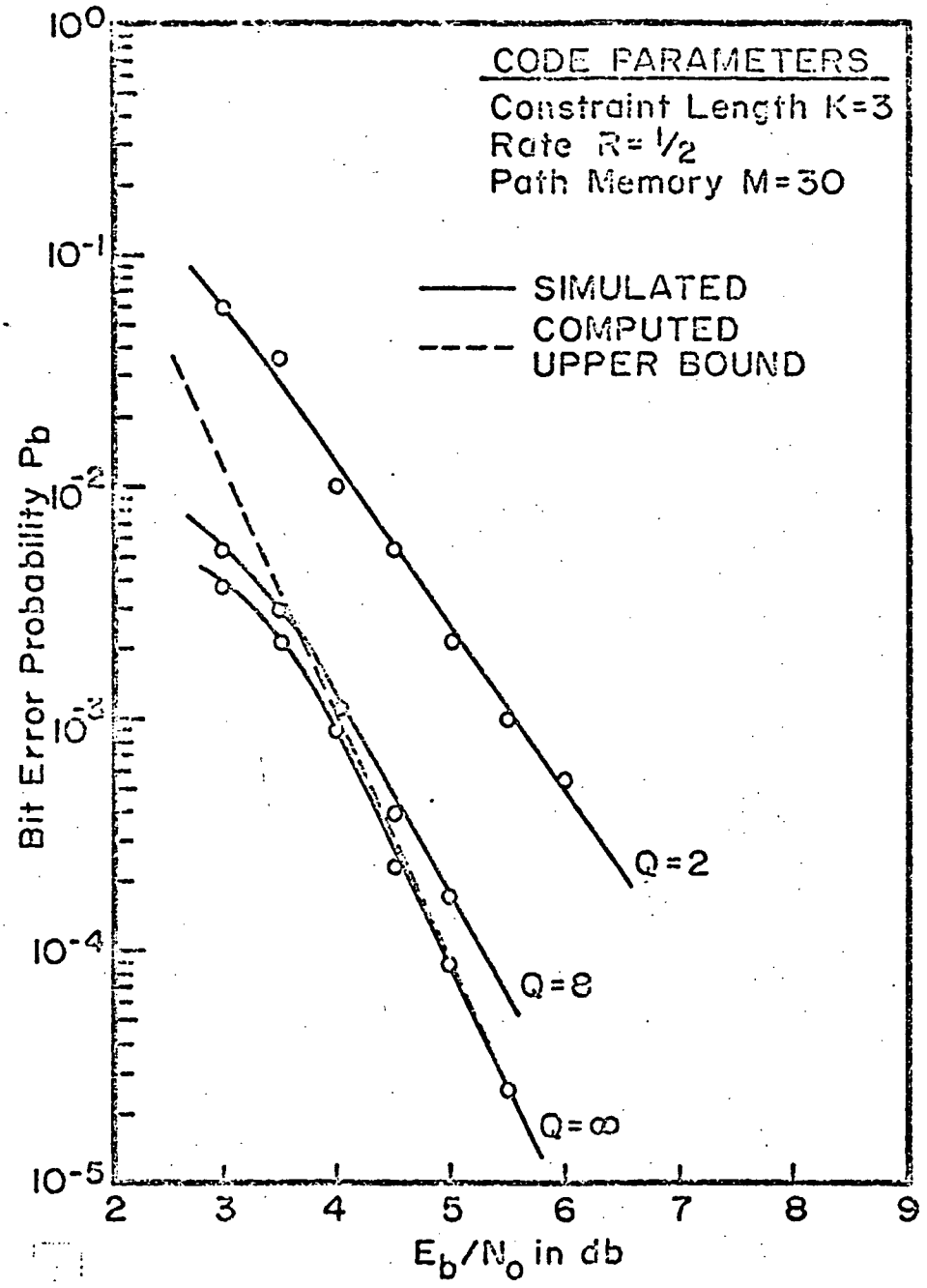

Figure 2-5

Simulated Bit Error Probability
Performance for K=3, R=1/2 Code

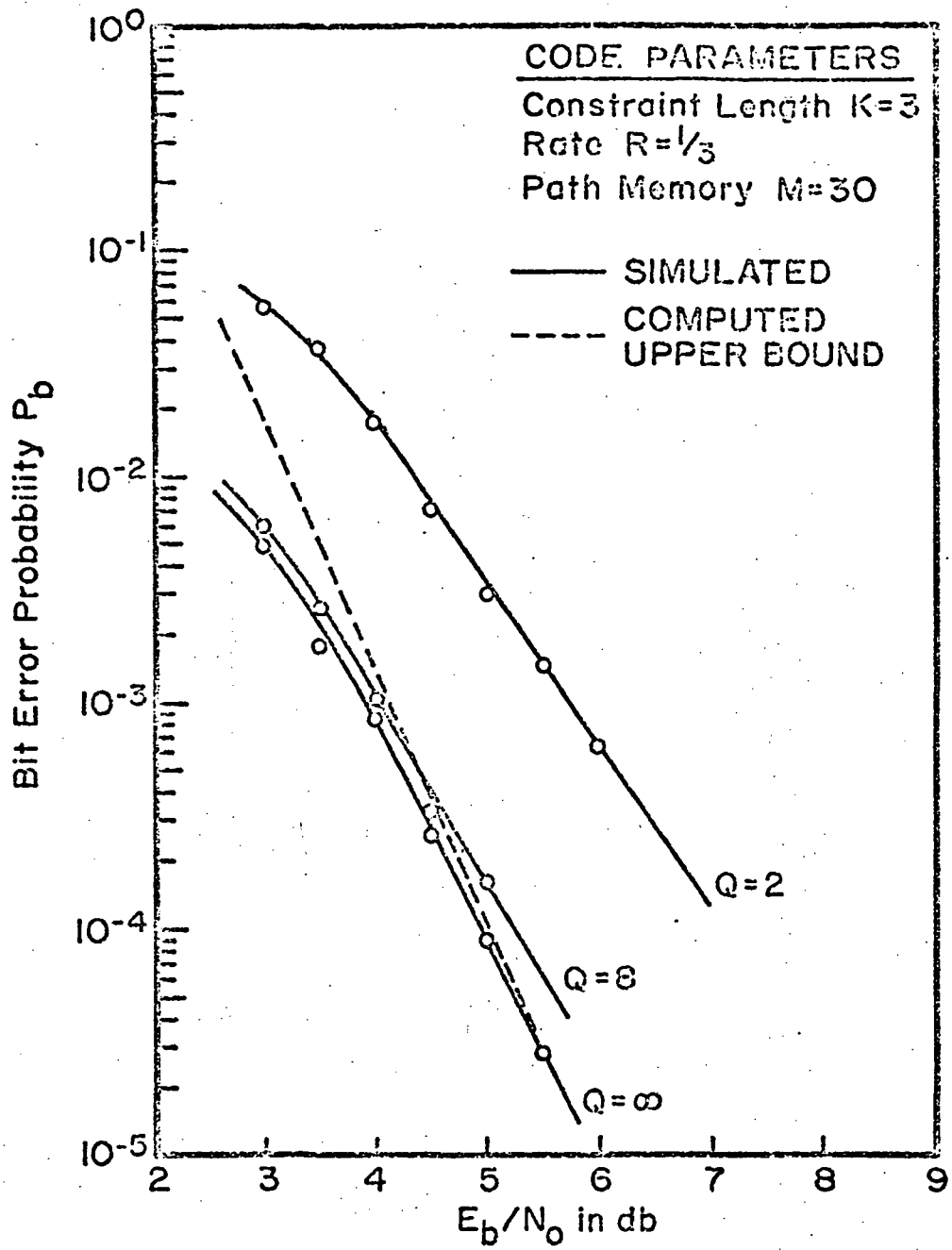

Figure 2-6

Simulated Bit Error Probability
Performance for K=3, R=1/3 Code

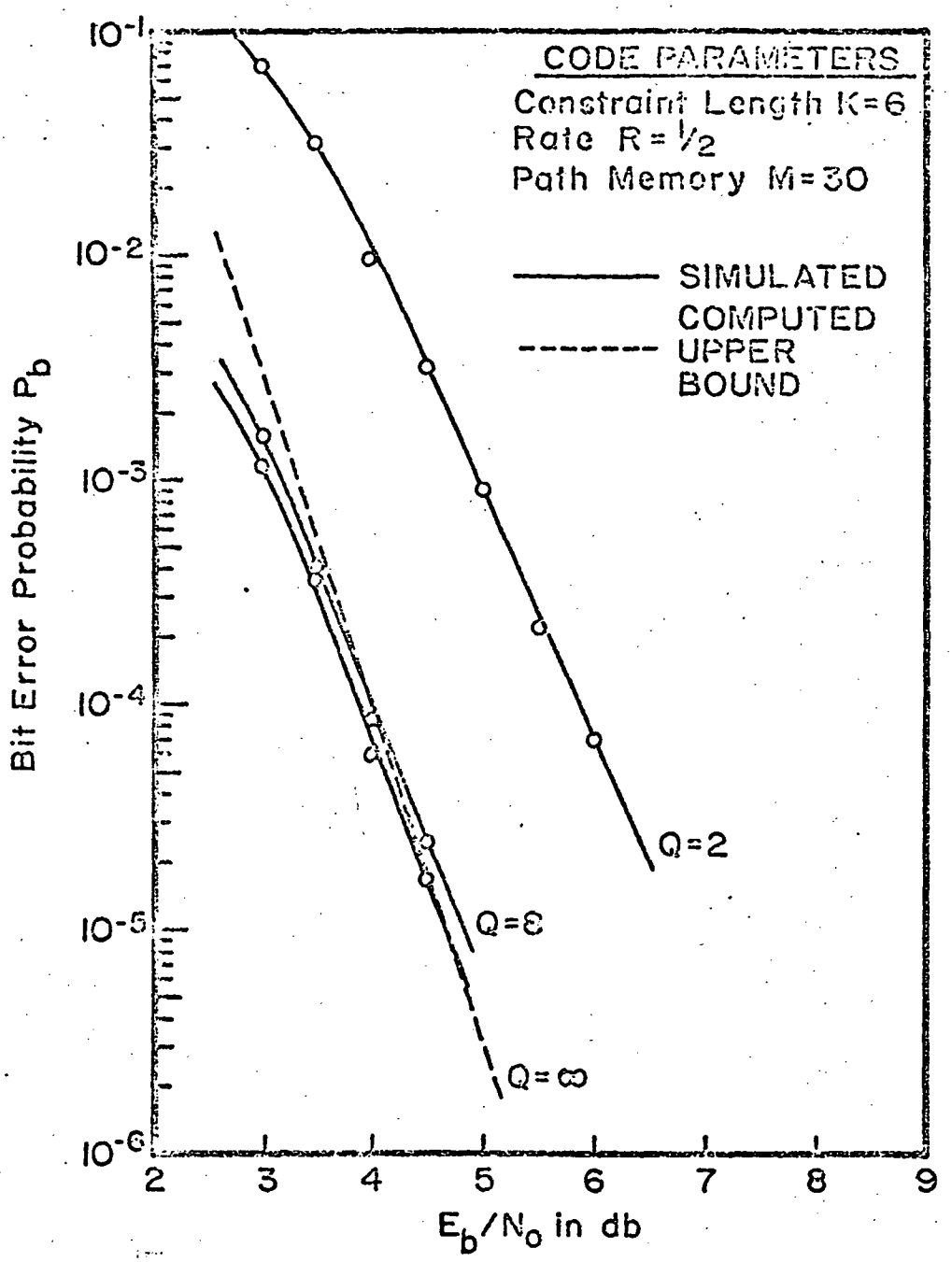

Figure 2-7

Simulated Bit Error Probability
Performance for K = 6, R = 1/2 Code

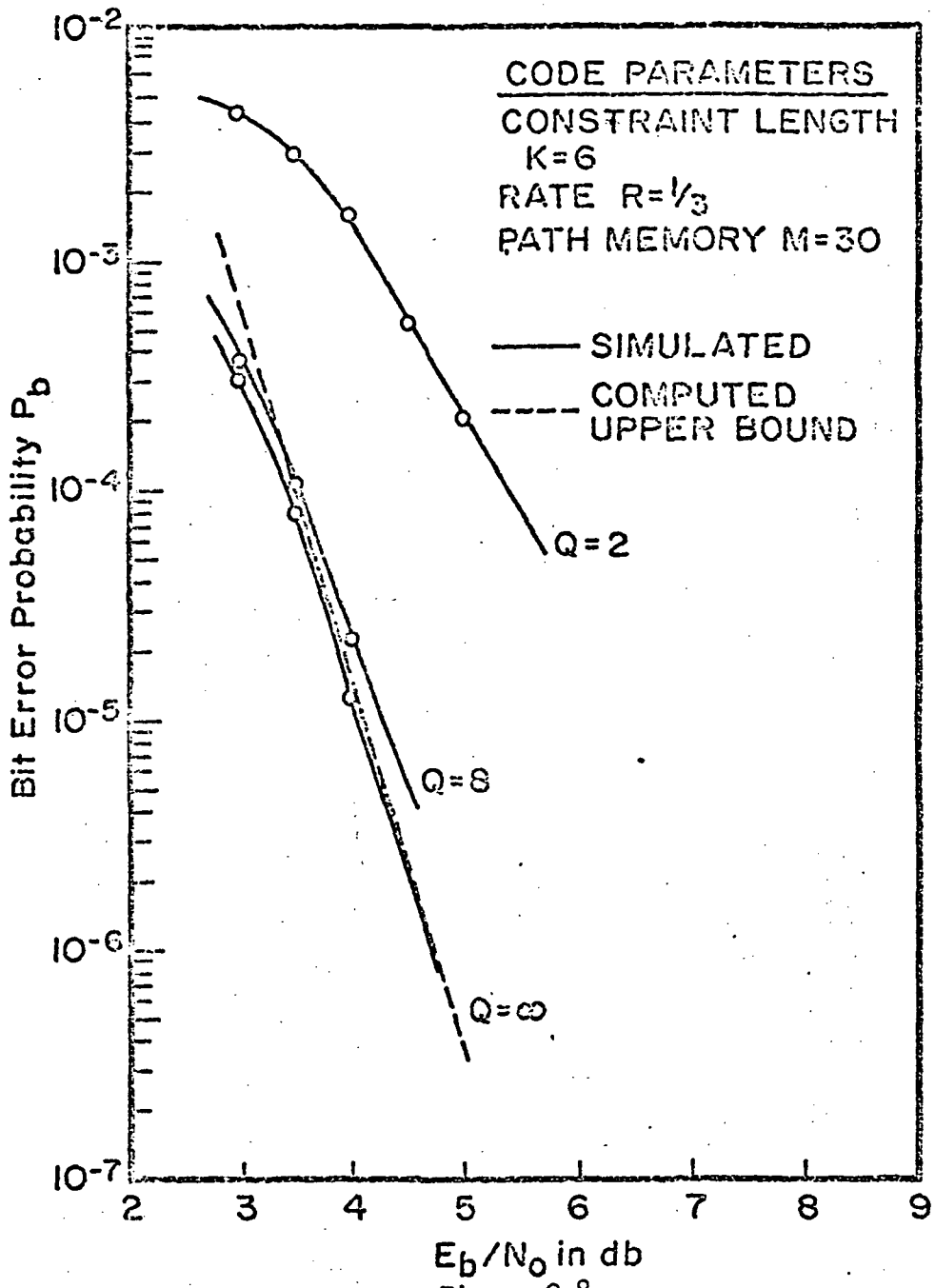

Figure 2-8

Simulated Bit Error Probability
Performance for K = 6, R = 1/3 Code

If $\{\tilde{r}_i\}$ represents the sequence of quantized matched filter outputs then $\tilde{r}_i = q_j$ if $I_{j-1} < r_i \leq I_j$ $j = 1, 2, \ldots, Q$. The receiver quantization is then completely determined by specification of the quantities I_j, $j = 1, 2, \ldots, \frac{Q}{2} - 1$. We have taken in all our studies the uniform quantization grid such that

$$I_j - I_{j-1} = \Delta ; \qquad j = 2, \ldots, Q/2 \tag{2.9}$$

Simulation results have suggested that Δ values as indicated in Table 2-1 are close to optimum and will be utilized in all simulations to be reported here

Q	Δ
4	1.0
8	0.5
16	0.25
32	0.125

Table 2-1
Approximately Optimum Uniform Quantization Spacing

The results illustrated in Figures 2-5 through 2-8 are in complete agreement with those reported previously by Heller and Jacobs [1] and serves as a useful check on the accuracy of the simulation program.

2.2 Fano Decoder

An important and useful parameter in characterizing the performance of sequential decoding schemes in general and the Fano algorithm in particular is the critical rate R_o (sometimes called the computational cutoff rate R_{comp}) which for coherent BPSK modulation and equally probable signaling is given by (cf. [4], Chap. 6)

$$R_o = 1 - \log_2 \left[1 + \int_{-\infty}^{\infty} \sqrt{p\{r|x=1\}\; p\{r|x=-1\}}\; dr \right] \tag{2.10}$$

where $p\left\{ r|x = i \right\}$ is the a posteriori probability of having observed a receiver output value r during any one channel signaling interval given that the corresponding transmitted symbol was $x = i$ for $i = \pm 1$. For the AWGN channel, the receiver outputs are described by (2.6) and the sequel with the result

$$p\left\{ r|x \right\} = \frac{1}{\sqrt{2\pi}} \exp\left\{ -\frac{1}{2}\left(r - x\sqrt{\frac{2E_s}{N_o}}\right)^2 \right\} \tag{2.11}$$

Substituting into (2.10) and performing the indicated integration we obtain

$$R_o = 1 - \log_2\left[1 + \exp\left\{ -\frac{E_s}{N_o} \right\} \right] \tag{2.12}$$

For quantized receiver outputs, the value of R_o must be computed according to

$$R_o = 1 - \log_2\left[1 + \sum_{j=1}^{Q} \sqrt{p\left\{ \tilde{r} = q_j|x=1 \right\}\ p\left\{ \tilde{r}=q_j|x=-1 \right\}} \right] \tag{2.13}$$

where now $p\left\{ \tilde{r} = q_j|x=i \right\}$ is the a posteriori probability that the quantized receiver output assumes the j^{th} quantization level q_j, $j = 1, 2, \ldots, Q$ during any signaling interval given that the corresponding transmitted symbol was $x = i$ with $i = \pm 1$. A plot of R_o vs. E_s/N_o is provided in Figure 2-9 for different amounts of receiver quantization. In Table 2-2 we illustrate how closely the value of R_o for uniform quantization approaches that with optimum quantization for selected values of E_s/N_o. This table is taken from Richer [11].

One of the principal problems encountered in the practical implementation of sequential decoding schemes in general and the Fano algorithm in particular is the variability of the amount of computation required to decode a message block. In particular, if C_N is the total number of computations required to decode a message block consisting of N bits, then it can be shown [12] - [13] that the number of computations per decoded information bit $C=C_N/N$ has a probability distribution

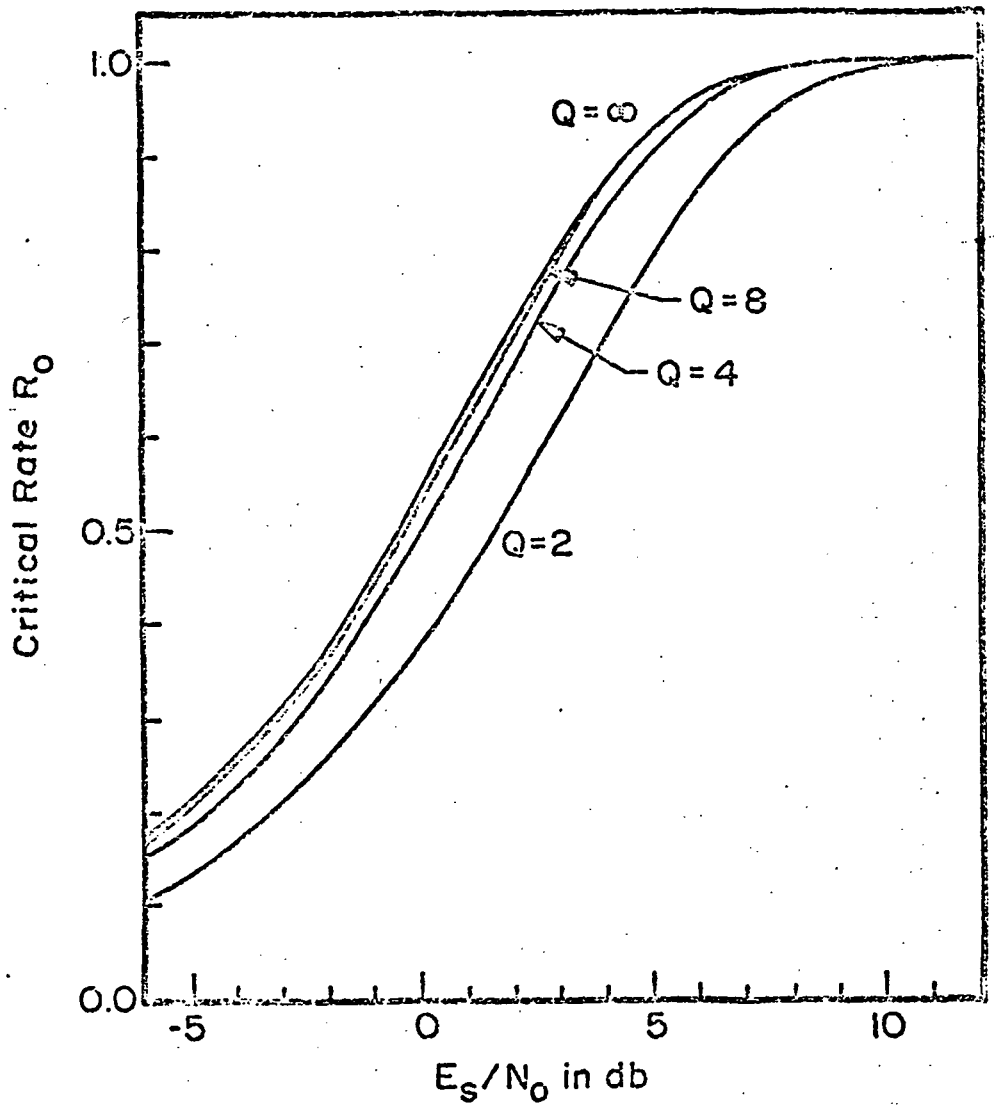

Figure 2-9

Critical Rate R_o vs. E_s/N_o

E_s/N_o	Number of Quantization Intervals Q	R_o	
		Optimum	Uniform
-17 db	4	0.0127	-
	8	0.0139	0.0138
	16	0.0142	0.0141
	32	0.0143	0.0143
	∞	0.0144	-
-9 db	4	0.0773	-
	8	0.0844	0.0841
	16	0.0865	0.0861
	32	0.0871	0.0870
	∞	0.0874	-
-3 db	4	0.283	-
	8	0.306	0.305
	16	0.313	0.312
	32	0.315	0.315
	∞	0.316	-

Table 2-2

Comparison of R_o for Optimum and
Uniform Quantization at Selected Values of E_s/N_o

which is approximately Pareto (cf. Cramer [14], page 248) of the form

$$P\left\{C \geq X\right\} \approx A\, X^{-\alpha} \tag{2.14}$$

where the approximation holds only for large X. The quantities A and α in (2.14) depend primarily on the channel and, in particular, on the quantity R/R_o through its dependence on E_s/N_o. Here R/R_o is the code information rate normalized by the critical rate R_o and is easily computed with the aid of Figure 2-9 as a function of E_s/N_o. For $\alpha > 1$, the expected value of the number C of computations per decoded information bit exists and is finite while for $\alpha \leq 1$ it does not exist. Furthermore, it can be shown that $\alpha > 1$ for $R/R_o < 1$ while $\alpha \leq 1$ for $R/R_o \geq 1$. It is for this reason that R_o has been called the critical or computational cutoff rate of sequential decoding. Our interest in sequential decoding will be confined to a particular code and block length. In particular, we consider a K = 32, R = 1/2 code described by Massey and Costello [15]. Although not a systematic code, this code has the unique ability of recovering the transmitted data sequence by simple modulo-two addition of the hard decisioned received data sequence. In all cases we consider a block length of N = 250 bits and Q = 8 level quantization. The decoder utilizes threshold spacing T_o = 4 bits. In Figure 2-10 we illustrate the empirically derived probability distribution of C_N for several values of R/R_o determined by simulation on the basis of 10^4 successive transmissions of the 250 bit message.* A computational cutoff of 5×10^4 computations per block has been imposed in these simulations. Table 2-3 lists other pertinent results of these simulations.

*The number of computations per decoded information bit C can then be determined as $C = C_N/N$ with N = 250.

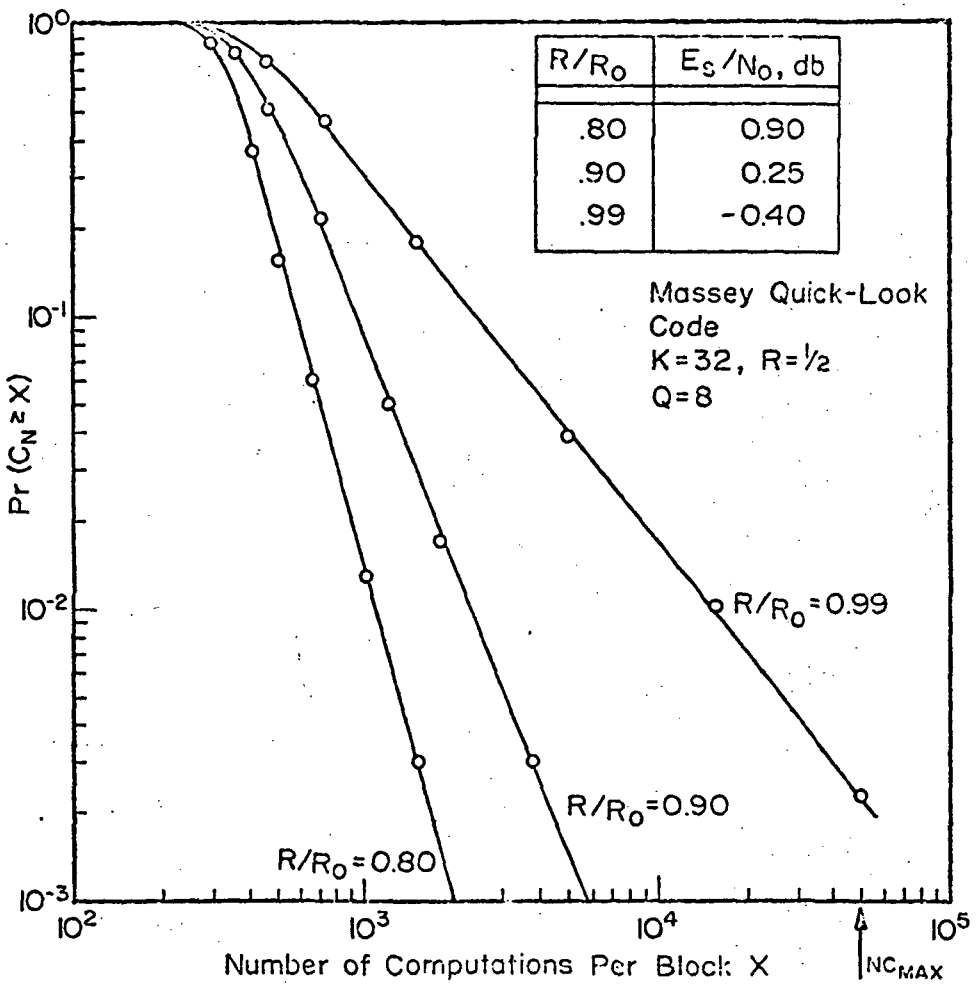

Figure 2-10

Empirical Probability Distribution of Computational Count for Fano Decoder in AWGN Channel

R/R_o	Block Error Probability P_E	Quit Probability* P_Q	A	α
0.80	0.00	0.00	4.5×10^8	3.50
0.90	0.00	0.00	2.5×10^7	2.82
0.99	0.00	0.002	1.1×10^3	1.20

*Based upon an imposed computational cutoff of 5×10^4 computations per 250 bit block.

Table 2-3

Other Pertinent Results of Fano Decoder Simulations in AWGN Channel

2.3 Zigangirov-Jelinek (ZJ) Decoder

The Fano algorithm treated in the preceding section has been used extensively in sequential decoding applications. It has been thoroughly investigated and its behavior well documented [16] - [20] and generally understood. Recently an alternative sequential decoding algorithm has been proposed independently by Zigangirov [21] and Jelinek [22] sometimes referred to as the Zigangirov-Jelinek or simply the ZJ algorithm. This algorithm differs from the Fano algorithm in that it saves all information on path segments which have been previously examined for possible future use. It can be shown [23] that the performance of the two algorithms are identical in the sense that, for all practical purposes, the sets of nodes examined by both algorithms are the same as are the paths ultimately selected. The significant difference is in the search strategies. With the ZJ algorithm, a node may be extended at most once, while the Fano algorithm allows repeated visits to a node in the process of decoding a received data sequence. There is an obvious tradeoff here between the smaller number of computations of the ZJ algorithm and the reduced memory requirements of the Fano algorithm. In

light of the potential computational advantage of the ZJ algorithm, and the relatively low and continually decreasing cost of memory, the ZJ algorithm is the more likely candidate for providing near real-time decoding of long constraint length convolutional codes.

The details of a digital computer program for simulating the performance of the ZJ algorithm under a variety of channel conditions has been described previously in [24] and need not be repeated at this time. The basic ZJ algorithm is characterized by the use of a memory table or "stack" to store node or cumulative path metrics associated with paths previously examined and extended. Each table entry consists of the identification of the most recent node on each path previously explored together with the cumulative path metric up to that node in the code tree. It is to be noted that there is exactly one entry for each previously explored path. The table entries are ordered in terms of decreasing path metrics so that, in particular, a pointer directed to the top of the stack will always be pointing to the node which currently possesses the largest cumulative path metric associated with it. The ZJ decoder then consistently attempts to extend the path through the node currently identified with the top entry in the stack. More specifically, the ZJ algorithm proceeds according to the following rules:

1.) Initialize by clearing the memory table and creating one entry corresponding to the root of the code tree. The cumulative path metric associated with this entry is set equal to zero.

2.) Retrieve the entry with the largest cumulative path metric currently residing at the top of the stack. If the associated node is at the end of the code tree,

decoding is completed - announce the corresponding N-bit message as having been transmitted. Otherwise continue to step 3.

3.) Compute the cumulative path metrics associated with the two successors of the node identified in step 2.

4.) Entries are created for these two successor nodes and inserted in the stack at appropriate positions while the entry for the predecessor node is deleted.

5.) Go to step 2.

There are several comments appropriate to this basic ZJ algorithm. First, observe that since there are a finite number of nodes in the code tree the algorithm will eventually terminate although possibly with an erronous decision. Indeed, even when a correct decision is eventually made a large number of computations may be required. Second, it is to be noted that a decoding table with at least 2^N entries is required to avoid overflow although under typical noise conditions only a small percentage of this number will actually be used. For large N it becomes unfeasible to provide the required memory so that the ZJ algorithm will be forced to operate with a reduced table size. Under such conditions it is, of course, possible that momentarily atypical noise conditions can result in the only entry associated with the correct path being purged from the stack. As a result, the decoder will have great difficulty in extending any of the remaining incorrect paths to the end of the code tree. It is clear, however, that given enough time the decoder will eventually make a decision although in error. If the table size is to be reduced then, it would appear appropriate to terminate decoding with declaration of an erasure if the number

C of computations* per decoded information bit exceeds a fixed preset limit C_{max}, or equivalently if the total number of computations exceeds NC_{max}. This will surely reduce the block error probability P_E but at the expense of an increase in the quit probability P_Q. This is tolerable provided that C_{max} is not so low as to result in the decoder quitting an appreciable percentage of the time when the correct path is in fact still represented in the decoding table. As part of the description of the ZJ decoder then we must specify the table size $T \leq 2^N$ and the imposed computational cutoff C_{max}. Other than some experimental work by Richer [11] there is little information to aid in this choice. In Figure 2-11 we illustrate the empirically derived probability distribution of C_N for the ZJ decoder for several values of R/R_o again using the K = 32, R = 1/2 Massey quick-look code. These results were obtained on the basis of 10^4 successive transmissions of the 250 bit message with an imposed computational cutoff of 5×10^4 computions as in the case of the Fano decoder. Again the computational distribution exhibits Pareto behavior although the computation count for a specified R/R_o is, as expected, reduced considerably over that for the Fano decoder. The table size T in these simulations was chosen to consist of a maximum of 5×10^3 entries and is sufficient to insure that the probability of purging the correct path is negligible. Indeed, Figure 2-12 illustrates the empirically determined probability distribution of the required table size for several values of R/R_o, again for the Massey K = 32, R = 1/2 code. This data was obtained by monitoring the maximum depth into the decode table or stack achieved by the table entry corresponding to the correct path. Interestingly enough this distribution again exhibits Pareto behavior although we have not made any great effort to pursue this result. It is clear, however, from Figure 2-12

*Here a computation will be taken to mean a single iteration of the steps 1-5 describing the basic ZJ algorithm.

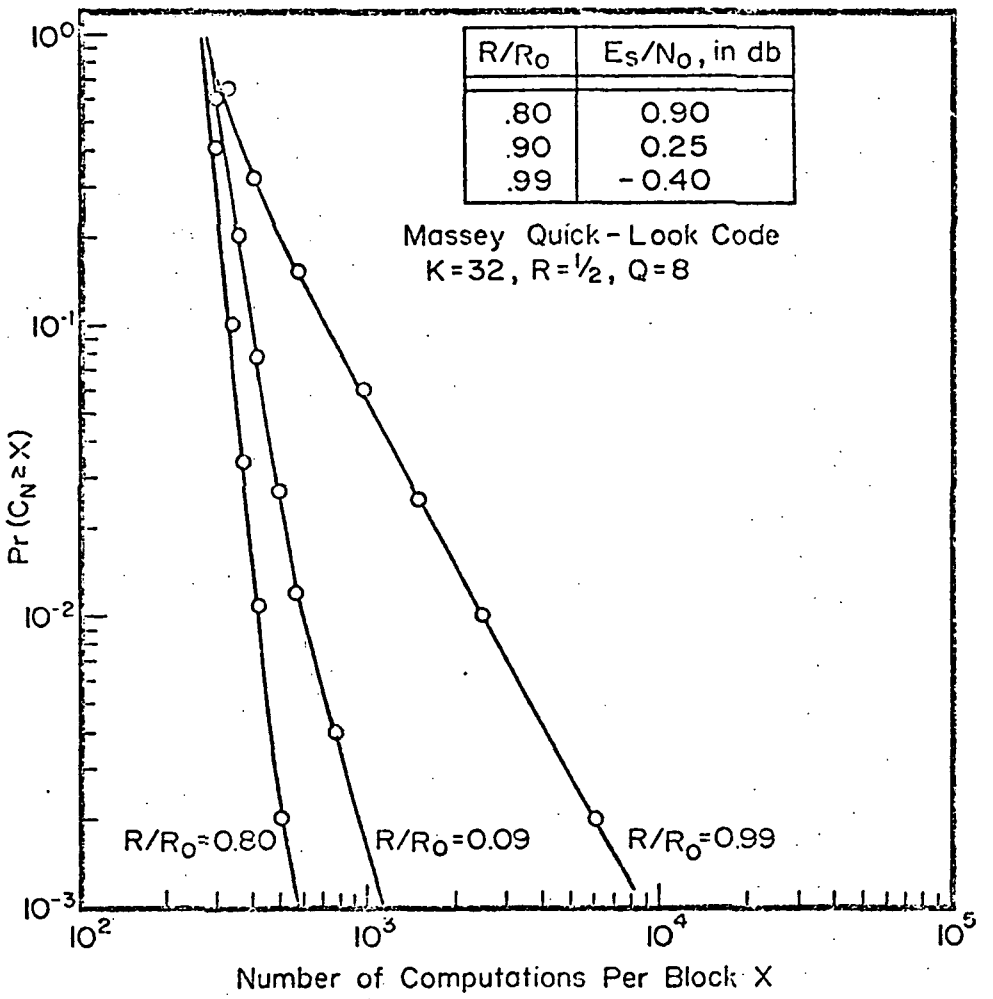

Figure 2-11

Empirical Probability Distribution of Computational Count for ZJ Decoder in AWGN Channel

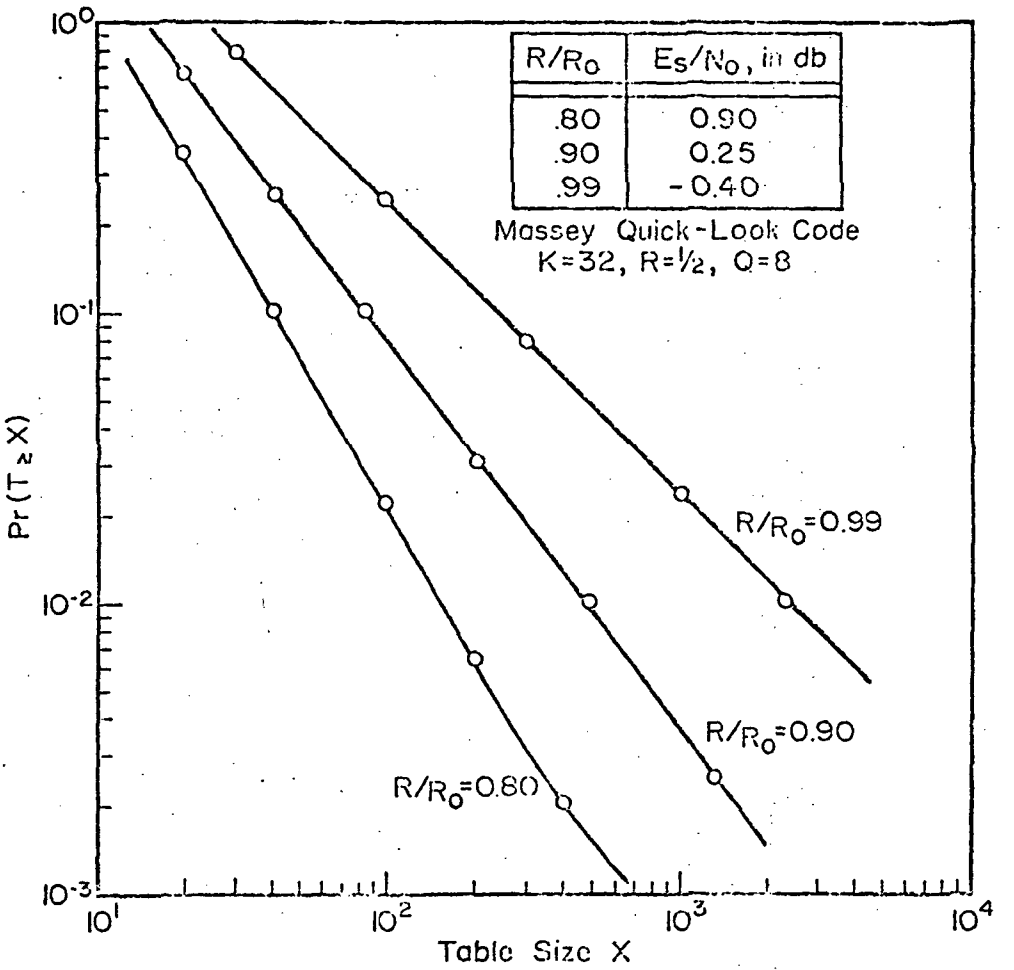

Figure 2-12

Empirical Probability Distribution of Required Table Size for ZJ Decoder in AWGN

that only moderate table sizes are required to provide reliable decoding in the presence of AWGN. Table 2-4 lists some other pertinent simulation results.

R/R_o	Block Error Probability P_E	Quit Probability* P_Q	A	α
0.80	0.00	0.00	1.4×10^{23}	9.60
0.90	0.00	1.5×10^{-4}	7.9×10^{4}	2.40
0.99	0.00	8.0×10^{-3}	2.5×10^{3}	1.36

*Based upon an imposed computational cutoff of 5×10^4 computations per 250 bit block and a decode table consisting of 5×10^3 entries.

Table 2-4

Other Pertinent Results of ZJ Decoder Simulations in AWGN Channel

It is to be noted that the computational advantages of the ZJ decoder vis-à-vis the Fano decoder is offset somewhat by the more complicated nature of a typical ZJ computation. In particular, even for decode tables of modest size, the sort and merge (or insert) operation represented by step 4 of the basic ZJ algorithm can be extremely time consuming if not performed intelligently. As a result, the computational advantage of the ZJ algorithm can be severely compromised if careful attention is not given to the data file organization and/or search strategy of the decode table. We have not investigated this topic to any great extent. It is felt, however, that with appropriate care given to such details the ZJ decoder does indeed appear a more attractive alternative to the Fano decoder for providing near-real time decoding of long constraint length convolutional codes.

3.0 Fading Channel Characterization

The transmitted channel waveform s(t) for BPSK modulation has been given previously by (2.2) and the sequel. It will be more convenient in what follows to consistently use complex signal representations. In particular, s(t) can be expressed in the form

$$s(t) = \mathrm{Re}\left\{\sqrt{2E_s}\sum_i x_i\, u_o(t-iT_s)\, e^{j\omega_o t}\right\} \tag{3.1}$$

where $u_o(t)$ is the complex envelope of the transmitted channel signal during any one signaling interval. More specifically, in this case

$$u_o(t) = p(t)\, e^{j\theta} \tag{3.2}$$

where p(t) and θ have been defined previously in conjunction with (2.1). From (2.2) it follows that

$$\int_0^{T_s} |u_o(t)|^2\, dt = 1 \tag{3.3}$$

The transmitted signal s(t) can be written in the still more convenient form

$$s(t) = \mathrm{Re}\left\{u(t)\, e^{j\omega_o t}\right\} \tag{3.4}$$

where now

$$u(t) = \sqrt{2E_s}\sum_i x_i\, u_o(t-iT_s) \tag{3.5}$$

The received signal is similarly of the form

$$u(t) = \mathrm{Re}\left\{w(t)\, e^{j\omega_o t}\right\} \tag{3.6}$$

where now w(t) is the complex envelope of the received waveform and will be assumed of the form

$$w(t) = z(t) + n(t) \tag{3.7}$$

Here the quantity $z(t)$ is the complex amplitude of the received scattered signal component and $n(t)$ is a signal independent zero-mean stationary complex Gaussian random process with

$$E\left\{n(t)\ n(t_o)\right\} = 0 \tag{3.8a}$$

and

$$E\left\{n(t)\ n^*(t_o)\right\} = N_o\ \delta(t-t_o) \tag{3.8b}$$

where $\delta(\cdot)$ is the Dirac delta function and $N_o/2$ is the double-sided noise spectral density of the inphase and quadrature components in watts/Hz. We have assumed that $z(t)$ can be expressed in the form (cf. [25])

$$z(t) = \left[\Gamma + a(t)\right]\ u(t) \tag{3.9}$$

Here $\Gamma = \gamma e^{j\psi}$ is a complex quantity whose amplitude γ is a fixed deterministic quantity while the phase ψ is uniformly distributed over $[-\pi, \pi]$. The quantity $a(t)$ is a complex zero-mean Gaussian random process completely described in terms of a channel scattering function as described previously in [25]. We will assume that σ^2 is the common variance of the inphase and quadrature components of $a(t)$ (actually $\sigma^2 = \sigma_a^2/2$ in the notation of [25]). Under these conditions, the probability density function (p.d.f.) of*

$$r(t) = \left|\ \Gamma + a(t)\ \right| \tag{3.10}$$

is given by the Rayleigh-Rice distribution

$$f_R(r) = \frac{r}{\sigma^2} \exp\left\{-\frac{r^2+\gamma^2}{2\sigma^2}\right\} I_o\left(\frac{r\gamma}{\sigma^2}\right); \qquad r \geq 0$$
$$= 0 \qquad\qquad\qquad\qquad\qquad\qquad ; \qquad r < 0 \tag{3.11}$$

---

*Hopefully it will not cause confusion that we are using $r(t)$ to represent the envelope of the received signal component and $\{r_i\}$ to represent the sequence of matched filter outputs.

where $I_o(x)$ is the modified Bessel function of the first kind of order zero. If $\gamma = 0$ (or equivalently $\Gamma = 0$), this reduces to the Rayleigh distribution.

$$f_R(r) = \frac{r}{\sigma^2} \exp\left\{-\frac{r^2}{2\sigma^2}\right\} \quad ; \quad r \geq 0$$
$$= 0 \quad ; \quad r < 0 \tag{3.12}$$

The mean-square value of the Rayleigh-Rice distribution is easily seen to be given by

$$E\left\{r^2\right\} = 2\sigma^2 + \gamma^2 = \sigma^2\left[2 + \alpha^2\right] \tag{3.13}$$

where $\alpha \triangleq \gamma/\sigma$ allowing γ^2 to be measured in units of σ^2.

It should be noted, that a number of theoretical propagation studies concerned with RF signal fading in the Venusian atmosphere (cf. [26], [27]) have been concluded indicating that instead of (3.9), the received signal component is described by

$$z(t) = \tilde{a}(t)\, u(t)$$

where the amplitude $r(t) \triangleq \left|\tilde{a}(t)\right|$ is lognormal, i.e.,

$$r(t) = e^{\chi(t)} \tag{3.14}$$

with $\chi(t)$ a real zero-mean Gaussian random process with variance σ_χ^2 and the phase $\phi(t) = \arg\left\{\tilde{a}(t)\right\}$ is likewise a real zero-mean Gaussian random process with variance σ_ϕ^2. It follows that under the lognormal assumption $r(t)$ has mean

$$E\left\{r\right\} = \exp\left\{\sigma_\chi^2/2\right\} \tag{3.15}$$

and mean-square value

$$E\left\{r^2\right\} = \exp\left\{2\sigma_\chi^2\right\} \tag{3.16}$$

Table 3-1 summarizes some pertinent information on the log-amplitude process $\chi(t)$ and the phase process $\phi(t)$ taken directly from [27].

The results of these previously referenced propagation studies have been discussed in [28] where arguments have been advanced in support of the Gaussian model represented by (3.9) and the sequel. These arguments will not be repeated here. Let us note, however, that for the most part our simulation studies have neglected phase fluctuations and have concentrated on the effects of amplitude fluctuations alone. The important question in a choice of fading channel model is then how closely the Rayleigh-Rice and lognormal distributions resemble each other. At least for the relatively small values of σ_χ^2 indicated in Table 3-1, the lognormal distribution is closely approximated by the Rayleigh-Rice distribution for appropriate choice of γ and σ^2. This is particularly true in the region of small values of r relative to the rms value ($r_{rms} = \sqrt{E\{r^2\}}$) which essentially determines the performance with coding. In particular, consider the exceedence probability given by $Q_R(r) = 1 - F_R(r)$ where $F_R(r)$ is the cumulative distribution function (c.d.f.) corresponding to either the lognormal or Rayleigh-Rice distribution. For the former we have

$$\begin{aligned} Q_R(r) &= 1 - \Phi\left\{\frac{\ln r}{\sigma_\chi}\right\}; && r \geq 0 \\ &= 1 && ; \quad r < 0 \end{aligned} \tag{3.17}$$

with $\Phi(x)$ the unit Gaussian c.d.f., while for the Rayleigh-Rice distribution we have

$$\begin{aligned} Q_R(r) &= Q(\alpha, r/\sigma) && ; \quad r \geq 0 \\ &= 1 && ; \quad r < 0 \end{aligned} \tag{3.18}$$

L*, km	σ_χ^2	σ_ϕ^2, rad^2	B_χ^{**}, Hz
55	0.056	0.2282	0.436
30	0.018	0.134	0.59
10	0.0025	0.05	1.02
5	0.0007	0.025	1.45
1	4×10^{-5}	0.005	3.23

* L is depth of penetration into Venusian atmosphere

** B_χ is 3 db single-side bandwidth of the log-amplitude spectra

Data based upon homogeneous turbulence below 55 km with structure constant

$$C_n = 2.024 \times 10^{-6} \quad m^{-1/3} \quad \text{(inferred from Venera 4)}$$

and wind shear velocity

$$v_\perp = 50 \text{ m/sec and uniform (Venera 4 data)}$$

Table 3-1

Summary of Log-Amplitude and Phase Fluctuation Results

where

$$Q(\alpha, \beta) \triangleq \int_{\beta}^{\infty} x \exp\left\{-\frac{x^2+\alpha^2}{2}\right\} I_o(\alpha x)\, dx$$

is Marcum's Q-function (cf. [29]). The quantity $Q_R(r)$ is plotted in Figure 3-1 for selected σ_χ^2 and α. It is clear that there is a close resemblence for appropriate parameter choices. We have not attempted to determine an optimum choice of parameter values in any sense. Instead we have chosen to evaluate code performance parametrically as a function of both γ and σ_χ^2. In particular, for fixed γ we have equated mean-square values for both the Rayleigh-Rice and the lognormal distributions to obtain an empirical relationship between α and σ_χ^2. Equating mean-square values we obtain

$$2\sigma^2 + \gamma^2 = \exp\left\{2\sigma_\chi^2\right\} \tag{3.20}$$

so that for fixed choice of σ_χ^2 and γ^2 we can solve for σ^2 (or equivalently σ_a^2) with the result

$$\sigma_a^2 = 2\sigma^2 = \exp\left\{2\sigma_\chi^2\right\} - \gamma^2 \tag{3.21}$$
$$\approx (1-\gamma^2) + 2\sigma_\chi^2$$

where the approximation is justified due to the relatively small values of σ_χ^2 as indicated in Table 3-1. It follows that

$$\alpha^2 = \left(\frac{\gamma}{\sigma}\right)^2 = \frac{2\gamma^2}{(1-\gamma^2) + 2\sigma_\chi^2} \tag{3.22}$$

which is the desired empirical relationship. For the small values of σ_χ^2 considered here the choice $\gamma = 1$ appears to provide the best match. For example with $\sigma_\chi^2 = 0.056$ and $\gamma = 1$ we have from (3.22) $\alpha \approx 4.2$ while $\alpha \approx 7.5$ for $\sigma_\chi^2 = 0.018$. In either case, the match between the Rayleigh-Rice and lognormal distributions as illustrated in Figure 3-1 is quite good and, improves with smaller values of σ_χ^2.

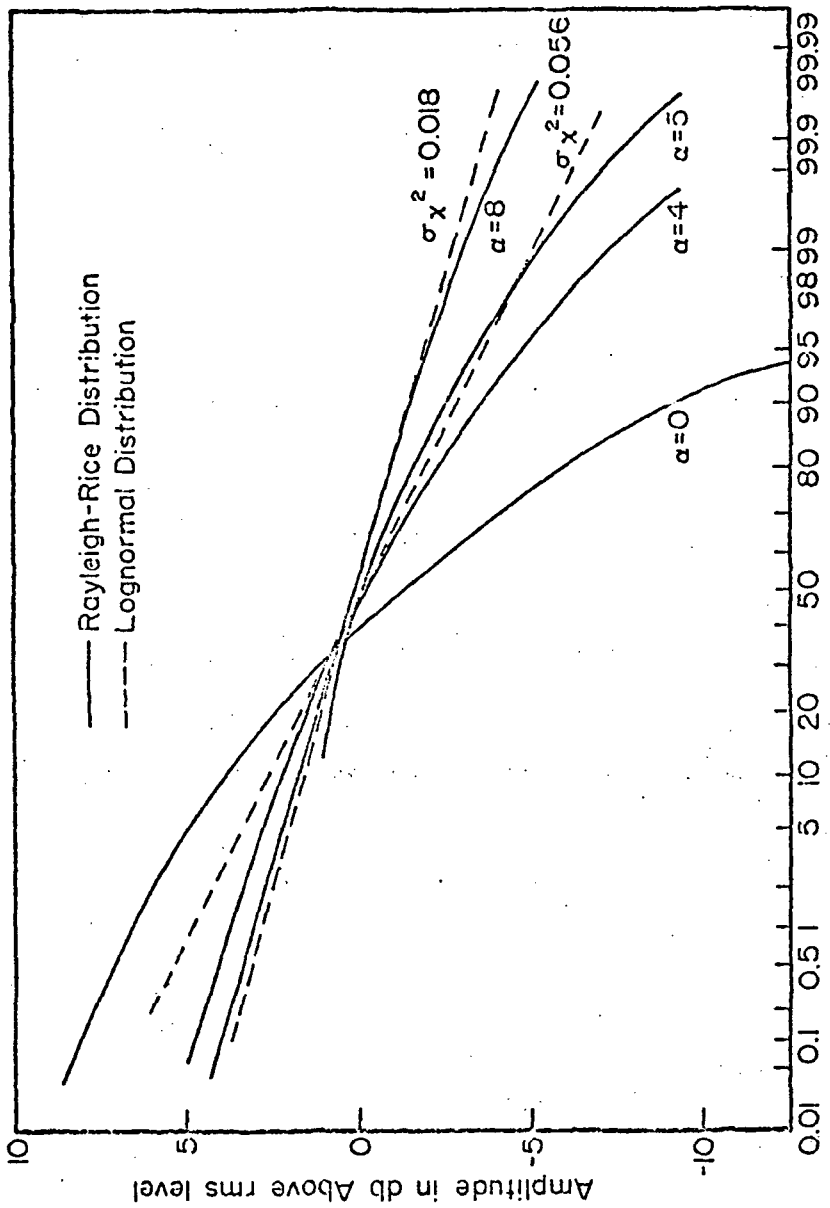

Figure 3-1
Comparison of Lognormal and Rayleigh-Rice
Amplitude Distribution

Indeed, as argued in [28] it is only for small values of σ_χ^2 that the lognormal distribution for the scattered signal amplitude can be considered valid.

Although the case $\gamma = 1$ appears to provide a best fit to the lognormal distribution it remains of interest to consider performance over a wide range of γ values. Due primarily to limitations on computer processing time, however, we have been forced to limit our consideration of γ values. As a result, we have chosen to concentrate on the two cases $\gamma = 0$ and $\gamma = 1$. This should essentially bound the range of anticipated channel conditions.

In previous work [25], [28] we choose to restrict attention to channel frequency dispersion functions of the form

$$\tilde{\sigma}(f) = \frac{\sigma_a^2}{2\pi} \frac{B_o}{B_o^2 + f^2} \tag{3.23}$$

where B_o is the coherence bandwidth of the channel in Hz. As a result the autocorrelation function of the a(t) process in (3.9) is given by

$$\begin{aligned} R_{aa}(\tau) &= E\left\{ a(t+\tau)\, a^*(t) \right\} \\ &= \sigma_a^2\, e^{-2\pi B_o |\tau|} \end{aligned} \tag{3.24}$$

A relationship between B_o and B_χ was derived in [28] with the result

$$B_o = \sqrt{2}\, \sigma_\chi\, B_\chi \tag{3.25}$$

With σ_χ^2 and B_χ specified as in Table 3-1 it is a simple matter to tabulate appropriate values of the two important parameters σ_a^2 and B_o. This is provided in Table 3-2.

L^*, km	σ_x^2	B_x, Hz	$B_o = \sqrt{2}\,\sigma_x B_x$, Hz	σ_a^2	
				$\gamma = 0$	$\gamma = 1$
55	0.056	0.436	0.146	1.118	0.112
30	0.018	0.59	0.112	1.037	0.036
10	0.0025	1.02	0.071	1.005	0.005
5	0.007	1.45	0.054	1.001	0.001
1	4×10^{-5}	3.23	0.029	1.000	-

*L is depth of penetration into Venusian atmosphere

Data taken from Table 3-1.

Table 3-2

Summary of Fading Channel Model Parameters

It is to be recalled that in [25] it was assumed for simulation purposes that the process $a(t)$ varies slowly relative to an elementary signaling interval of T_s seconds duration so that it can be considered constant over any such interval but allowed to vary from interval-to-interval. It was remarked that this is a realistic assumption for $B_o T_s << 1$. From Table 3-2 it is seen that this restricts us to signaling rates in excess of approximately one channel symbol/second which is felt quite reasonable for planetary entry missions. We will assume that some mechanism is available to allow perfect phase tracking of the signal component of the received signal. Admittedly this is somewhat unrealistic and later in this report we will describe in some detail the effects of imperfect phase tracking. For the time being, however, let us assume that a perfect carrier phase reference is available. The receiver output, after suitable normalization, is then the sequence.

$$r_i = x_i \sqrt{\frac{2E_s}{N_o}} \left| \Gamma + a_i \right| + n_i \; ; \qquad i = 1, 2, \ldots \tag{3.26}$$

which replaces that given previously in (2.6). Here a_i represents the value of the a(t) process throughout the i^{th} signaling interval and can be described by the first order regression

$$a_{i+1} = \rho a_i + w_i \; ; \qquad i = 1, 2, \ldots \tag{3.27}$$

The sequence $\{ w_i \}$ is an i.i.d. sequence of zero mean complex Gaussian random variates such that

$$E \{ w_i w_i \} = 0 \tag{3.28a}$$

and

$$E \{ w_i w_j^* \} = (1 - \rho^2) \; \sigma_a^2 \; \delta_{ij} \tag{3.28b}$$

with δ_{ij} the Kronecker delta function, $\rho = e^{-2\pi B_o T_s}$ and T_s the duration of an elementary signaling interval. This scheme has been described previously in [25] and need not be repeated. Simulation studies have been performed parametrically as a function of $B_o T_s$ and allows conclusions to be drawn as a function of signaling rate $f_s = 1/T_s$.

Finally, it is to be noted that one of the major concerns in the simulation results to be described in the following sections is to establish the efficacy of interleaving in combatting the channel memory represented by the time-correlated fading. For short constraint length codes the quantity of interest is the amount of interleaving required to achieve a given error probability for specified E_b/N_o as a function of the parameters describing the channel model, the code and the receiver operation. Of particular importance will be the interleaving requirements as a function of the channel coherence bandwidth B_o with other parameters held fixed. For longer constraint length codes we are interested in the effectiveness

of interleaving in reducing the computational and/or storage requirements of sequential decoders in the presence of fading. While there are many interleaving techniques possible, we shall employ a particularly simple approach until such time as a superior approach becomes apparent. We shall call this approach block interleaving and is described as follows: The encoded serial bit stream is first blocked into blocks of length L bits where $L = \ell n$ for some $\ell = 1, 2, \ldots$ and n is related to the code rate $R = 1/n$. An I x L block interleaver then transmits each of the L successive bits in a block separated by I - 1 bits from I - 1 other blocks. The storage requirements are then N = I x I bits.

4.0 Simulation Results for Viterbi Decoding

In this section we will describe some of the simulation results obtained to date for short constraint length convolutional codes in conjunction with Viterbi maximum likelihood decoding. The channel model will be as described in the preceding section. The codes considered in this study are listed in Table 4-1. In

R bits/channel use	Constraint Length K
1/2	3, 7, 10
1/3	3, 6

Table 4-1
Short Constraint Length Codes Considered in Simulation Study

each case we utilize the Odenwalder/Larsen codes (cf. [8], [9]) as discussed previously in Section 2.0. The K = 3 code for both rate 1/2 and 1/3 is included since its performance is relatively easy to simulate. In cases where $\gamma = 0$ we have simulated only the case $\sigma_a^2 = 1$ since Table 3-2 indicates the actual value will be very close to unity for a wide range of mission parameters. For $\gamma = 1$, on the other hand, we have considered only the value $\sigma_a^2 = 0.1$ as this appears representative of worst case values appearing in Table 3-2.

Let us first consider the effects of σ_a^2 and/or γ on the bit error probability P_b when there is little or no memory on the channel. This is obtained by setting B_oT_s equal to some relatively large value, say $B_oT_s = 10.0$.* The resulting performance then represents an ultimate limit for fixed γ and σ_a^2 which can be approached with sufficiently large interleaving. The simulated performance with infinitely fine quantization is illustrated in Figures 4-1 and 4-2 for $\gamma = 0$ and $\sigma_a^2 = 1.0$ and in Figures 4-3 and 4-4 for $\gamma = 1.0$, $\sigma_a^2 = 0.1$ with selected rate 1/2 and 1/3 codes. These results should be compared with Figures 2-5 through 2-8 for performance over the AWGN channel. It should be clear from Figures 4-3 and 4-4 that, for $\gamma = 1.0$ and $\sigma_a^2 = 0.1$, performance close to that obtained in the absence of fading can be achieved provided the channel is memoryless. For smaller values of σ_a^2, the performance approaches the upper bound for the AWGN channel even more closely. The case $\gamma = 1.0$ and $\sigma_a^2 = 0.1$ then, according to the discussion of the previous section, provides a useful measure of representative performance when the scale of amplitude fading represented by σ_x^2 is small. Although large values of σ_x^2 have not been predicted by propagation studies, the case $\gamma = 0$, $\sigma_a^2 = 1.0$ nevertheless provides a useful measure of performance for large σ_x^2 and in this sense provides a worst case performance bound.

In Figures 4-5 through 4-8 we illustrate the expected performance as a function of the dimensionless quantity B_oT_s when there is no interleaving and infinitely fine receiver quantization is employed. It is apparent that severe degradation in performance results with increasing channel memory represented by small values of B_oT_s. In particular some degree of interleaving must be provided if the signaling rate is such that $B_oT_s \leq 0.1$. Referring to Table 3-2, for a penetration of 55 km into the Venusian atmosphere this would imply a maximum

*Care must be taken in the interpretation of the large B_oT_s results. As stated, they provide a useful measure of the ultimate performance which can be approached with sufficiently large interleaving. The actual performance for large B_oT_s (i.e., fast fading) must take into account the decorrelation loss in the detectors. We have not pursued this question.

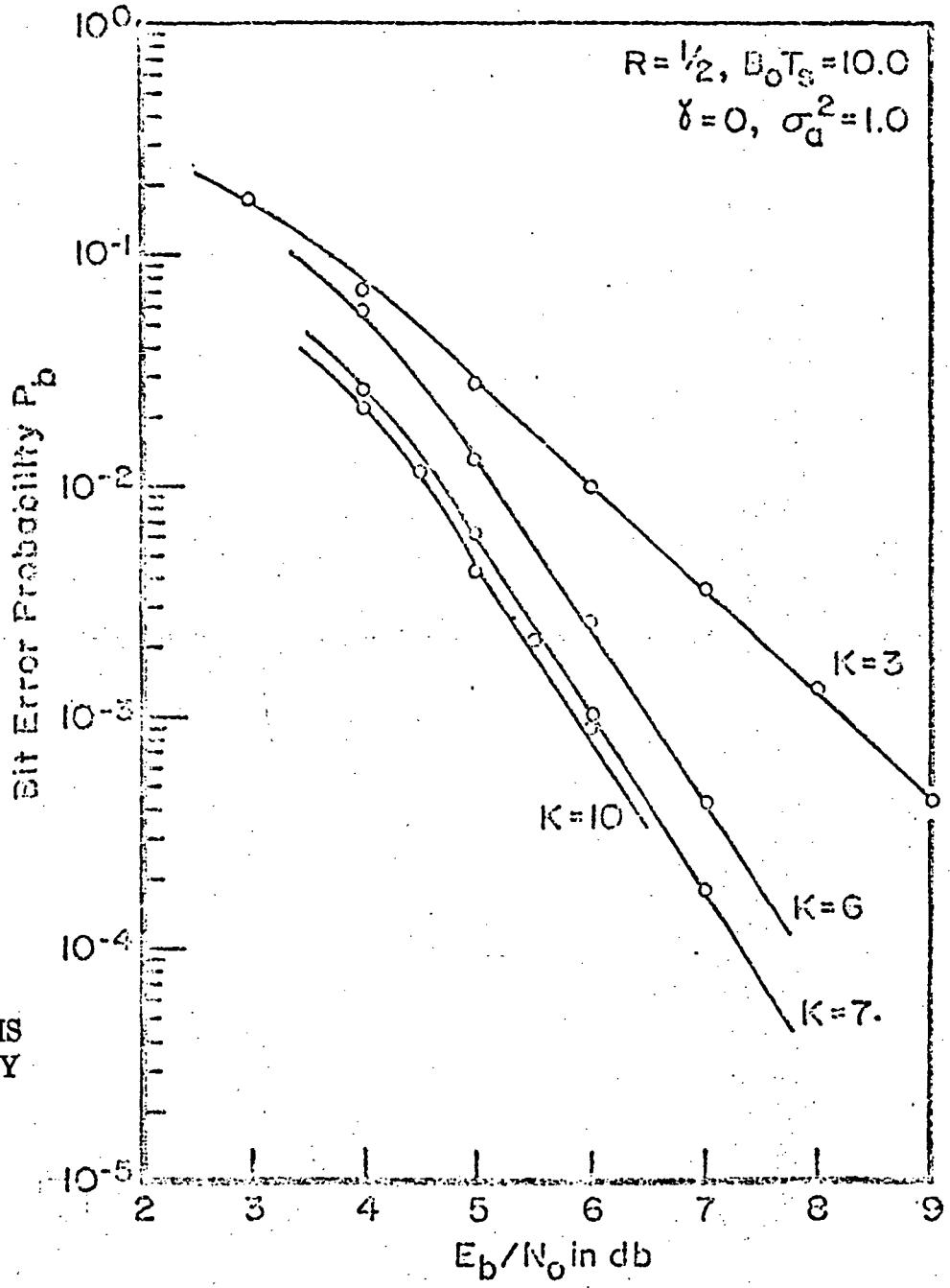

Figure 4-1

Simulated Performance of Selected Rate 1/2 Codes with B_oT_s = 10.0, γ = 0 and σ_a^2 = 1.0

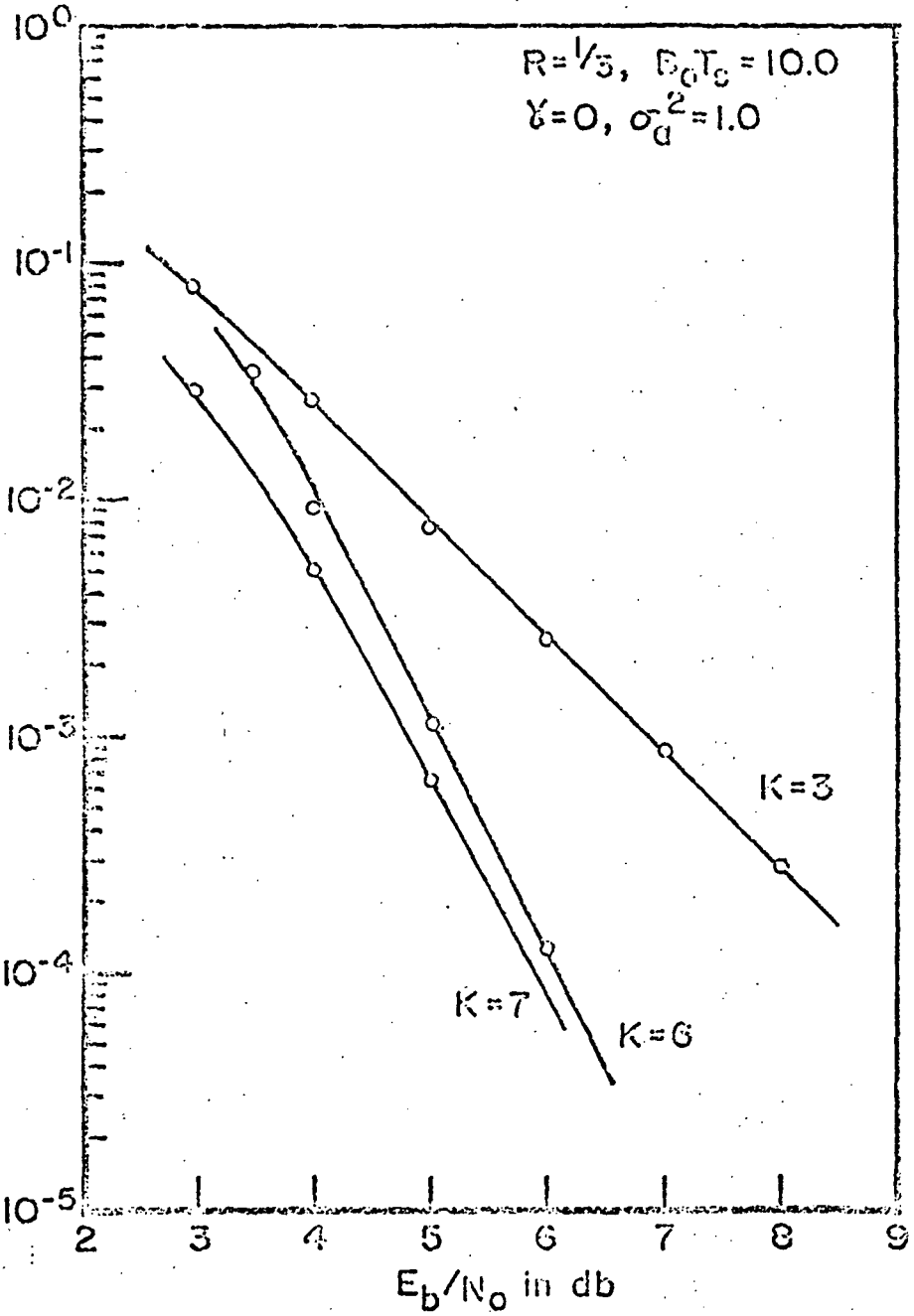

Figure 4-2

Simulated Performance of Selected Rate 1/3 Codes with B_oT_s = 10.0, γ = 0 and σ_a^2 = 1.0

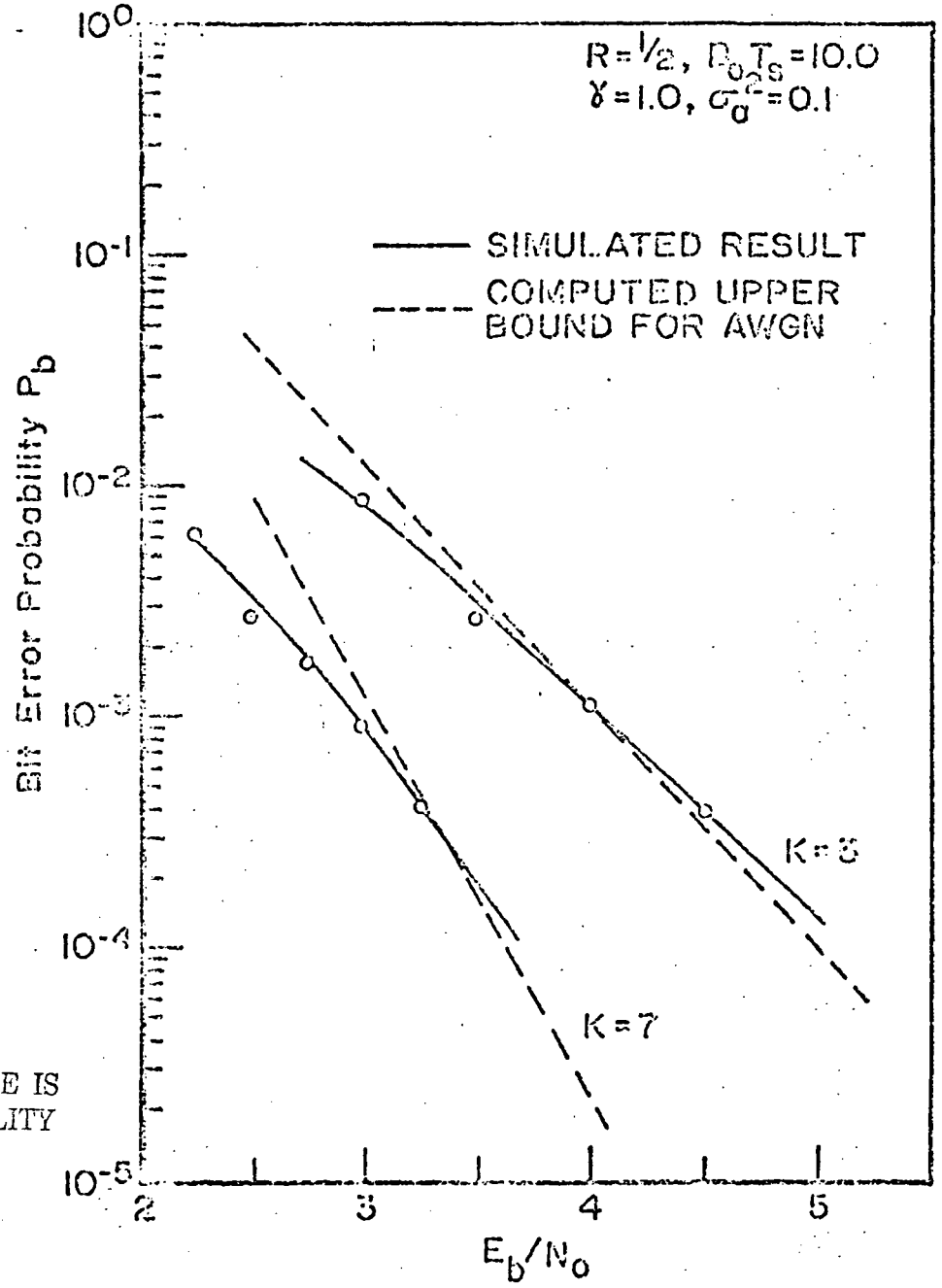

Figure 4-3

Simulated Performance of Selected Rate 1/2 Codes with B_oT_s = 10.0, γ = 1.0 and σ_a^2=0.1

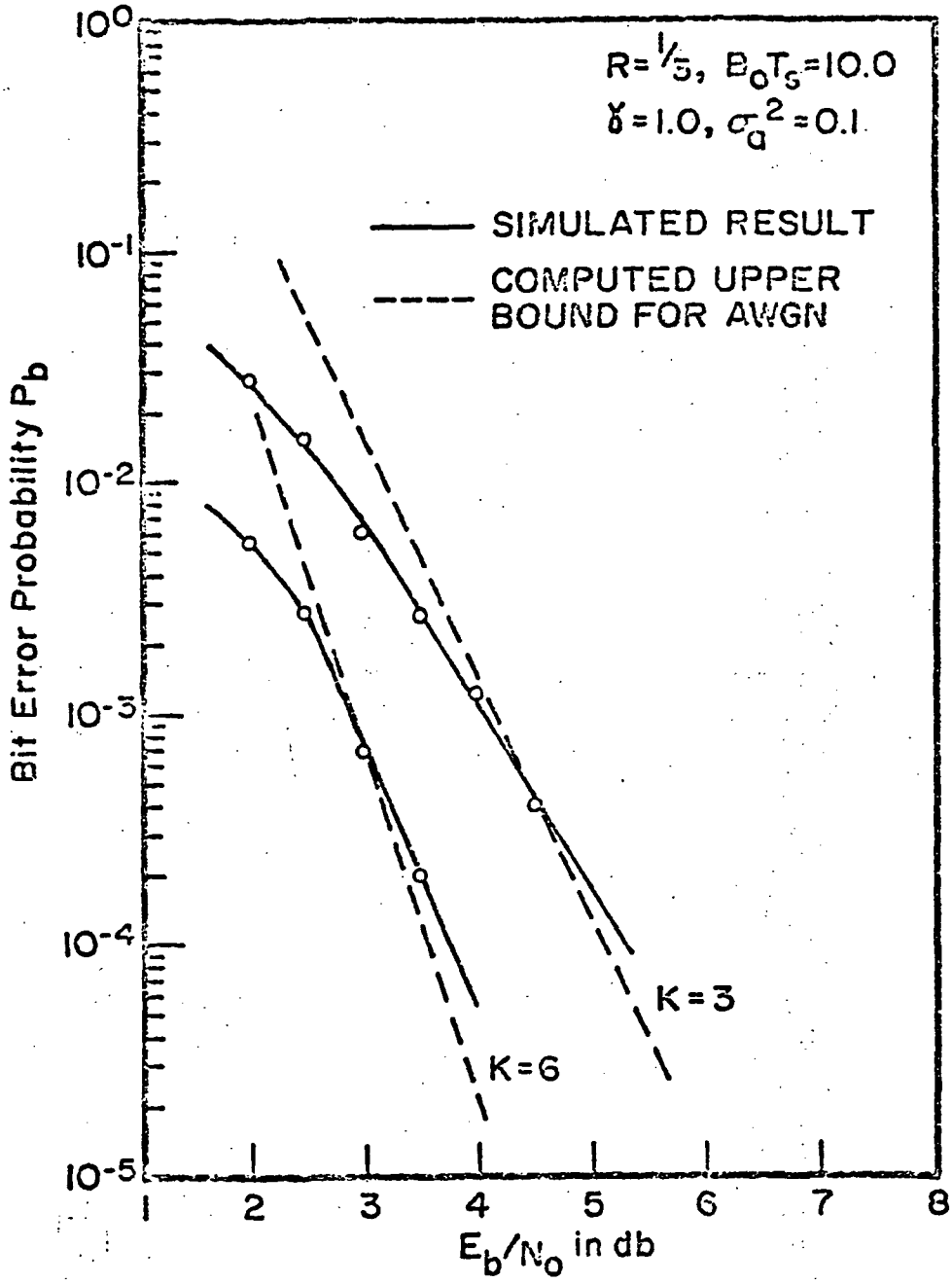

Figure 4-4

Simulated Performance of Selected Rate 1/3 Codes with B_oT_s = 10.0, γ = 1.0 and σ_a^2=0.1

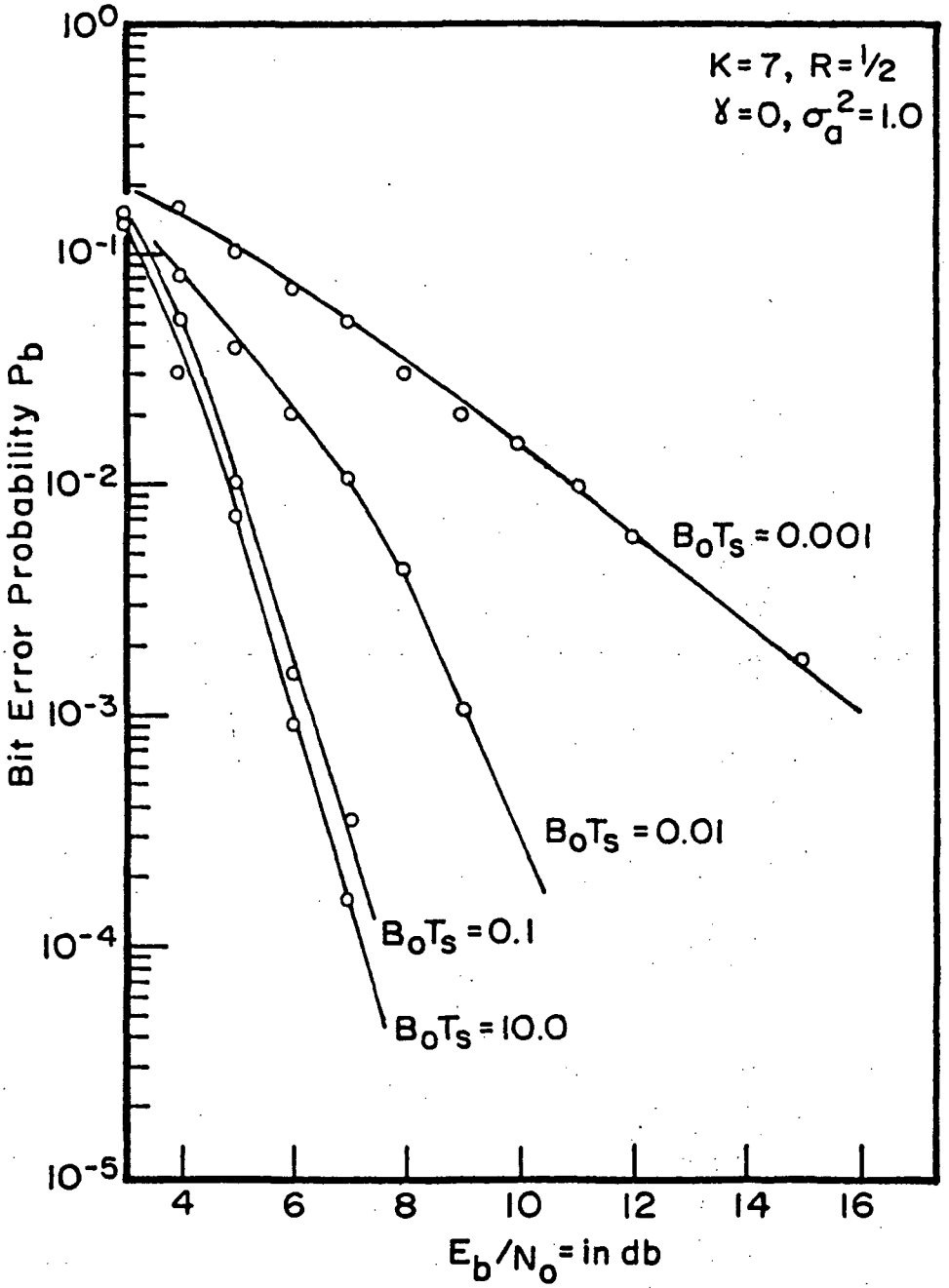

Figure 4-5

Simulated Performance of K = 7, R = 1/2 Code for Different Values of B_oT_s without Interleaving and with $\gamma = 0$, $\sigma_a^2 = 1.0$

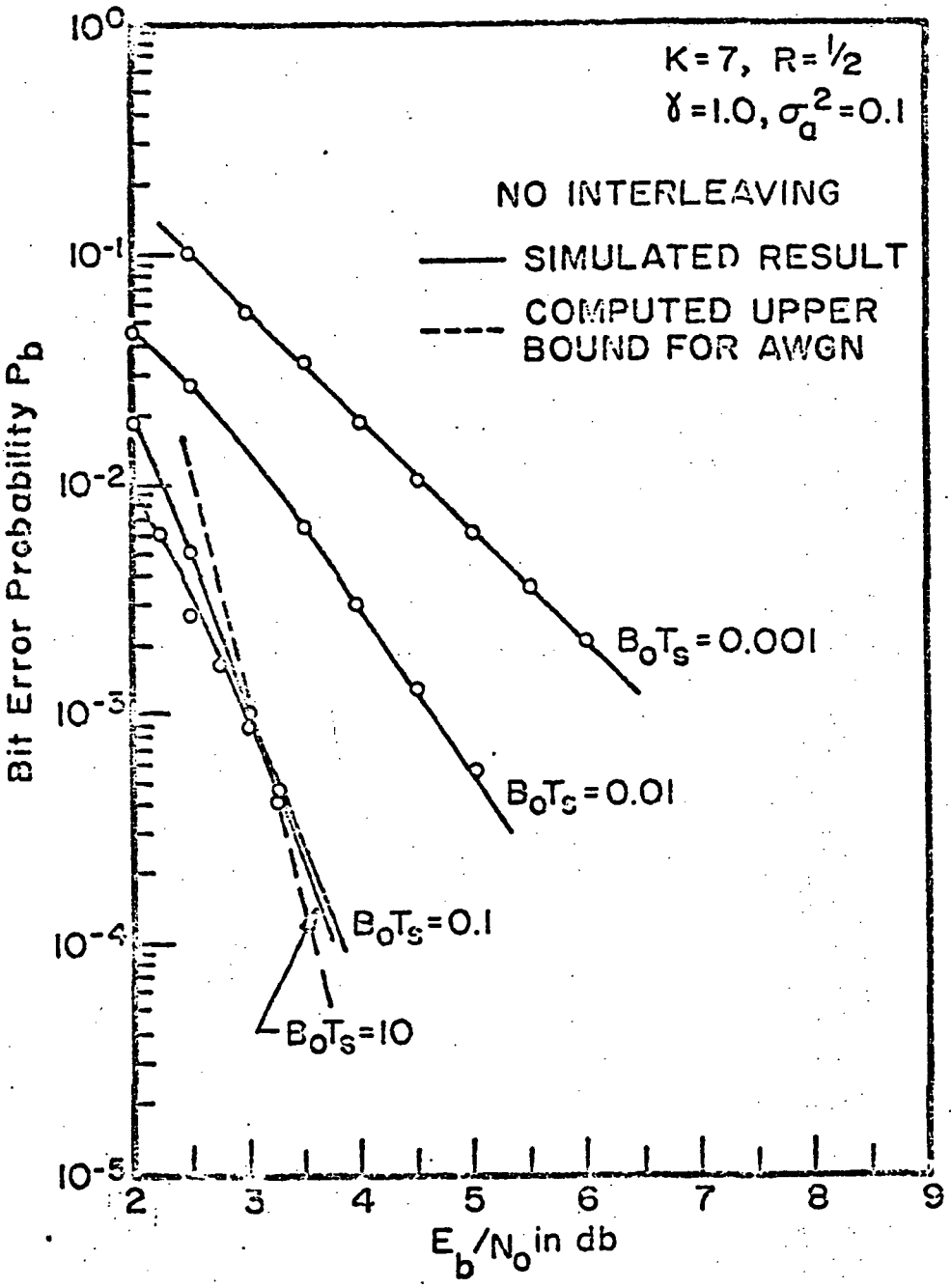

Figure 4-6

Simulated Performance of K = 7, R = 1/2 Code for Different Values of B_oT_s without Interleaving and with $\gamma = 1.0$, $\sigma_a^2 = 0.1$

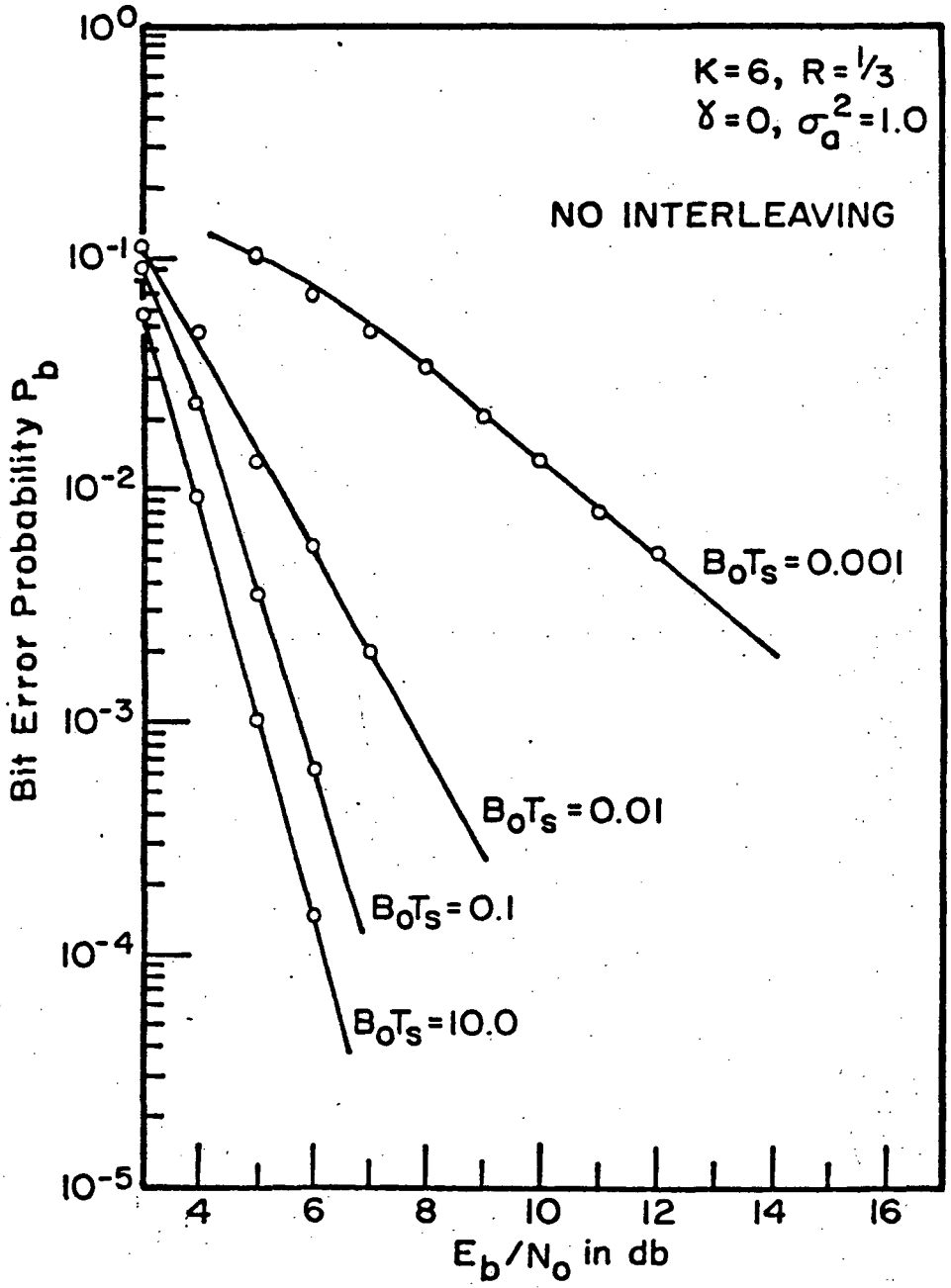

Figure 4-7

Simulated Performance of K = 6, R = 1/3 Code for Different Values of B_0T_s without Interleaving and with $\gamma = 0$, $\sigma_a^2 = 1.0$

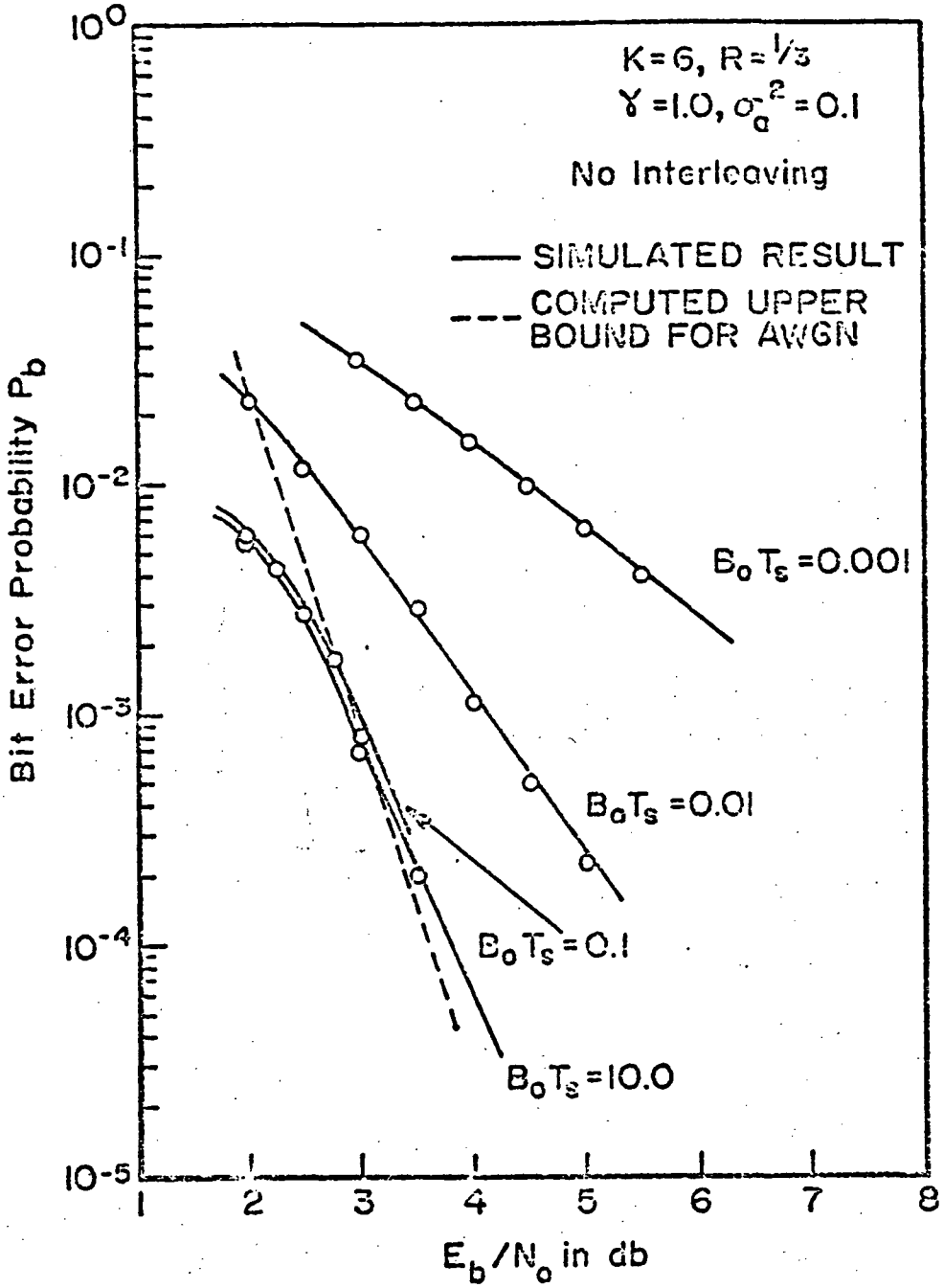

Figure 4-8

Simulated Performance of K = 6, R = 1/3 Code for Different Values of $B_o T_s$ without Interleaving and with $\gamma = 1.0$, $\sigma_a^2 = 0.1$

signaling rate of approximately 1 channel symbol per second if interleaving is to be avoided. It should be noted that at higher altitudes σ_a^2 is smaller and the effects of channel memory are not as severe. This is offset, however, by the corresponding decrease in B_o. At any rate, the conclusions to be drawn are that some degree of interleaving is required if reasonable signaling rates are to be achieved.

4.1 Interleaving Considerations

A number of simulations have been performed to establish the efficacy of interleaving in reducing the channel memory and thereby avoiding the severe degradations in error probability performance for small B_oT_s demonstrated in the preceding section. While considerably more work is required in this area, some tentative conclusions can be drawn on the basis of simulation results obtained as part of this study.

An Illustration of typical improvement in bit error probability to be realized with the use of a simple block interleaver structure is provided in Figures 4-9 and 4-10 for a K = 7, R = 1/2 code with $B_oT_s = 0.001$. In all cases we have employed an I x L block interleaver as described in Section 3.0 with $L = \ell n$ for some n = 1, 2,... and n is related to the code rate by R = 1/n. We have found it convenient in simulating interleaver performance for convolution codes of different rates to parameterize results in terms of the two quantities I and ℓ. As a result we have consistently labeled curves in terms of the literal product I x ℓ. Note that no interleaving is implied in the case 1 x ℓ for any value of ℓ. It is clear from Figures 4-9 and 4-10 that, at least for this code, an interleaver of size in excess of 30 x 30 is required to approach within 1 db of the limiting performance for B_oT_s in the vicinity of 0.001. Similar conclusions can be drawn from Figures 4-11 and 4-12 for a K = 6, R = 1/3 code and in Figure 4-13 for a K = 3, R = 1/2 code again with $B_oT_s = 0.001$ in each case. For larger values

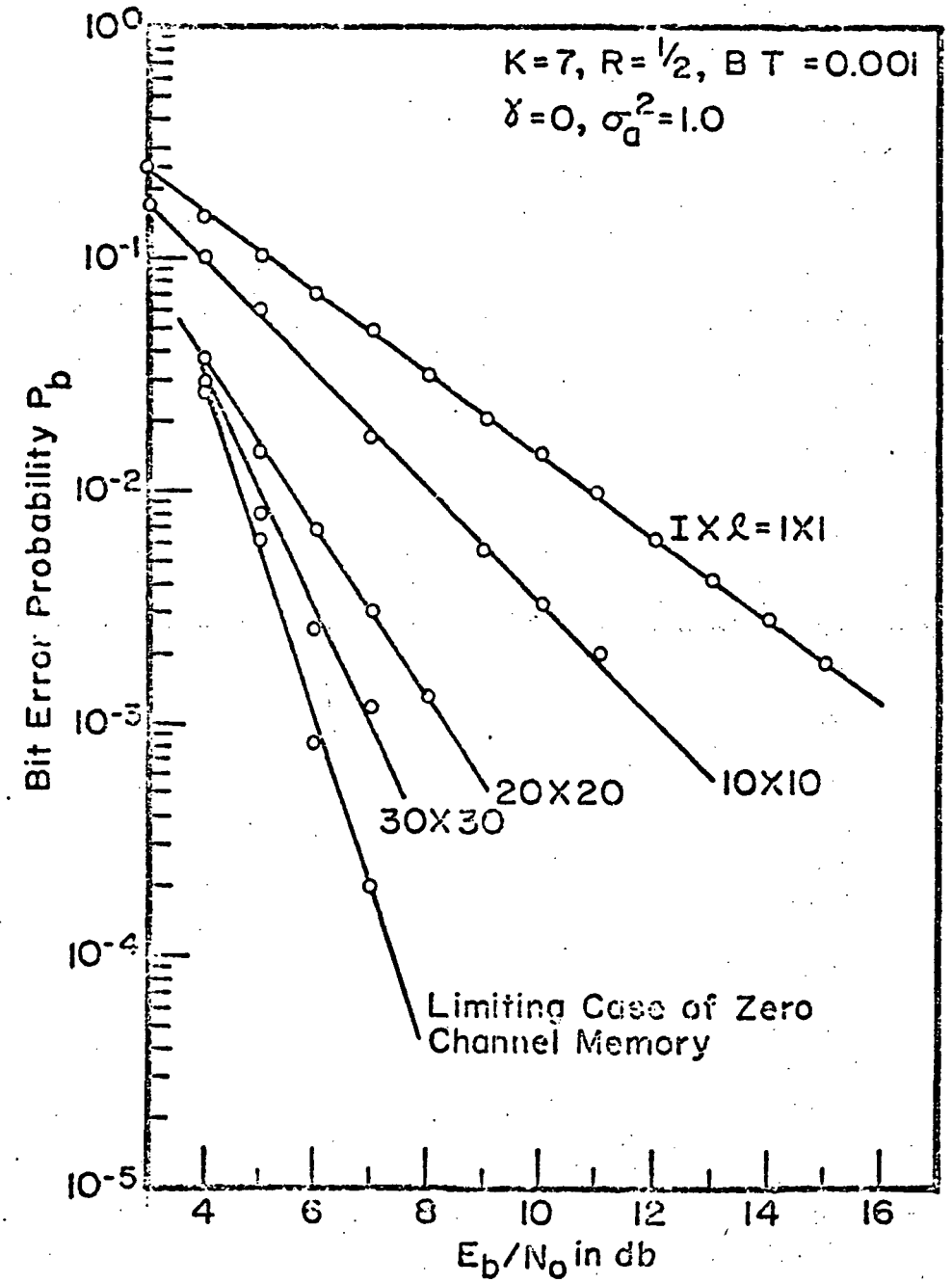

Figure 4-9

Effects of Block Interleaving for K = 7, R = 1/2 Code with $B_o T_s$ = 0.001 and γ = 0, σ_a^2 = 1.0

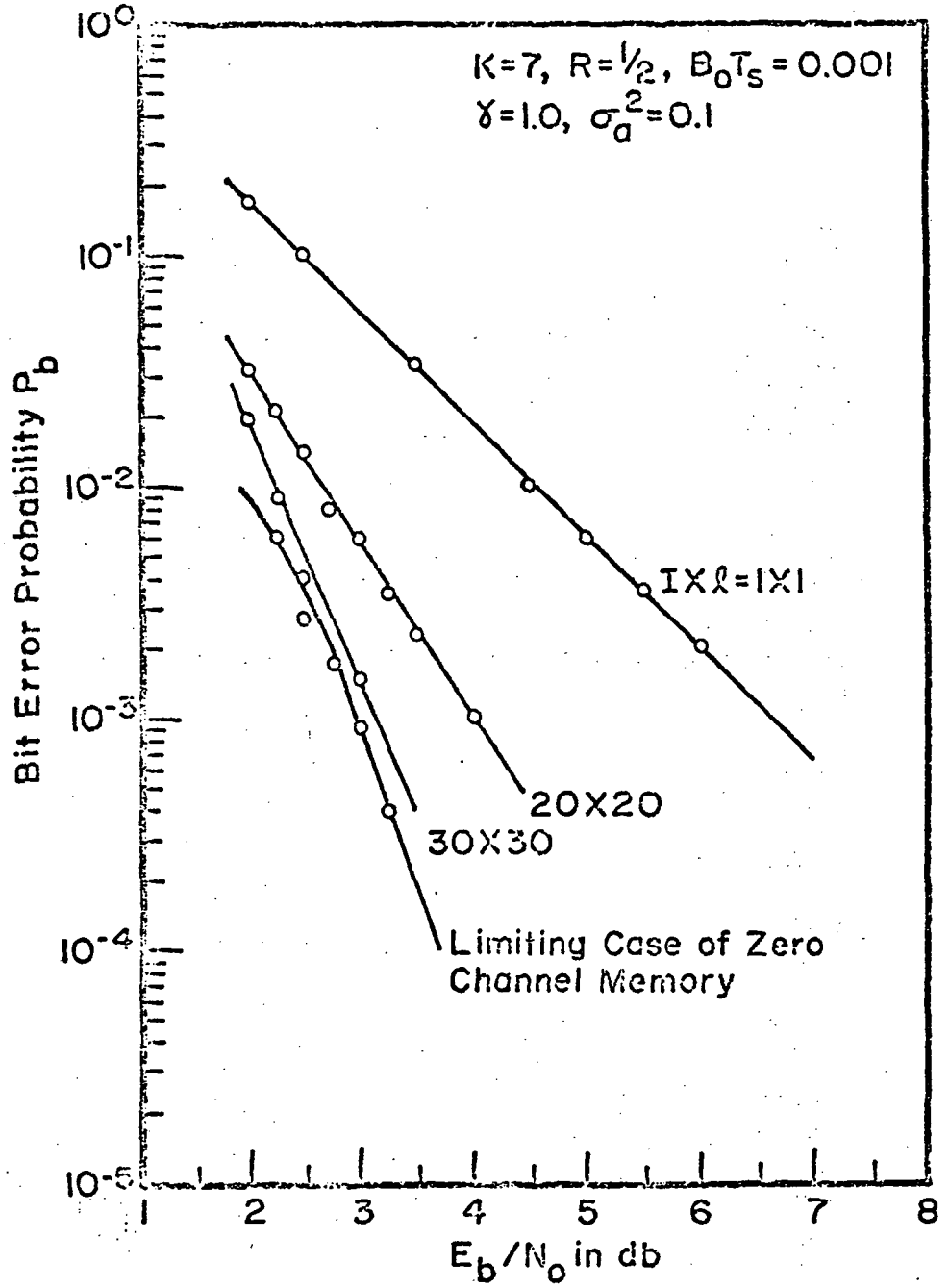

Figure 4-10

Effects of Block Interleaving for K = 7, R = 1/2 Code with B_oT_s = 0.001 and γ = 1.0, σ_a^2 = 0.1

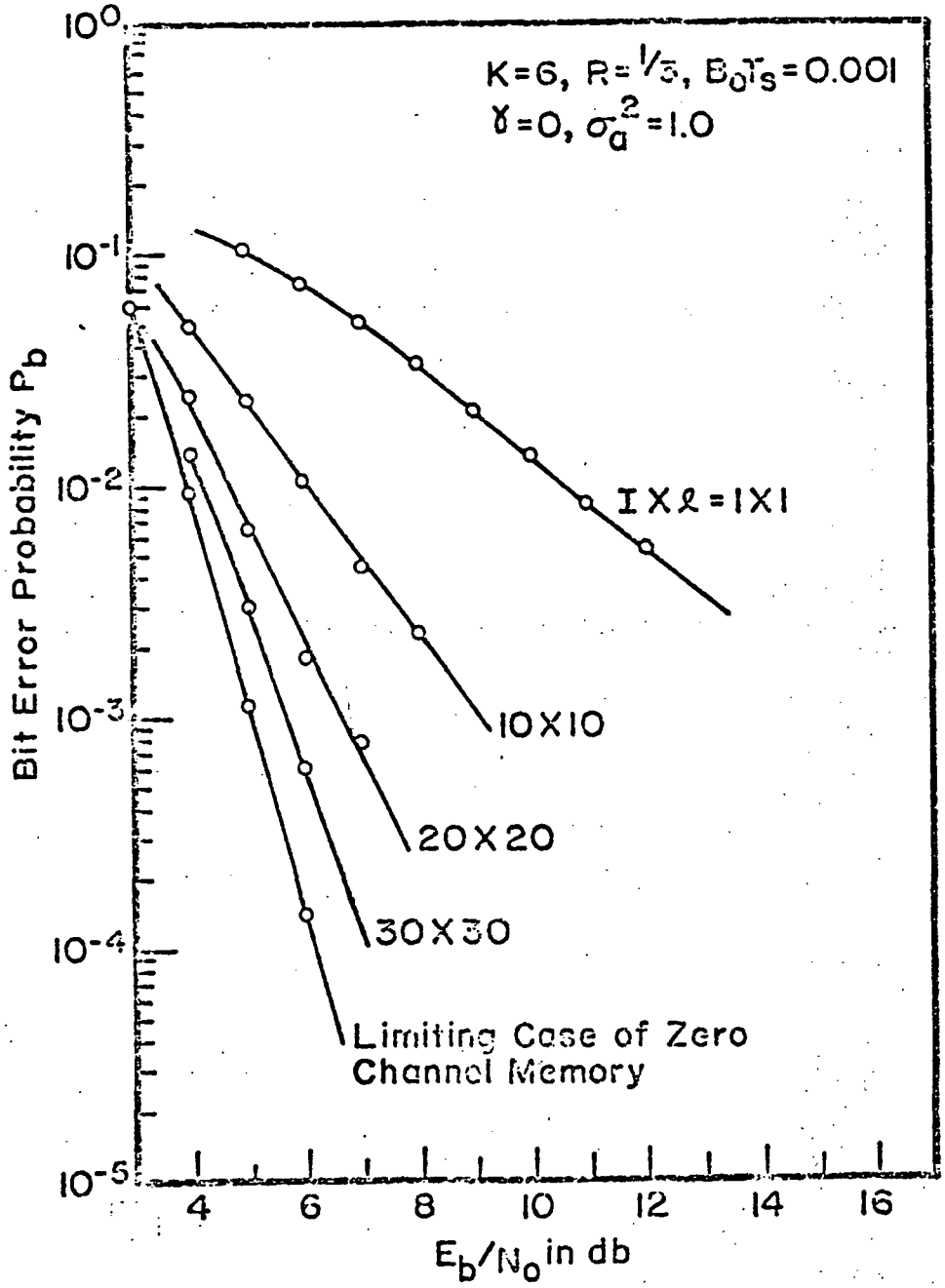

Figure 4-11

Effects of Block Interleaving for K = 6, R = 1/3 Code with B_oT_s = 0.001 and γ = 0, σ_a^2 = 1.0

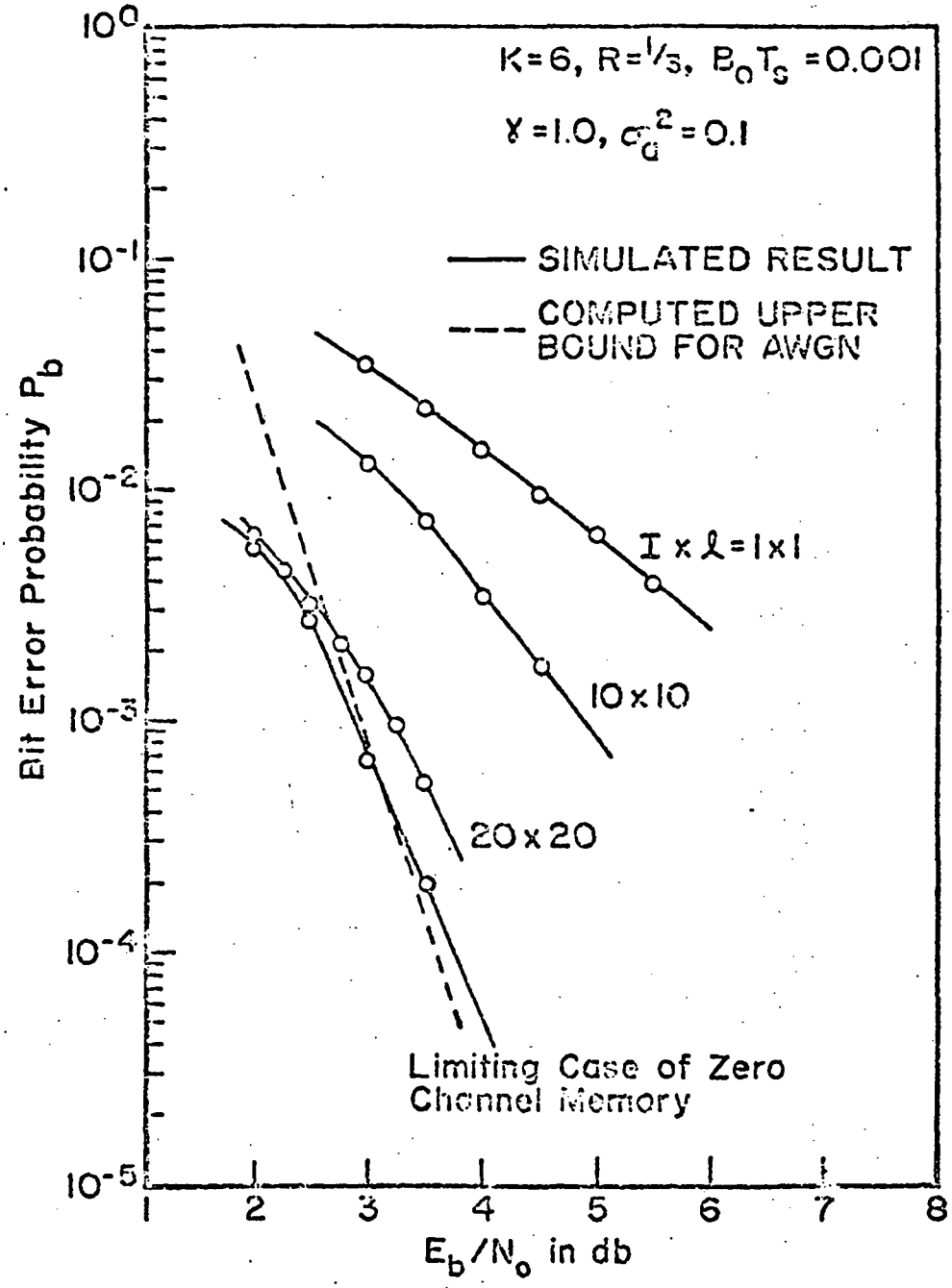

Figure 4-12

Effects of Block Interleaving for K = 6, R = 1/3 Code with B_oT_s = 0.001 and γ = 1.0, σ_a^2 = 0.1

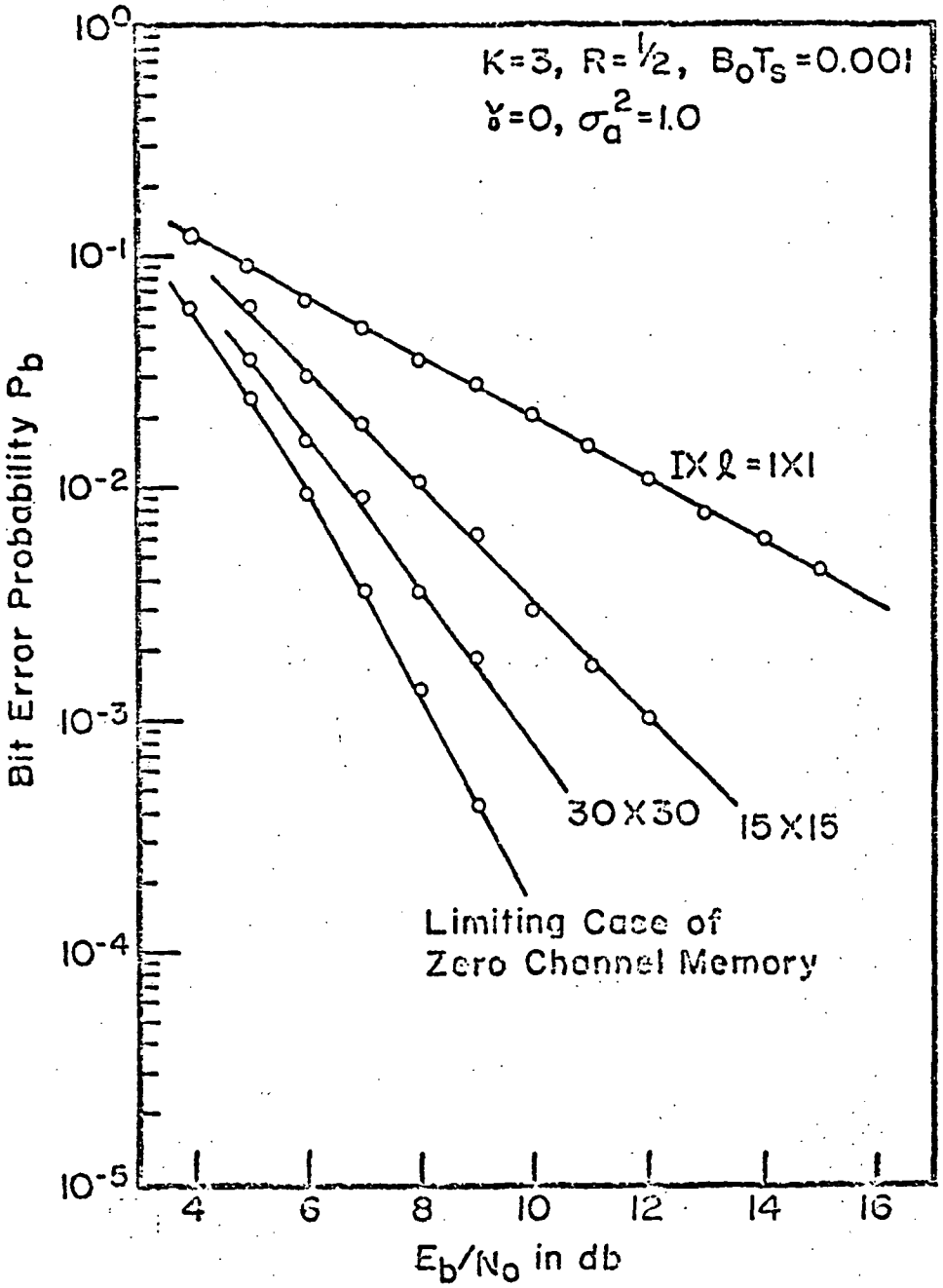

Figure 4-13

Effects of Block Interleaving for K = 3, R = 1/2 Code with B_oT_s = 0.001 and γ = 0, σ_a^2 = 1.0

of B_oT_s, of course, the interleaving requirements are less severe. This is illustrated in Figures 4-14 and 4-15 for a K = 6, R = 1/3 code with $B_oT_s = 0.01$ and $B_oT_s = 0.1$ respectively. The effects of interleaving have shown a surprising insensitivity to both code rate and constraint length depending instead only upon the value of B_oT_s. It is somewhat surprising that such small amounts of interleaving can be so effective in combatting the memory effects of the channel. This behavior is easily explained by reference to Figure 4-16 which illustrates in some detail the approach of the bit error probability performance to the limiting case of zero channel memory as a function of B_oT_s for a K = 3, R = 1/2 code. Observe that for $B_oT_s = 0.001$ initially, a 30 x 30 interleaver results in an "effective" time-bandwidth product of 0.03 which according to Figure 4-16 should provide performance within 1 db of the limiting case. In general an interleaver of size I x ℓ results in an "effective" time-bandwidth product of B_oT_s x I since successive symbols are then separated by I channel symbols reducing the memory or equivalently increasing the coherence bandwidth by the factor I. This is illustrated in Figure 4-17 for a K = 7, R = 1/2 code with an initial $B_oT_s = 0.001$. It is demonstrated that the performance obtained with interleaving compares favorably with that obtained with the corresponding "effective" value of B_oT_s. As a rule of thumb it would appear that if performance within a few tenths of a db of the limiting performance is to be obtained, the "effective" B_oT_s should be in the vicinity of 0.1. Table 4-2 provides a summary of the interleaving requirements as a function of B_oT_s.

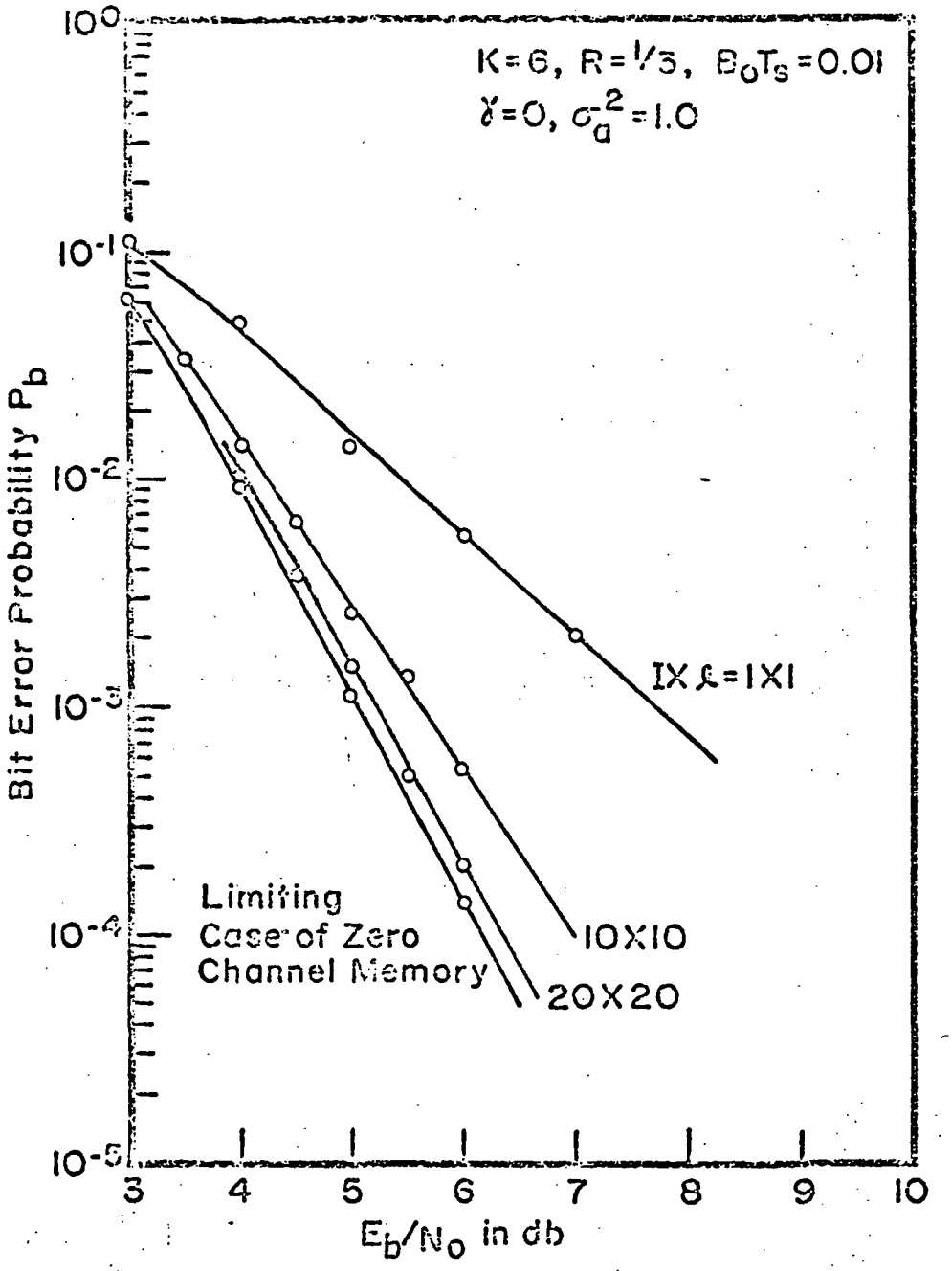

Figure 4-14

Effects of Block Interleaving for K = 6, R = 1/3 Code with B_oT_s = 0.01 and γ = 0, σ_a^2 = 1.0

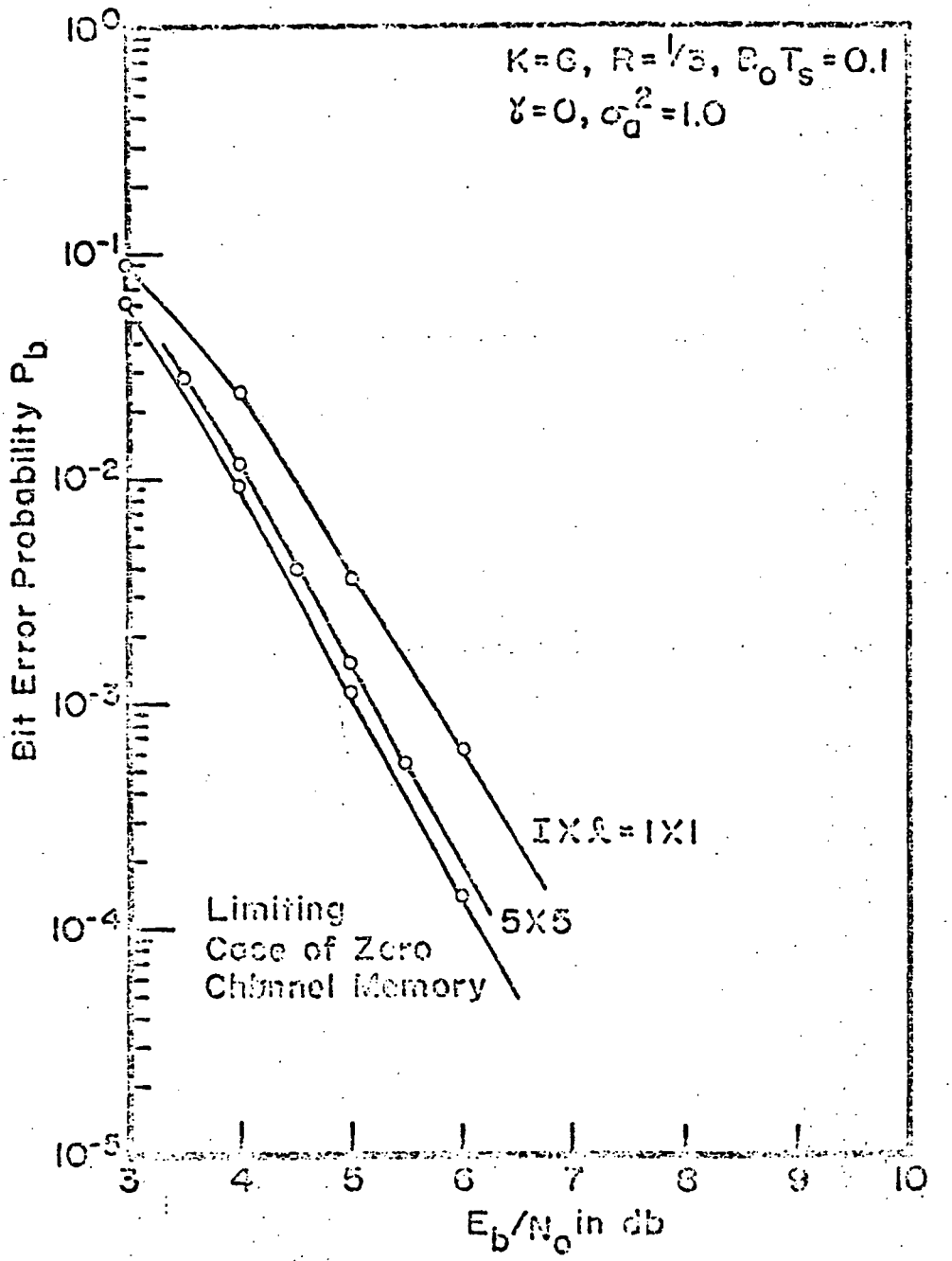

Figure 4-15

Effects of Block Interleaving for K=6, R=1/3

Code with B_oT_s=0.1 and γ=0, σ_a^2=1.0

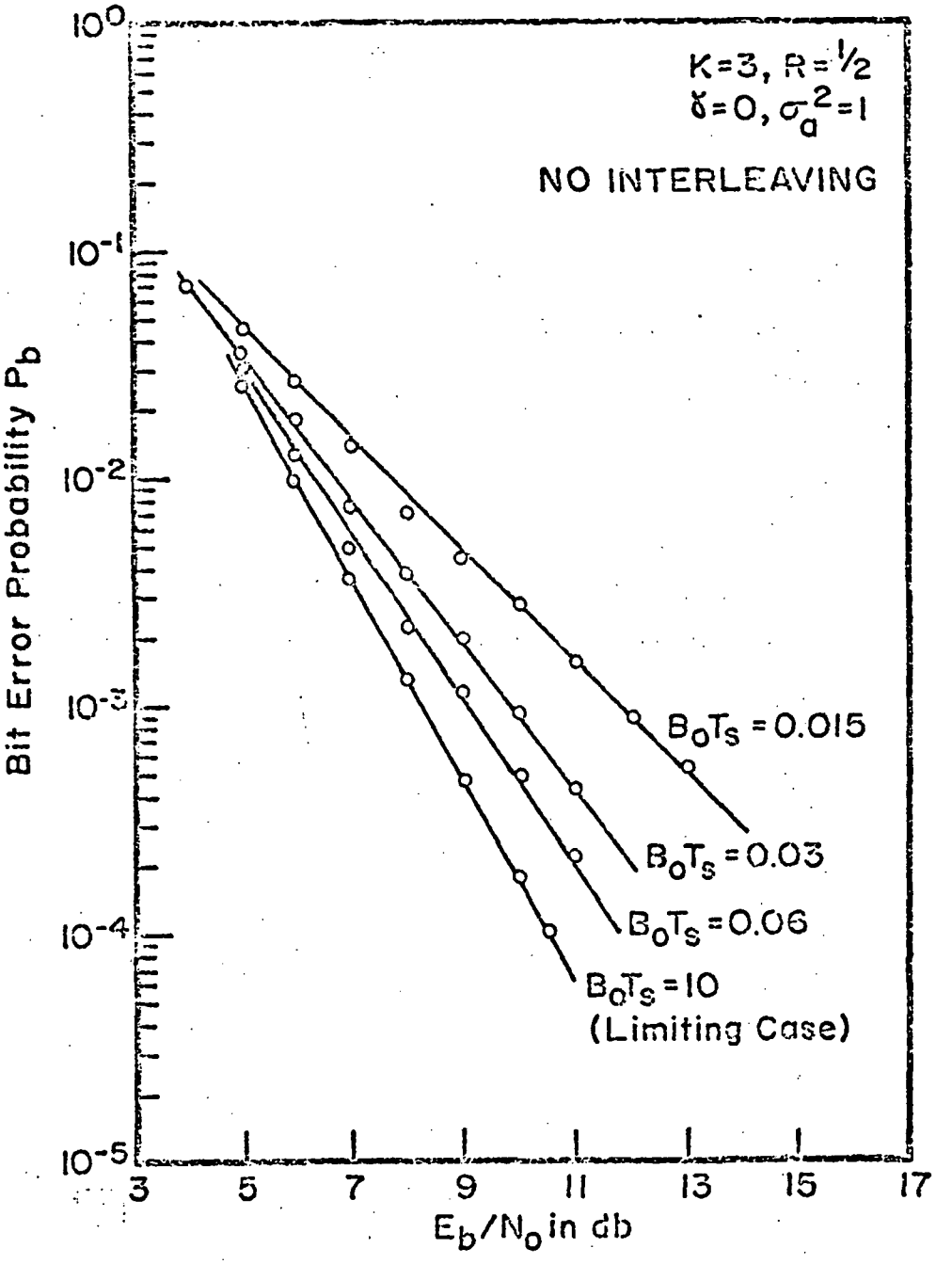

Figure 4-16

Approach of Performance with K = 3, R = 1/2 Code to Limiting Performance with Increasing B_oT_s

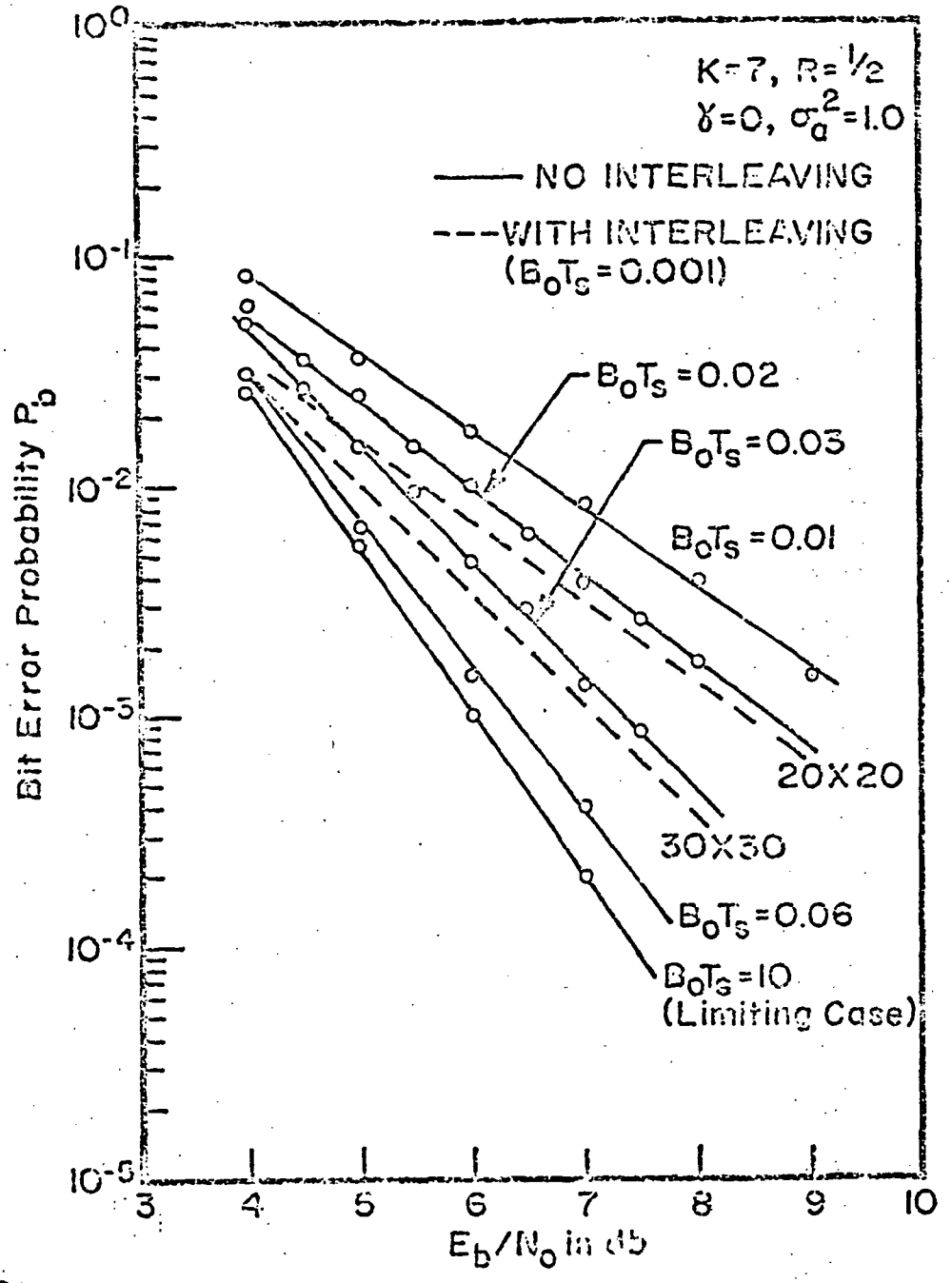

Figure 4-17

Comparison of Performance of K=7, R=1/2 Code for Various Amounts of Interleaving with Corresponding "Effective" B_oT_s

B_oT_s	Required I x ℓ
.1	1 x 1
.01	10 x 10
.001	100 x 100

Table 4-2

Summary of Interleaving Requirements as a Function of B_oT_s to Obtain Performance within a Few Tenths of a db of Limiting Performance

Finally it is to be noted that in all of the preceding work we have considered only square interleaver structures. It is to be expected that performance should be an insensitive function of the dimension ℓ and hence economies can be realized by reducing this dimension considerably. Figure 4-18 illustrates typical results for a K = 3, R = 1/2 code utilizing non-square interleaving. Obviously there is a finite limit to how small ℓ can be made without seriously degrading performance. This is a subject of continuing study.

4.2 Quantization Effects:

In all the simulations described so far infinitely fine quantization was employed. It remains to determine the effects of receiver quantization. The effects of receiver quantization are in clear evidence in Figure 4-19 and Figures 4-20 and 4-21 for a K = 6, R = 1/3 code and B_oT_s = 10.0 and B_oT_s = 0.01 respectively. In each case no interleaving is employed. It appears, as in the case of the AWGN channel, that a degradation of only a few tenths of a db result with Q = 8 level quantization. We do not expect the previously drawn conclusions on interleaving requirements to be altered if 8 level receiver quantization is employed.

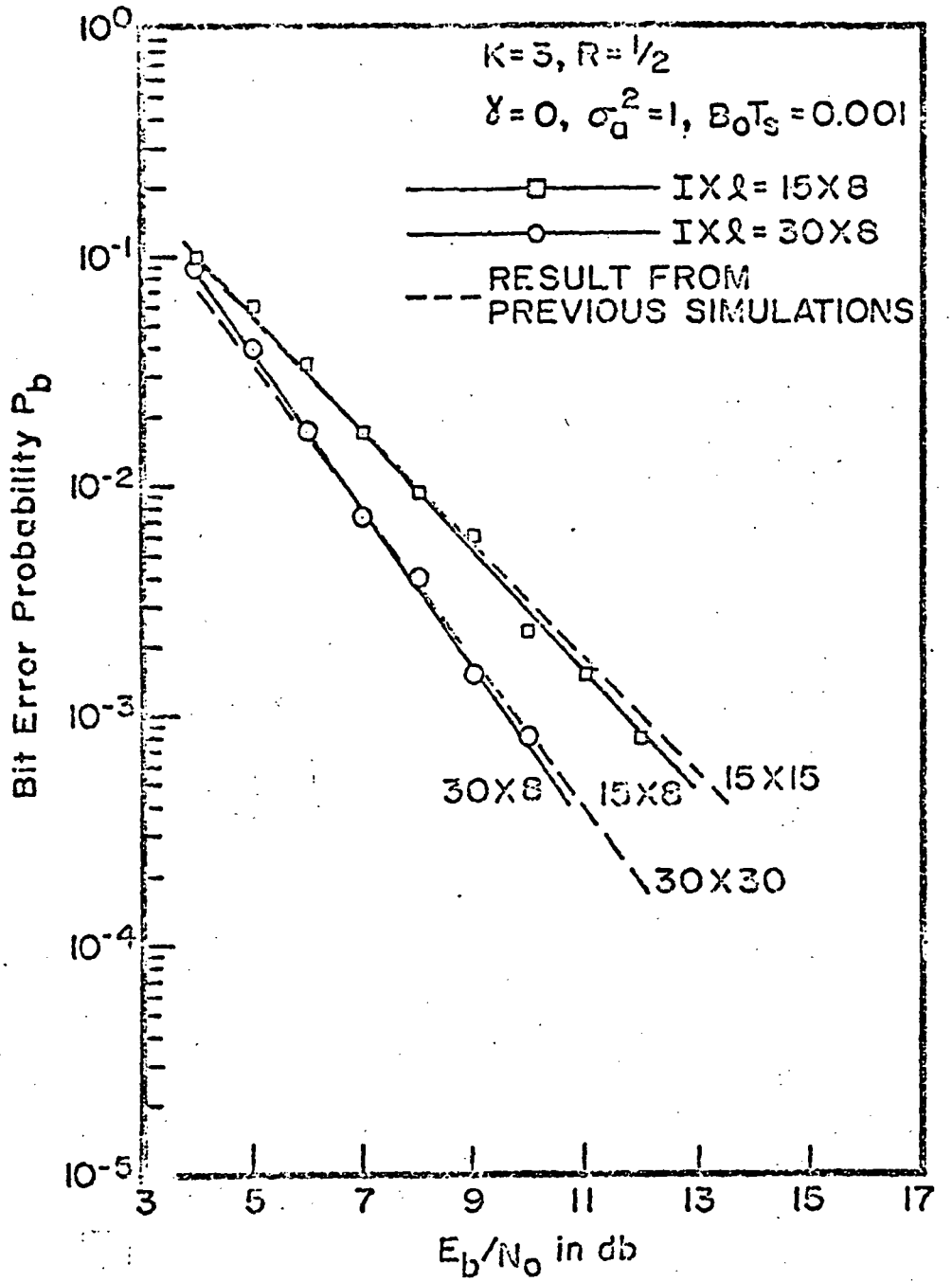

Figure 4-18

Performance of K = 3, R = 1/2 Code
with Non-Square Interleaver

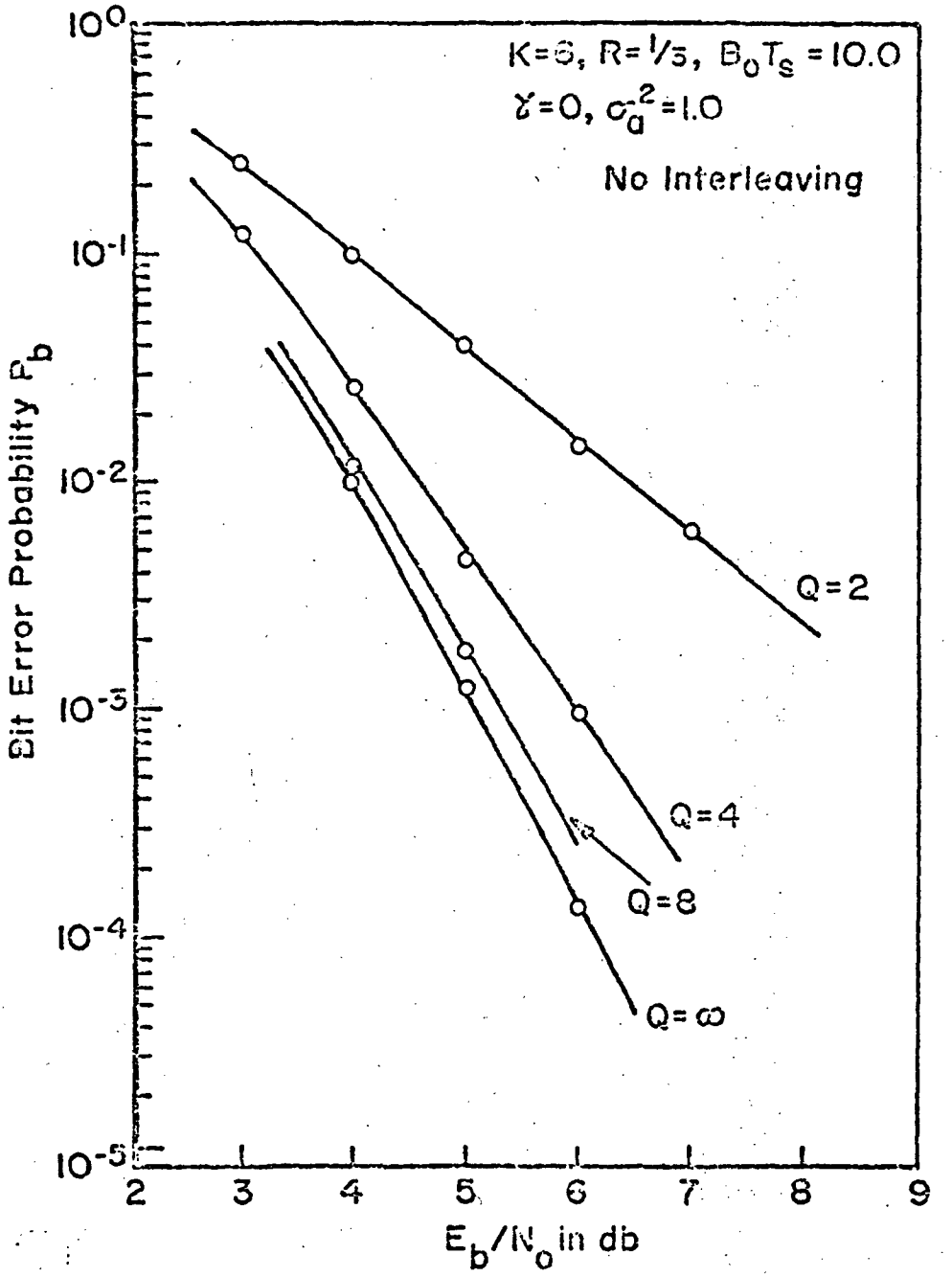

Figure 4-19

Effects of Quantization on K = 6, R = 1/3 Code with B_oT_s = 10.0 and γ = 0, σ_a^2 = 1.0

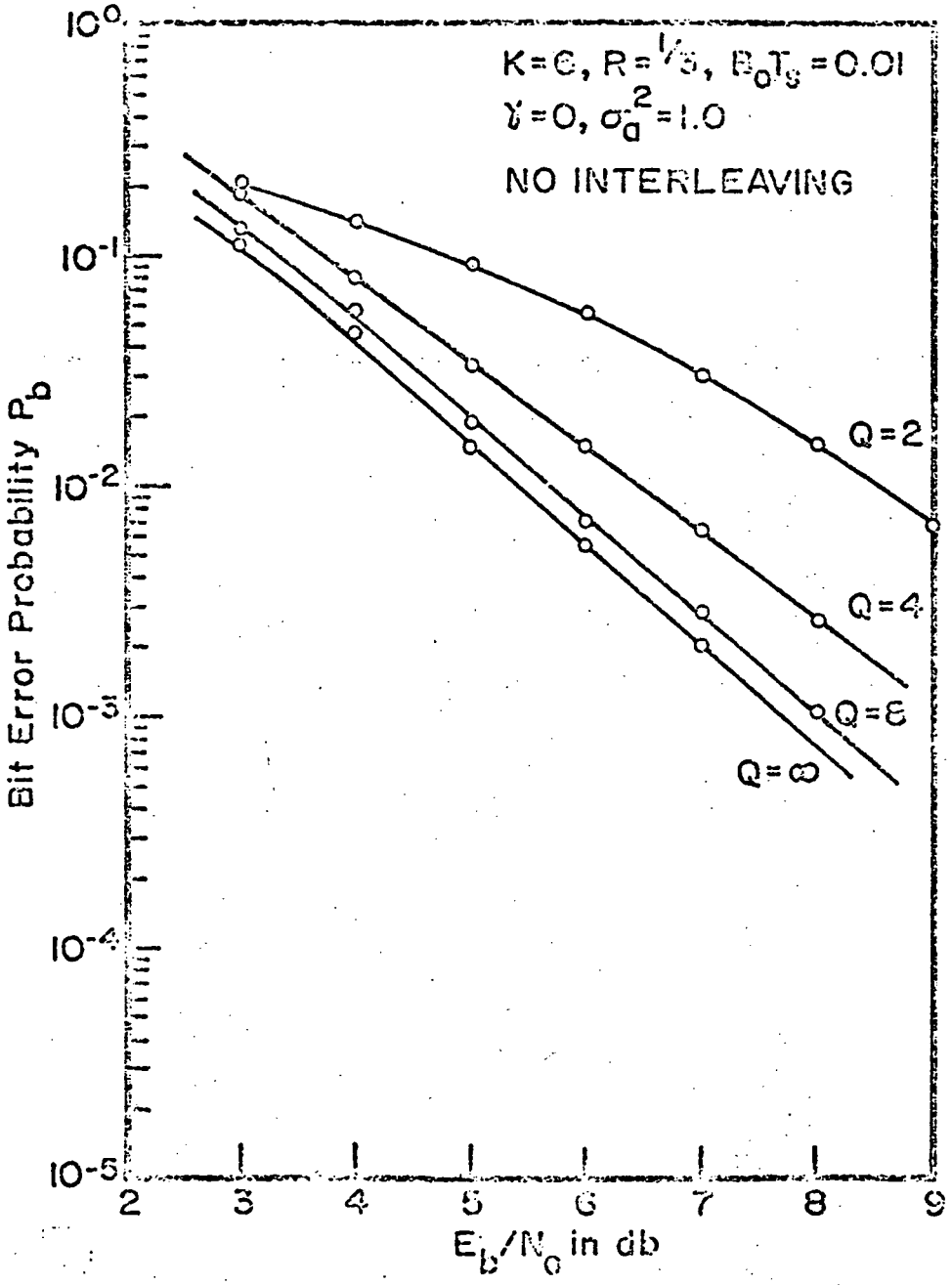

Figure 4-20

Effects of Quantization on K=6, R=1/3 Code with B_oT_s=0.01 and γ=0, σ_a^2=1.0

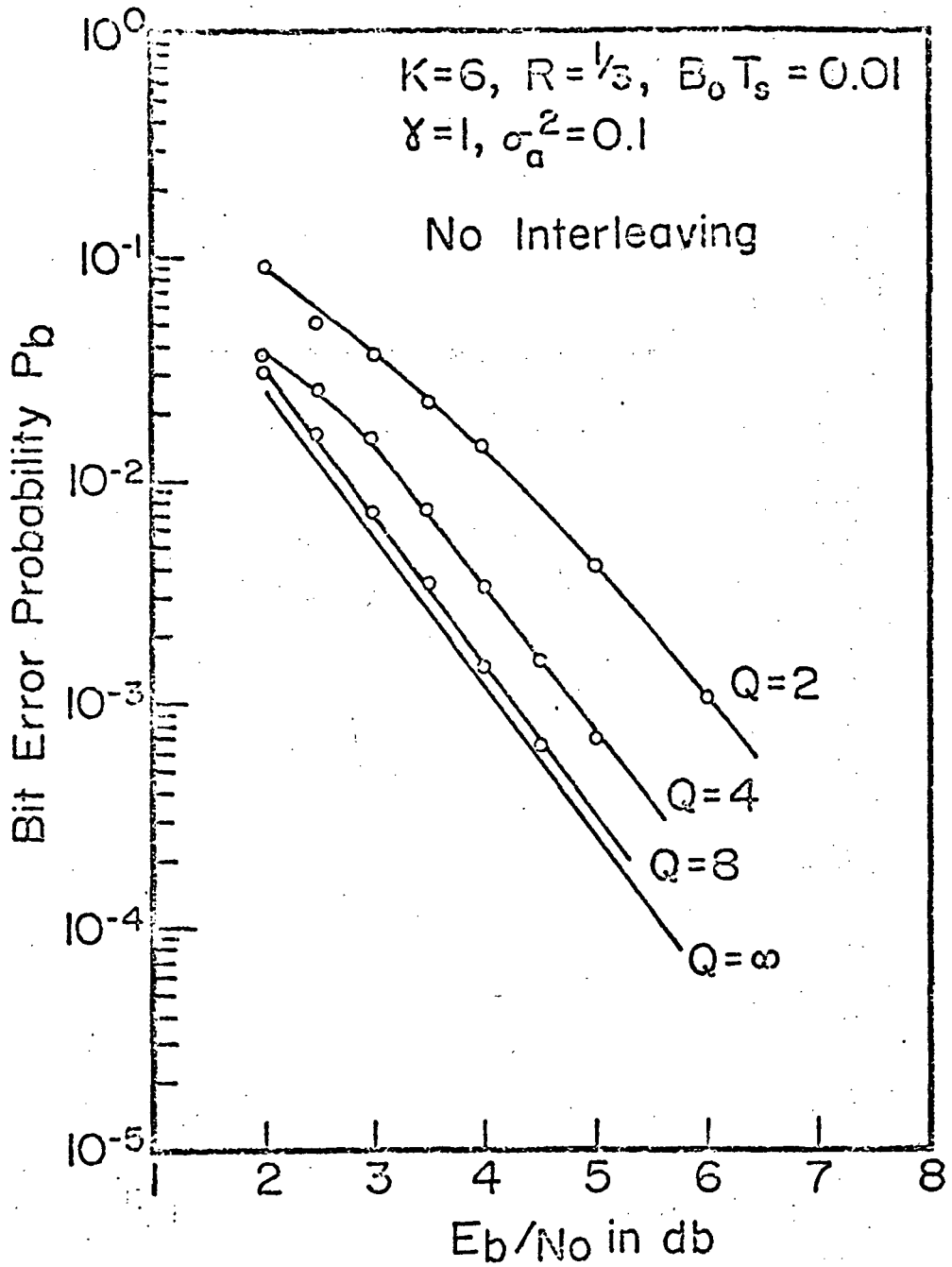

Figure 4-21

Effects of Quantization on K = 6, R = 1/3 Code with $B_o T_s$ = 0.01 and γ = 1.0, σ_a^2 = 0.1

4.3 Comparison of Results With Lognormal Amplitude Distribution

While there is some theoretical justification of the lognormal amplitude distribution there is also reason to believe that the Rayleigh-Rice amplitude distribution provides a more realistic model of actual fading channel behavior. It is of some interest to compare simulation results obtained under both assumptions. This is illustrated in Figure 4-22 for a K = 3, R = 1/2 code and $B_o T_s = 0.001$. For the lognormal distribution we take $\sigma_\chi^2 = 0.056$ and $\sigma_\chi^2 = 0.018$ with B_χ related to B_o through (3.25). The parameters of the Rayleigh-Rice distribution have been chosen as $\gamma = 1.0$ and σ_a^2 taken from Table 3-2. The simulated bit error probability performance compares favorably with the correspondence improving with smaller values of σ_χ^2.

4.4 Imperfect Phase Tracking

The simulation results reported in preceding sections have all assumed perfect phase tracking. As a result, the sequence of matched filter outputs can be described by (3.26) and the sequel. In reality, since the phase is not known at the receiver, quadrature matched filters must be employed. During the i^{th} signaling interval the inphase and quadrature matched filter outputs can be respectively represented as

$$r_{I,i} = x_i \sqrt{\frac{2E_s}{N_o}} \left| \Gamma_i + a_i \right| \cos \theta_i + n_{I,i} \; ; \qquad i = 1, 2, \ldots \tag{4.1a}$$

and

$$r_{Q,i} = x_i \sqrt{\frac{2E_s}{N_o}} \left| \Gamma_i + a_i \right| \sin \theta_i + n_{Q,i} \; ; \qquad i = 1, 2, \ldots \tag{4.1b}$$

Here $\{ n_{I,i} \}$ and $\{ n_{Q,i} \}$ are mutually independent i.i.d. zero-mean unit Gaussian sequences and

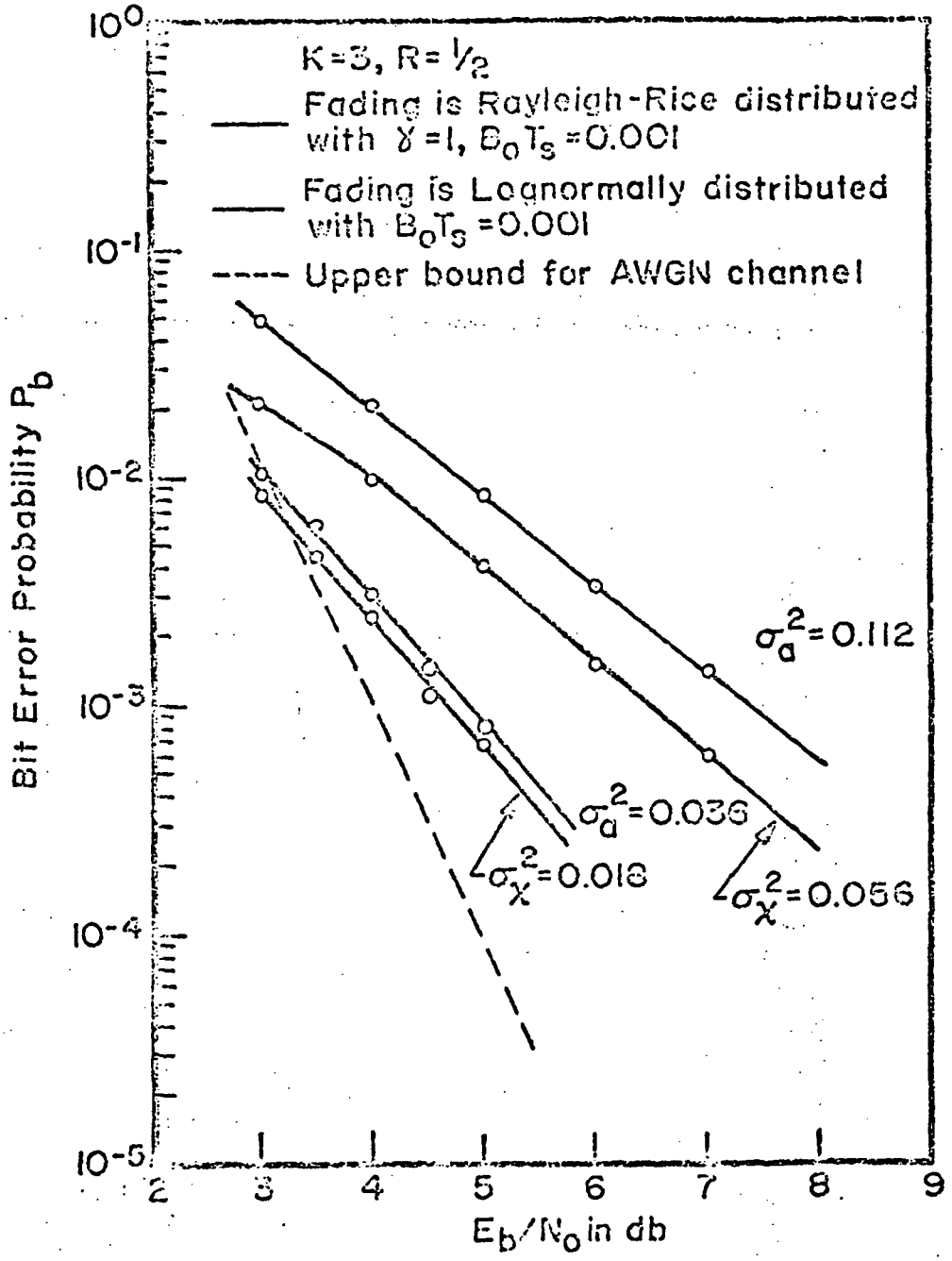

Figure 4-22

Comparison of Results for Rayleigh-Rice and Lognormal Distribution with K = 3, R = 1/2 Code

$$\theta_i = \arg\left[\Gamma + a_i\right] \qquad (4.2)$$

$$= \tan^{-1}\left[\frac{\gamma \sin \Psi + a_{Q,i}}{\gamma \cos \Psi + a_{I,i}}\right]; \qquad i = 1, 2, \ldots$$

represents the value of the true phase process $\theta(t)$ throughout the i^{th} signaling interval. The quantities $a_{I,i}$ and $a_{Q,i}$ are respectively the inphase and quadrature components of the complex quantity a_i described previously, i.e.,

$$a_i = a_{I,i} + j\, a_{Q,i}; \qquad i = 1, 2, \ldots \qquad (4.3)$$

as in [25]. It proves convenient to represent the quadrature matched filter outputs as

$$R_i = r_{I,i} + j\, r_{Q,i} \qquad (4.4)$$

$$= x_i \sqrt{\frac{2E_s}{N_o}}\left|\Gamma + a_i\right| e^{j\theta_i} + N_i; \qquad i = 1, 2, \ldots$$

where now

$$N_i = n_{I,i} + j\, n_{Q,i}; \qquad i = 1, 2, \ldots \qquad (4.5)$$

We have then made use of a phase estimator originally proposed by Jacobs [4] and easily shown to be related to that described by Arnstein [30]. In particular, we develop the estimate

$$\hat{\theta}_i = \pm \frac{1}{2} \arg\left\{\sum_{k=i-N}^{i-1} R_k^2\right\}; \qquad i = 1, 2, \ldots \qquad (4.6)$$

of the phase θ_i during the i^{th} signaling interval based upon N past observations of the matched filter output sequence represented by (4.4). The 180° phase ambiguity represented by the $\pm$ sign in (4.6) can easily be removed by periodic insertion of a known signal sequence and subsequent tracking of the phase during successive signaling intervals. An analysis of the estimation accuracy to be achieved with

this estimator is provided in [31] where it is shown that for large SNR the performance approaches that of a first order phase-locked loop (PLL) with tracking bandwidth $b_L = 1/NT_s$. The advantage of this approach is that it does not require carrier power. If the phase were truly constant for all time it would make sense to utilize as large a value of N in (4.6) as possible. The assumption of constant phase over the N preceding signaling intervals is approximately satisfied if $N < 1/B_oT_s$ where the dimensionless quantity B_oT_s has been defined previously. In our simulations we will assume that

$$N = \frac{\alpha}{B_oT_s} \tag{4.7}$$

when $0 < \alpha \leq 1$ is to be specified. The question remains as to how α is to be chosen as a function of the fading channel parameters. Figure 4-23 illustrates a typical simulation result for a K = 3, R = 1/2 code with $\gamma = 0$, $\sigma_a^2 = 1.0$ and $B_oT_s = 0.015$. With a choice $\gamma = 0$, the phase varies so rapidly that nothing is to be gained by employing N in excess of 3 ($\alpha = 0.05$ in this case). In Figure 4-24 we illustrate the performance of the phase tracker for a K = 3, R = 1/3 code now with $\gamma = 1.0$, $\sigma_a^2 = 0.1$ and $B_oT_s = 0.001$. Here the phase varies so slowly that performance within a few tenths of a db of that afforded by perfect phase tracking can be achieved with N = 100 ($\alpha = 0.1$). Additional results are illustrated in Figures 4-25 and 4-26. It would appear that for $\gamma = 1.0$, $\sigma_a^2 = 0.1$, which we feel are typical channel parameters for a Venusian atmosphere, a value α in the range $0.25 \leq \alpha \leq 0.1$ should provide performance within a few tenths of a db of that obtainable with perfect phase tracking.

5.0 Simulation Results for Sequential Decoding

In this section we will describe some of the simulation results obtained for both Fano and ZJ decoding of long constraint length convolutional codes. We

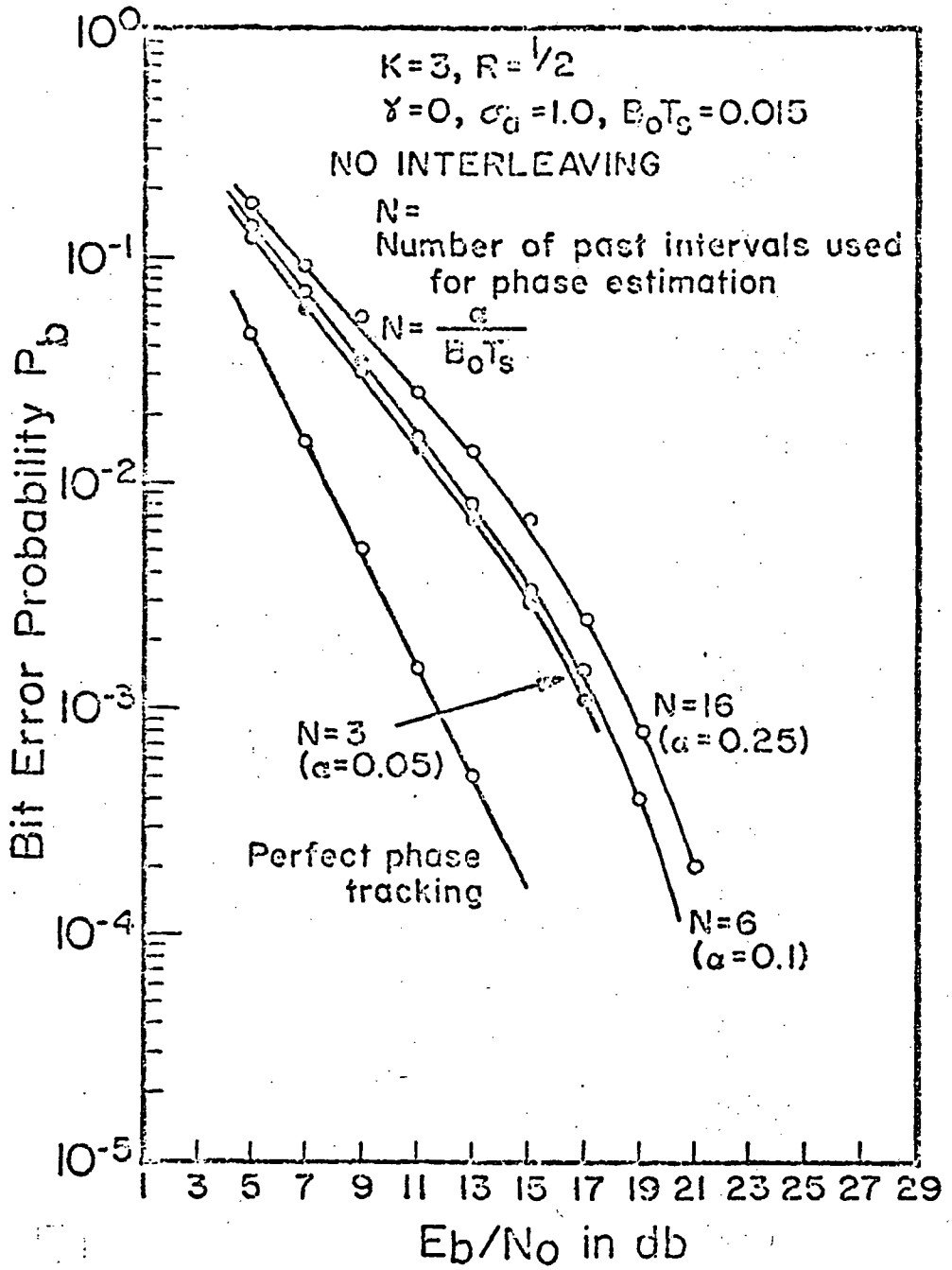

Figure 4-23

Effects of Imperfect Phase Tracking on K = 3, R = 1/2 Code with $\gamma = 0$, $\sigma_a^2 = 1.0$ and $B_o T_s = 0.015$

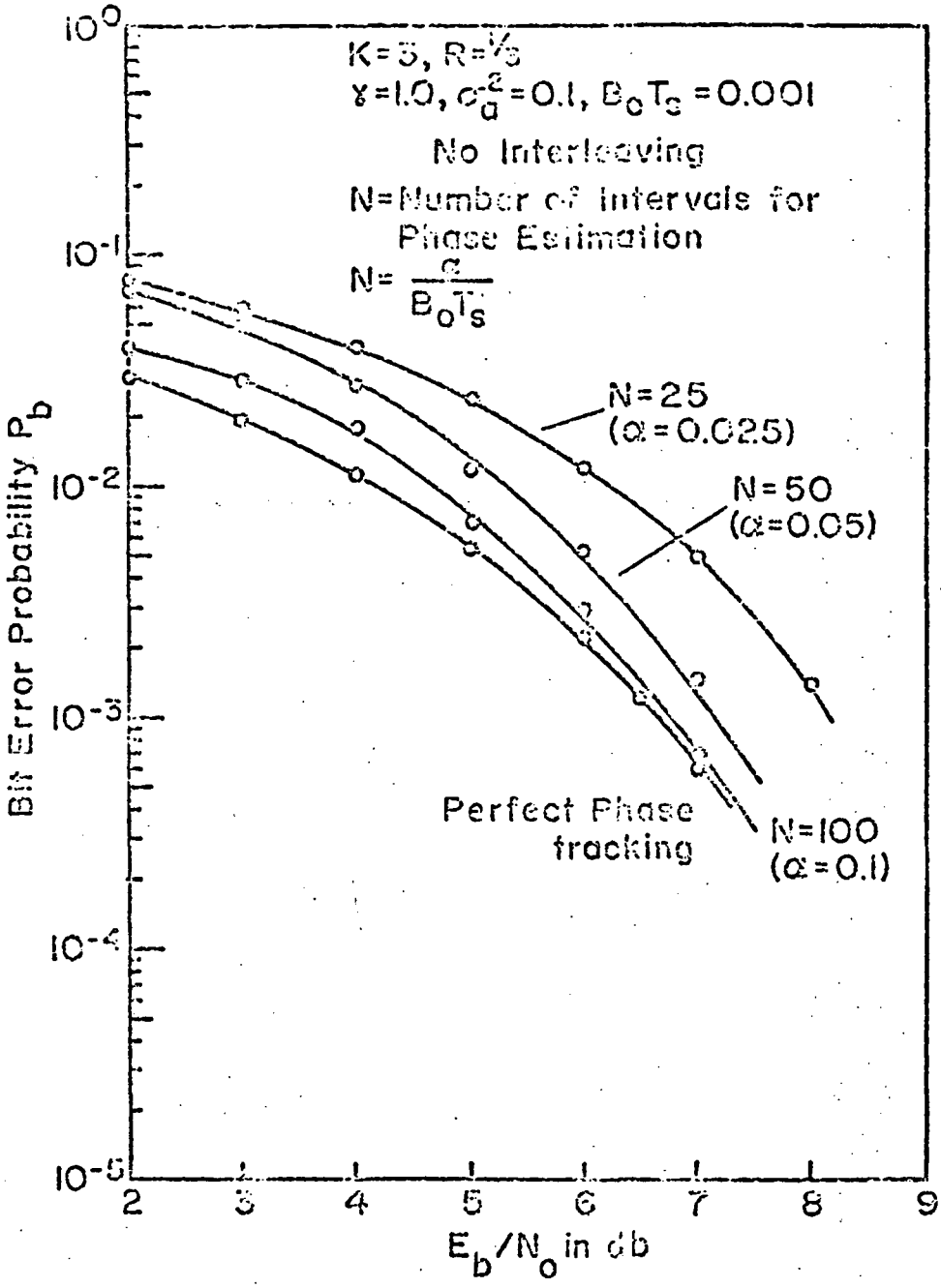

Figure 4-24

Effects of Imperfect Phase Tracking on K = 3, R = 1/3 Code with $\gamma = 1.0$, $\sigma_a^2 = 0.1$ and $B_oT_s = 0.001$

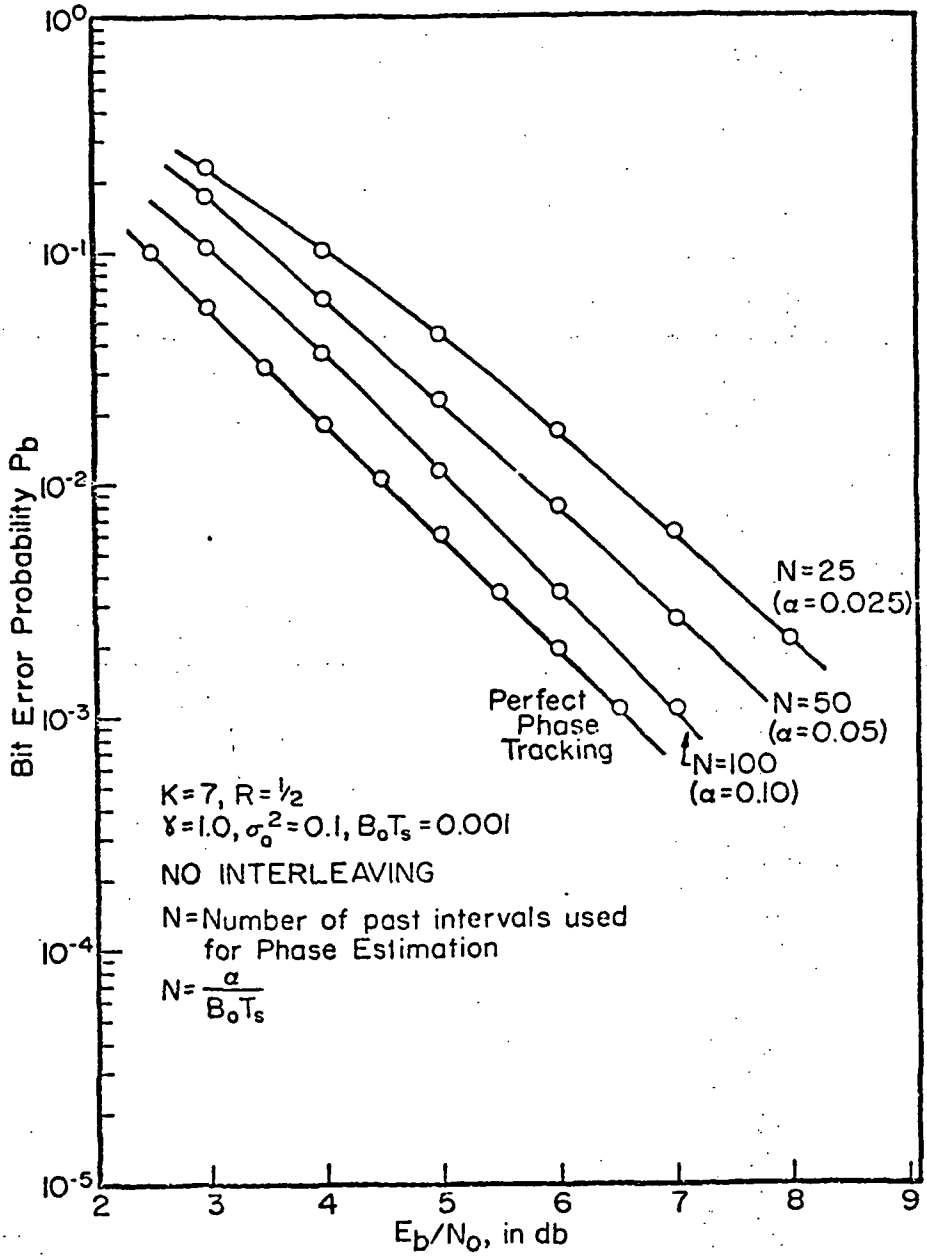

Figure 4-25

Effects of Imperfect Phase Tracking on K = 7,
R = 1/2 Code with γ = 1.0,
σ_a^2 = 0.1 and B_oT_s = 0.001

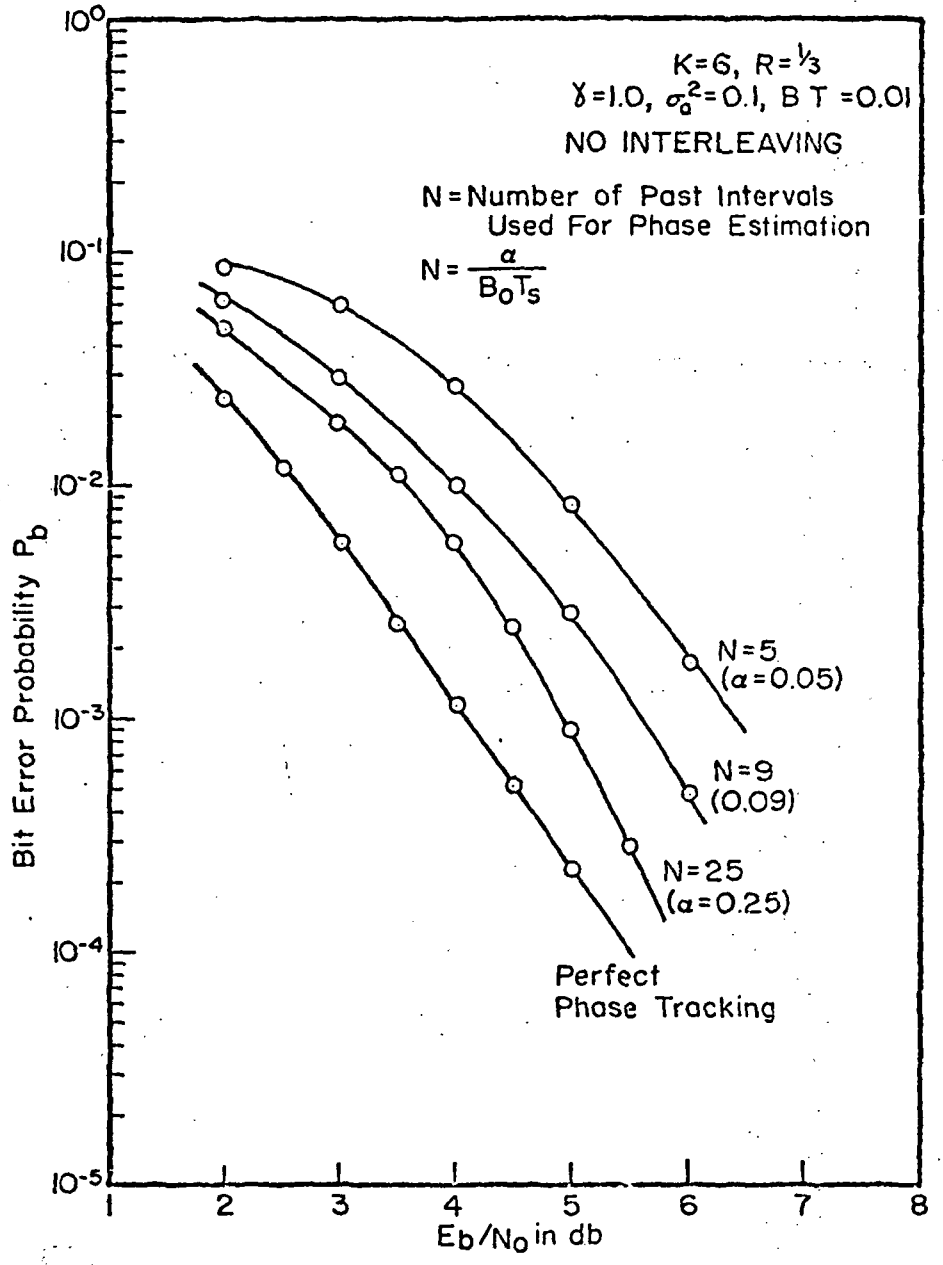

Figure 4-26

Effects of Imperfect Phase Tracking on $K = 6$, $R = 1/3$ Code with $\gamma = 1.0$, $\sigma_a^2 = 0.1$ and $B_o T_s = 0.01$

will attempt to parallel the discussion of the Viterbi decoding results presented in the preceding section to the extent possible. It is to be emphasized at the outset that considerably less simulation results have been obtained for sequential decoding vis-à-vis the results for Viterbi decoding. This is due chiefly to the time consuming and expensive nature of the computer processing required in order to obtain statistically significant data. As a consequence, the results and conclusions reported here should be considered tenative based as they are on a limited number of simulation results. It is expected, however, that all substantive issues will be resolved in the course of work presently in progress.

In all simulations of sequential decoder performance we have made use of the Massey quick-look code described previously in Section 2 with constraint length $K = 32$ and rate $R = 1/2$. Each frame or block consisted of 250 information bits to which 31 tail zeros were added. The receiver employed uniform quantization with $Q = 8$ levels. All simulation results are reported on the basis of 10^4 successive transmissions of the 250 bit message. A computational cutoff of 5×10^4 computations was imposed for both the Fano and ZJ decoder. The ZJ algorithm employed a decode table consisting of a maximum of 5×10^3 entries although only a small percentage of this number were ever required. Both the Fano and ZJ decoders employed a bias $\lambda_o = 1/2$ (i.e., equal to the rate) while the Fano decoder employed a threshold spacing $T_o = 4$ bits. We have found it convenient to present simulation results for fixed values of R/R_o. Here R_o refers to the computational cutoff rate or critical rate in the absence of fading, i.e., in the AWGN channel as determined by (2.13) and the sequel. It is recognized that the actual critical rate is effectively lowered in the presence of fading although no attempts have been made to explicitly compute this quantity

as a function of the underlying channel parameters. In what follows then we will continue to use the normalized rate R/R_o referred to the critical rate of the original AWGN channel as a convenient parameter in describing the behavior of sequential decoders in the planetary entry channel.

In Figures 5-1 and 5-2 we illustrate the empirically determined computational distribution of the Fano decoder as a function of the dimensionless quantity B_oT_s for $R/R_o = 0.8$ and 0.9 respectively. Here the channel parameters were chosen as $\gamma = 1.0$ and $\sigma_a^2 = 0.1$. For the case $R/R_o = 0.99$, the probability of exceeding the imposed computational cutoff of 5×10^4 computations per block was close to unity even for $B_oT_s = 10.0$ so that results are not plotted. Similarly, for the choice of channel parameters $\gamma = 0.0$ and $\sigma_a^2 = 1.0$ the quit probability P_Q was consistently found to be close to unity for $R/R_o \geq 0.8$. As a result, this worst case has been eliminated from further consideration. On Figures 5-1 and 5-2 we have indicated the performance in AWGN for comparison purposes. The case $B_oT_s = 10.0$ represents, for all practical purposes, the limiting case of zero channel memory which can be approached with sufficiently large interleaving. It is clear that even moderate amounts of channel fading can result in severe degradation of the computational performance of the Fano decoder. Furthermore, even if large amounts of interleaving is provided the best that one could expect is to approach the limiting case of zero channel memory represented by the case $B_oT_s = 10.0$. For R/R_o close to unity, this performance can in turn be orders of magnitude worse than the computational requirements in the AWGN channel. Similar comments can be made for the ZJ decoder on the basis of the simulation results obtained to date. In the absence of fading, prudent system design would dictate choosing R/R_o close to unity. From the limited simulation results reported here it must then be concluded that, in the presence of even moderate amounts of channel

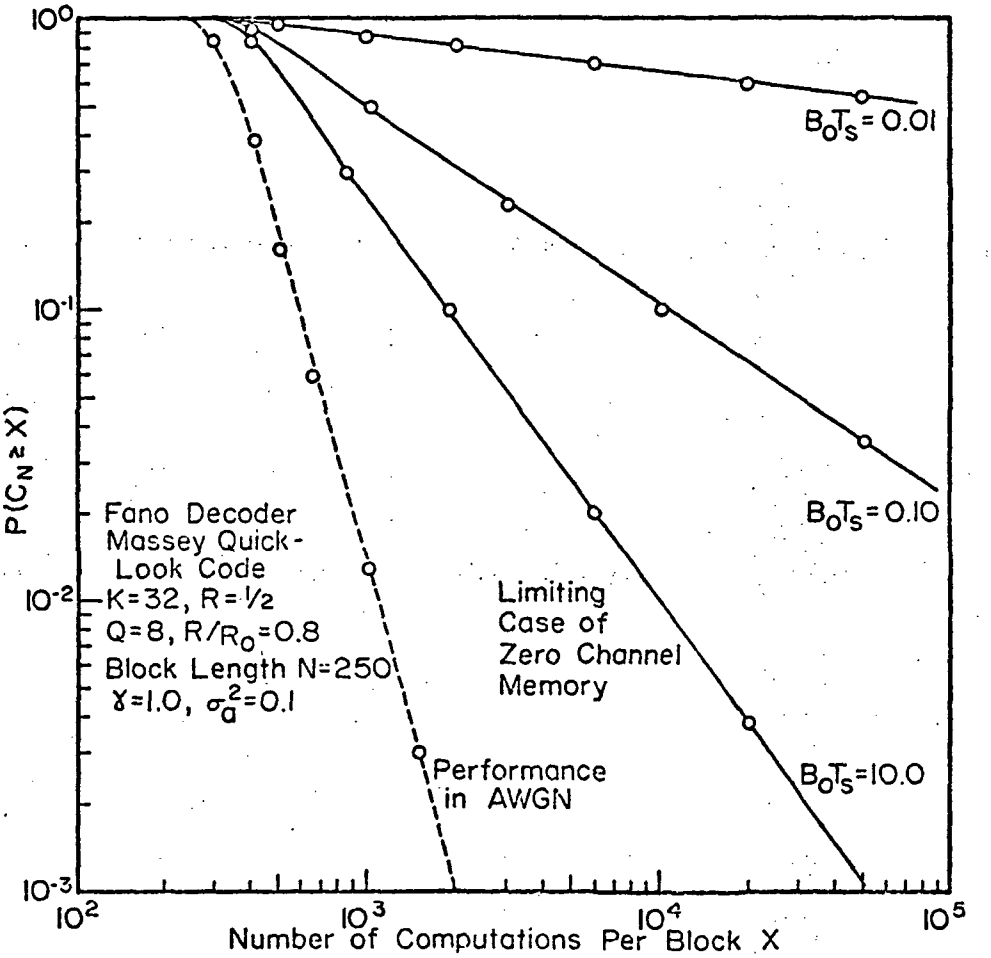

Figure 5-1

Empirical Probability Distribution of Computational Count for Fano Decoder with $\gamma = 1.0$, $\sigma_a^2 = 0.1$ and $R/R_o = 0.8$

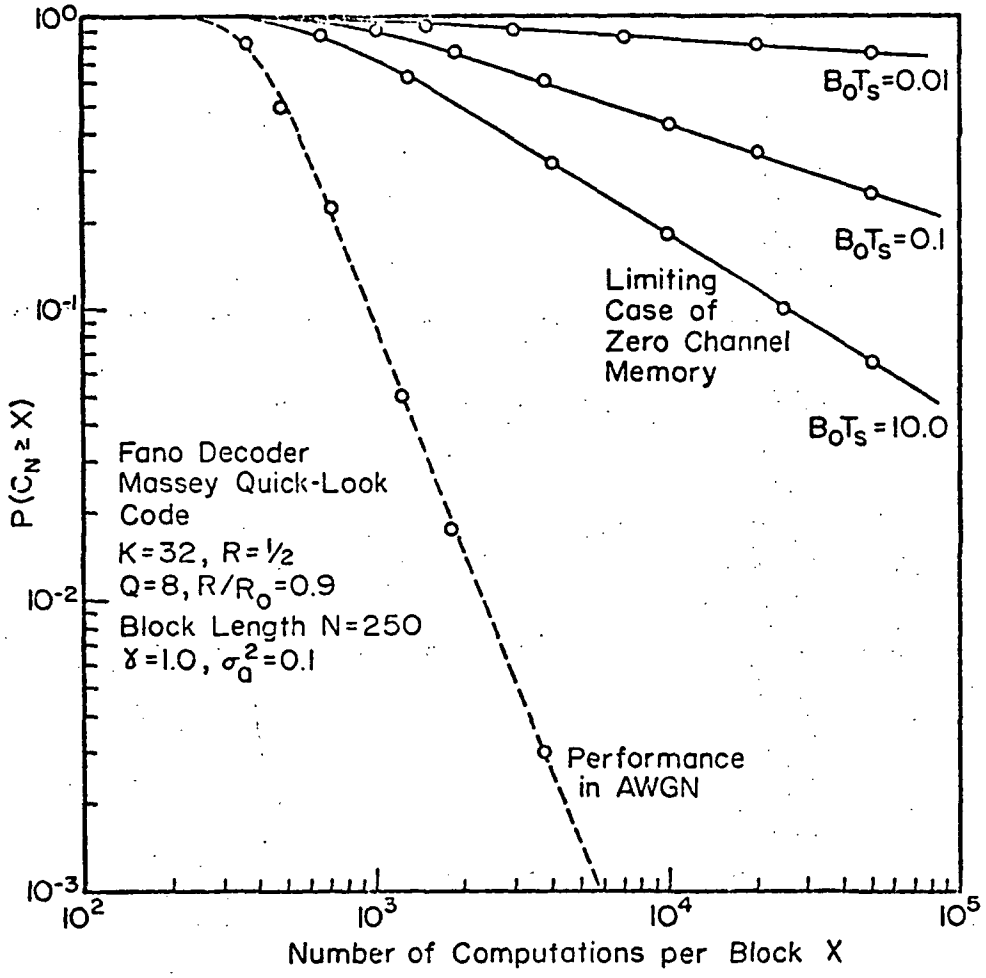

Figure 5-2

Empirical Probability Distribution of Computational Count for Fano Decoder with $\gamma = 1.0$, $\sigma_a^2 = 0.1$ and $R/R_o = 0.9$

fading, interleaving alone will not prove sufficient to insure computational requirements comparable to that of the AWGN channel. What is required is clearly a combination of interleaving and a simultaneous reduction in the operating R/R_o ratio. While it is felt that the required reduction in R/R_o can be explicitly calculated, no attempt was made to do so as part of this study. It is felt that this is a topic worthy of additional investigation.

5.1 Interleaving Considerations

A limited number of simulations have been performed to investigate the efficacy of simple block interleaving in combatting the channel memory and thereby reducing somewhat the computational requirements of sequential decoders for small values of B_oT_s. Typical results for a Fano decoder are illustrated in Figures 5-3 and 5-4 for $R/R_o = 0.8$ and 0.9 respectively with $B_oT_s = 0.01$ in either case. Here it would appear that an interleaver of size 50 x 50 will suffice to provide performance comparable to the memoryless channel if $R/R_o = 0.8$ while for $R/R_o = 0.9$ an interleaver of size 100 x 100 is required. Unfortunately time and computer processing costs have precluded obtaining additional simulation results. It is recommended that future investigations concerning the efficacy of interleaving consider the more meaningful range of R/R_o values such that $R/R_o \leq 0.8$.

6.0 Summary and Conclusions

An attempt has been made to describe an approach to the determination and parameterization of the performance of convolutional codes on fading channels typical of planetary entry missions. For short constraint length codes and Viterbi decoding we have considered the effects of amplitude fading alone under the assumption a perfect carrier phase reference is available and have shown the severe degradation which results unless some form of interleaving is utilized to combat the channel

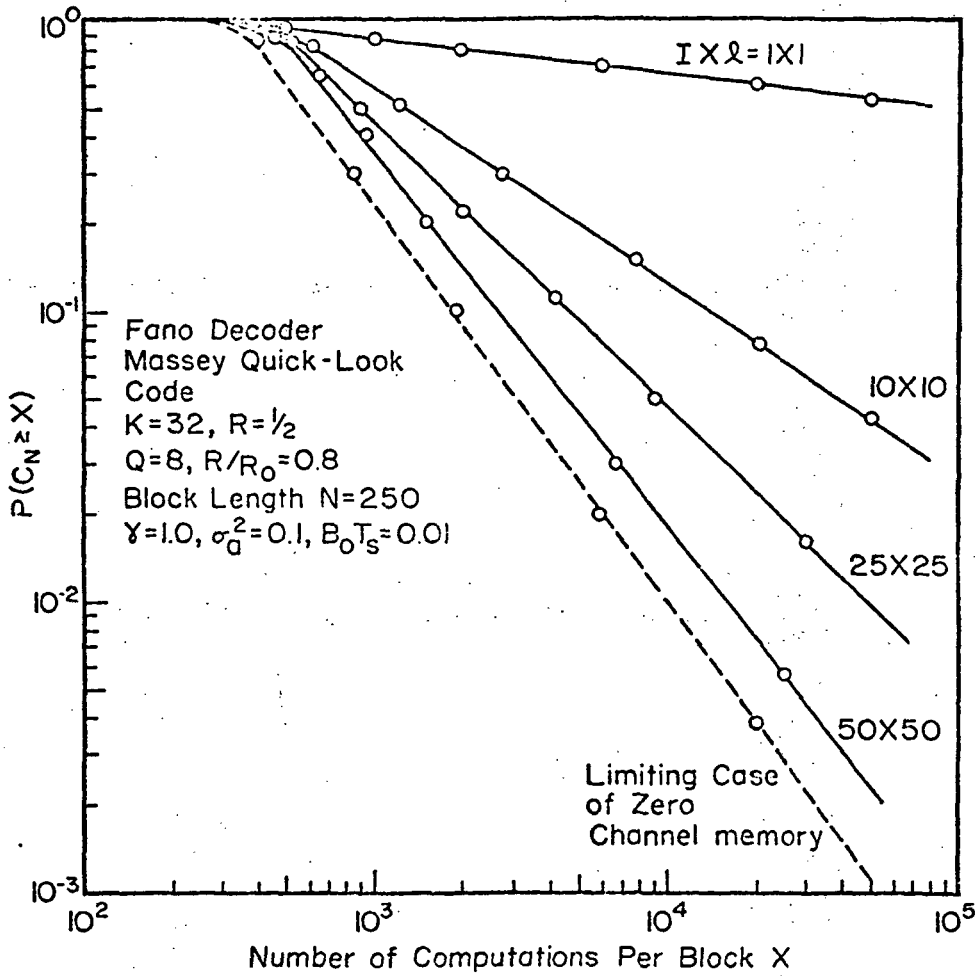

Figure 5-3

Effects of Block Interleaving on Computational Distribution of Fano Decoder with γ=1.0, σ_a^2=0.1, B_oT_s=0.01 and R/R_o=0.8

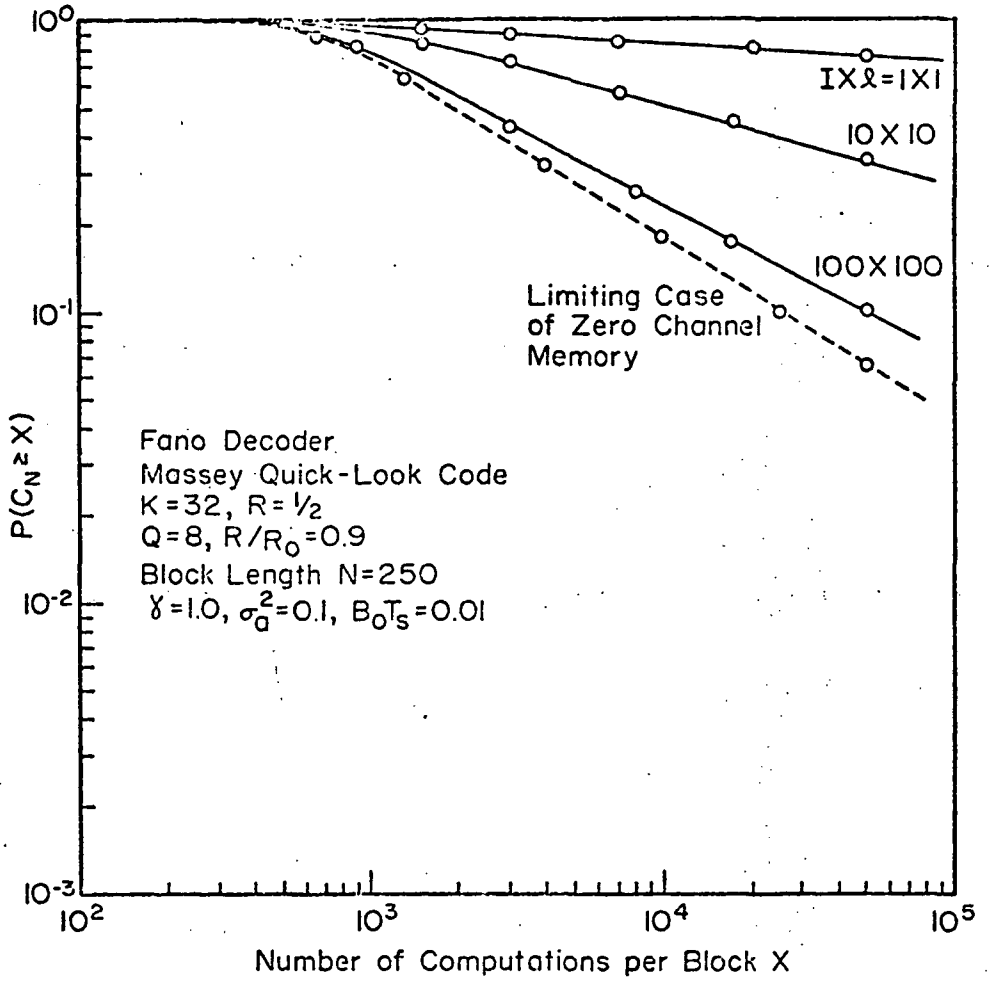

Figure 5-4

Effects of Block Interleaving on Computational Distribution of Fano Decoder with γ=1.0, σ_a^2 = 0.1, B_oT_s = 0.01 and R/R_o = 0.9

memory. The efficacy of simple block interleaving was investigated and shown to be quite effective in reducing the bit error probability P_b. The effects of imperfect carrier phase tracking was then considered and a simple phase estimator proposed which has shown to result in performance comparable to that of perfect phase tracking for reasonable E_b/N_o and provided the parameters of the phase tracker were chosen appropriately. Other than some additional work on the effects of phase tracking errors, it is felt that the treatment of short constraint length codes and Viterbi decoding is complete.

For longer constraint length codes and sequential decoding much more work remains. In particular, additional work should be done to establish the efficacy of block interleaving than has been reported here. The penality in operating R/R_o to maintain computational and/or storage requirements comparable to that for the AWGN channel should be investigated in detail. We have not studied the effects of imperfect phase tracking to any great extent and this subject is certainly worthy of detailed investigation. Finally, it appears that with suitable implementation, the ZJ decoder is capable of providing near real-time decoding of long constraint convolutional codes. This could be of considerable utility in relay links where decoding is provided onboard the spacecraft. Much work remains, however, before a complete understanding is available concerning the nature of the tradeoff between the block error probability P_E, the quit error probability P_Q and the computational and storage requirements. These topics are all subjects of continuing investigation.

References

1. Heller, J. A., and Jacobs, I. M., "Viterbi Decoding for Satellite and Space Communication," IEEE Trans. Comm. Tech., Vol. COM-19, No. 5, Oct. 1971, pp. 835-848.
2. Viterbi, A. J., "Error Bounds for Convolutional Codes and an Asymptotically Optimum Decoding Algorithm," IEEE Trans. Infor. Theory, Vol. IT-13, April 1967, pp. 260-269.
3. Viterbi, A. J., "Convolutional Codes and Their Performance in Communication Systems," IEEE Trans. Comm. Tech., Vol. COM-19, No. 5, Oct. 1971, pp. 751-772.
4. Jacobs, I. M., "Sequential Decoding for Efficient Communication from Deep Space," IEEE Trans. Comm. Tech., Vol. COM-15, Aug. 1967, pp. 492-501.
5. Wozencraft, J. M., and Jacobs, I.M., Principles of Communication Engineering, John Wiley and Sons, New York, 1965.
6. Gallager, R. G., Information and Reliable Communication, John Wiley and Sons, New York, 1968.
7. Modestino, J. W., "Computer Program to Compute Bit Error Probability Performance of Arbitrary Convolution Codes," unpublished RPI report.
8. Odenwalder, J. P., "Optimum Decoding of Convolutional Codes," Ph.D. thesis, Syst. Sci. Dept., Univ. California, Los Angeles, 1970.
9. Larsen, K. J., "Short Convolutional Codes with Maximal Free Distance for Rates 1/2, 1/3, and 1/4", IEEE, Trans. Inform. Theory, Vol. IT-19, No. 3, May 1973, pp. 371-372.
10. Peterson, H. C., and Pike, E. W., "RAN2(K), A New Random Number Generator," TM-S0078, Feb. 1967, MIT Lincoln Laboratory, Lexington, Mass.
11. Richer, I., "Sequential Decoding with a Small Digital Computer," MIT Lincoln Laboratory, TR-491, Jan. 1972.
12. Jordan, K. L., "The Performance of Sequential Decoding in Conjunction with Efficient Modulation," IEEE Trans. Comm. Tech., Vol. COM-14, No. 3, June 1960, pp. 283-297.
13. Savage, J., "The Computation Problem with Sequential Decoding," Ph.D. Thesis, Dept. of Elec. Eng., MIT, Cambridge, Mass. 1965.
14. Cramer, H., Mathematical Methods of Statistics, Princeton University Press, Princeton, N.J., 1966.
15. Massey, J. L. and Costello, D. T., "Nonsystematic Convolutional Codes for Sequential Decoding in Space Applications," IEEE Trans. Comm. Tech., Vol. COM-19, No. 5, Oct. 1971, pp. 806-813.

16. Bluestein, G., and Jordan, K., "An Investigation of the Fano Sequential Decoding Algorithm by Computer Simulation," MIT Lincoln Laboratory, Lexington, Mass., Group Report 62G-3, July 1963.

17. Falconer, D. D., and Niessen, C. W., "Simulation of Sequential Decoding for a Telemetry Channel," Research Lab. of Electronics, M.I.T., Cambridge, Mass., Quat. Prog. Rep. 80, Jan. 1966, pp. 183-193.

18. Jordan, L. L., Jr., "The Performance of Sequential Decoding in Conjunction with Efficient Modulation," IEEE Trans. Comm. Tech., Vol. COM-14, June 1966, pp. 283-297.

19. Lebow, I. L., and McHugh, P. G., "A Sequential Decoding Technique and Its Realization in the Lincoln Experimental Terminal," IEEE Trans. Comm. Tech., Vol. COM-15, August 1967, pp. 477-491.

20. Niessen, C. W., "An Experimental Facility for Sequential Decoding," Sc.D. Thesis, Dept. of Elec. Eng., M.I.T., Cambridge, Mass., Sept. 1965.

21. Zigangirov, K. Sh., "Some Sequential Decoding Procedures," Probl. Peredach. Inform., Vol. 2, 1966, pp. 13-25.

22. Jelinek, F., "A Fast Sequential Decoding Algorithm Using a Stack," IBM J. Res. Dev., Vol. 13, Nov. 1969, pp. 675-685.

23. Geist, J. M., "Search Properties of Some Sequential Decoding Algorithms," IEEE Trans. on Inform. Theory, Vol. IT-19, No. 4, July 1973, pp. 519-526.

24. Modestino, J. W., "Design of a Simulation Facility for Investigating the Performance of Convolutional Codes in Conjunction with Sequential Decoding," unpublished RPI report.

25. Modestino, J. W., "Simulation Facility for Investigating the Performance of Short Constraint Length Codes on Fading Channels," unpublished RPI report.

26. Croft, T. A., et. al., "Preliminary Review and Analysis of Effects of the Atmosphere of Venus on Radio Telemetry and Tracking of Engry Probes," Final Report under Contract NASA 2-7126, Stanford Electronics Laboratories, Stanford Univ., Stanford, Calif., Oct. 1972.

27. Woo, R., et. al., "Effects of Turbulence in the Atmosphere of Venus on Pioneer-Venus Radio-Phase I," Tech. Memo. 33-644, Jet Propulsion Laboratory, California Institute of Technology, June 1973.

28. Modestino, J. W., "Initial Simulation Results to be Obtained Concerning the Performance of Short Constraint Length Convolutional Codes on Fading Channels," unpublished RPI report.

29. Helstrom, C. W., Statistical Theory of Signal Detection, 2nd Edition, Pergamon Press, London, 1968.

30. Arnstein, D. S., "Phase Measurement Accuracy with Modulated Sounding Signals," IEEE Trans. Comm. Tech., Vol. COM-16, No. 3, June 1968, pp. 419-429.

31. Modestino, J.W., "Analysis of the Performance of a Phase Tracker for Use in Coded BPSK System," unpublished RPI report.